TAMPEREEN TEKNILLINEN YLIOPISTO
TAMPERE UNIVERSITY OF TECHNOLOGY

Sari Merilampi

The Exploitation of Polymer Thick Films in Printing Passive UHF RFID Dipole Tag Antennas on Challenging Substrates

Julkaisu 967 • Publication 967

Tampere 2011

Tampereen teknillinen yliopisto. Julkaisu 967
Tampere University of Technology. Publication 967

Sari Merilampi

The Exploitation of Polymer Thick Films in Printing Passive UHF RFID Dipole Tag Antennas on Challenging Substrates

Thesis for the degree of Doctor of Science in Technology to be presented with due permission for public examination and criticism in Auditorium 125, at Tampere University of Technology, Pori, on the 3rd of June 2011, at 12 noon.

Tampereen teknillinen yliopisto - Tampere University of Technology
Tampere 2011

ISBN 978-952-15-2578-0 (printed)
ISBN 978-952-15-2584-1 (PDF)
ISSN 1459-2045

Abstract

The main objective of this thesis was to study the usability of electrically conductive polymer thick film (PTF) inks and non-traditional substrate materials in passive Ultra High Frequency (UHF) radio frequency identification (RFID) tag antenna manufacturing. An important part of the work was to develop new applications for printed tags. The effect of the manufacturing method and the materials' electrical characteristics on tag performance was also investigated.

In recent years the use of radio frequency identification has become increasingly popular since it has many advantages over other identification systems. The integration of electronics, such as RFID tags, in different products is becoming more widespread with the growing need for greater functionality in products. With traditional electronic mass production techniques such as etching, the integration may not be technically or economically feasible. Printing, on the other hand, is a simple additive method which is suitable for mass production. Material loss and the use of chemicals are substantially less than in etching, and printing can also be performed on a variety of materials.

Although printing is a promising tag antenna manufacturing method, the printed tag materials are very different from those used in etched tags. This is challenging since the materials play a crucial role in tag functioning and their electrical properties are relatively unknown. In addition, the cost of an RFID tag is still too high for item level tracking. The price must decrease further and new applications must be found in order to gain maximum benefit from this technology. Rather than focusing on the reduction of tag costs, this thesis deals with the opportunities that novel materials and manufacturing methods offer.

The thesis consists of an introduction to the passive UHF RFID system, tag antenna performance, tag manufacturing and materials together with 9 publications. The publications present in detail the effect of the manufacturing method, the conductor material and the substrate effect on tag performance. The applications of printed tags are investigated through case studies.

The results obtained showed that competitive tags can be manufactured by printing, provided that the materials and manufacturing method are taken into account at the design stage. Indeed, the design process should be regarded as an integral part of the manufacturing process.

The use of PTF conductors, printing methods and non-traditional substrate materials facilitate the development of new applications and activities that could not be realised using traditional tag manufacturing and materials. The novel materials enable applications in which the printed tags are used for other purposes than product identification, such as tag-based sensing. This enhances the use of printable electronics as well as RFID technology.

Acknowledgements

This work was carried out at Tampere University of Technology (TUT), Pori, Electronics in close co-operation with the RFID research group of TUT, Department of Electronics, Rauma Research unit.

I would first like to thank my advisor Professor Pekka Ruuskanen for his guidance throughout this work. Pekka has provided me with much independence and responsibility but also support and advice whenever needed. I am also grateful to him for introducing me to the JOUSTE research project during the first year of my post graduate studies and for guiding me into the field.

Special thanks are also due to Professor Lauri Sydänheimo and Adjunct Professor Leena Ukkonen for all the opportunities they have given me in my research work. I am especially grateful for their encouragement and advice as well as the scope for networking. Without such co-operation this thesis would not have been possible in its present form. I would also like to thank Lauri Sydänheimo, Leena Ukkonen and Mr. Markku Paukkunen for the opportunity to complete my diploma thesis and for introducing me to my research interests. I am also grateful to Markku for his support throughout my career.

I wish to express my gratitude to professor Andrzej Dziedzic, Dean of Faculty of Microsystem Electronics and Photonics, Wroclaw University of Technology and Dr Jukka Voutilainen, CEO of Voyantic Ltd. for reviewing the manuscript of this thesis as well as Professor Aulis Tuominen of the University of Turku, Department of Information Technology (Electronics Productization) for agreeing to act as opponent at the public defense of this thesis.

Warm thanks also go to my close colleagues, Mr. Toni Björninen and Mrs. Teija Laine-Ma, for the fruitful co-operation and many enjoyable working days. I am also indebted to Adjunct Professor Antti Vuorimäki for his time, guidance and encouragement. I also wish to thank Mr. Veikko Haukka, Mr. Jussi Polvi and the other personnel of TUT, Pori, Electronics and TUT, Rauma research unit for a supportive and relaxed working environment. Mr. Alan Thompson I would like to thank for the English language revisions.

I would also like to thank Dean, Vice-President, Adjunct Professor Matti Lähdeniemi and Satakunta University of Applied Sciences for supporting me to finish my thesis.

I am grateful to Adjunct Professor Jari Palomäki for mentoring me during my post graduate studies and in the present research. Thanks are also due to Jari Palomäki, Professor Pekka Loula, Professor Hannu Jaakkola and Professor Tarmo Lipping for providing the opportunity to study at TUT, Pori doctoral school.

The financial support of the TUT, Pori doctoral school, Finnish Funding Agency for Technology (TEKES), the Emil Aaltonen Foundation, the Finnish Cultural Foundation - Satakunta Regional Fund, the Ulla Tuominen Foundation, High Technology Foundation of Satakunta and Porin akateemiset naiset are gratefully acknowledged.

Finally, I would like to express my heartfelt thanks to my family. Without their help and encouragement this work would never have been completed. I will always value the love and support of my parents, Maarit and Hannu Merilampi, during this work and throughout my life. I would also like to give special thanks to my brother Rami Merilampi who taught me to take nothing for granted. I am eternally grateful to my future husband, Antti Koivisto, for his unstinting love and patience throughout our years together.

Pori, April 2011

Sari Merilampi

List of publications

[P1] Merilampi S., Ukkonen L., Sydänheimo L., Ruuskanen P., Kivikoski M., Analysis of Silver Ink Bow-Tie RFID Tag Antennas Printed on Paper Substrates, International Journal of Antennas and Propagation, Volume 2007, 2007

[P2] Merilampi S., Laine-Ma T., Ruuskanen P., The Characterization of Electrically Conductive Silver Ink Patterns on Flexible Substrates, Microelectronics Reliability, Volume 49, Issue 7, 2009, pp. 782 - 790

[P3] Merilampi S., Haukka V., Ukkonen L., Ruuskanen P., Sydänheimo L., Kivikoski M., Loo C-H, Yang F., Elsherbeni A. Z., Printed RFID Tag Performance with Different Materials, The 5th International New Exploratory Technologies Conference (NEXT Conference), Turku, Finland, 2008, pp. 265 - 274

[P4] Björninen T., Merilampi S., Ukkonen L., Sydänheimo L., Ruuskanen P., The Effect of Fabrication Methods on Passive RFID Tags, The International Journal of Antennas and Propagation, Volume 2009, 2009

[P5] Merilampi S., Björninen T., Vuorimäki A., Ukkonen L., Ruuskanen P., Sydänheimo L., The Effect of Conductive Ink Layer Thickness on the Functioning of Printed UHF RFID Antennas, (IEEE Special Issue, RFID - A Unique Radio Innovation for the 21st Century), Proceedings of the IEEE, Volume 98, Issue 9, 2010, pp.1610 – 1619

[P6] Björninen T., Merilampi S., Ukkonen L., Ruuskanen P., Sydänheimo L., A Performance Comparison of Silver Ink and Copper Conductors for Microwave Applications, IET Microwaves, Antennas & Propagation, Volume 4, Issue 9, 2010, pp. 1224 - 1231

[P7] Merilampi S., Björninen T., Ukkonen L., Ruuskanen P., Sydänheimo L., Characterization of UHF RFID Tags Fabricated Directly on Convex Surfaces by Pad Printing, The International Journal of Advanced Manufacturing Technology, Volume 53, Issue 5, 2011, pp. 577-591

[P8] Merilampi S., Björninen T., Haukka V., Ruuskanen P., Ukkonen L., Sydänheimo L., Analysis of Electrically Conductive Silver Ink on Stretchable Substrates under Tensile Load, Microelectronics Reliability, Volume 50, Issue 12, 2010, pp. 2001-2011

[P9] Merilampi S., Björninen T., Ukkonen L., Ruuskanen P., Sydänheimo L., Embedded Wireless Strain Sensors Based on Printed RFID Tag, Sensor Review, Volume 31, Issue 1, 2011, pp. 32-40

Author's contribution

Publication 1 – "Analysis of Silver Ink Bow-Tie RFID Tag Antennas Printed on Paper Substrates" is contributed by the author with the help of co-authors. The author selected the tag materials, fabricated the prototypes and performed the measurements. The measurement set-up was planned by L. Ukkonen. The results were analyzed and the manuscript was written by the author with the help of the co-authors.

Publication 2 – "The Characterization of Electrically Conductive Silver Ink Patterns on Flexible Substrates" is contributed by the author with the help of the co-authors. The author fabricated the prototypes (excluding bending tests), planned the measurement set-up and performed the measurements (excluding bending tests). The bending test was performed by T. Laine-Ma. The results were analyzed and the manuscript was written by the author with the help of the co-authors.

Publication 3 – "RFID Tag Performance with Different Materials" is contributed by the author with the help of the co-authors. The author fabricated the prototypes with Veikko Haukka and selected the materials for them. The measurements were carried out by Matti Nikkari. The performance analysis and the manuscript writing were performed by the author together with the co-authors.

Publication 4 – "The Effect of Fabrication Methods on Passive RFID Tags" is contributed by the author together with the co-authors. The author fabricated the prototypes and selected the manufacturing methods and materials for the prototypes. Simulations were carried out by T. Björninen. The author performed the measurements with T. Björninen. The results were analyzed and the manuscript was written together with the co-authors.

Publication 5 – "The Effect of Conductive Ink Layer Thickness on the Functioning of Printed UHF RFID Antennas" is contributed by the author together with the co-authors. The author fabricated the prototypes and selected the materials for them. Simulations were carried out by T. Björninen. The measurement setup was planned and the measurements were performed by the author and T. Björninen. The results were analyzed and the manuscript was written by the author together with the co-authors.

Publication 6 – "A Performance Comparison of Silver Ink and Copper Conductors for Microwave Applications" is contributed by the author together with the co-authors. The author performed the prototype material selection and prototype manufacturing. The designs of the samples, simulations and measurements were performed by T. Björninen. The measurement results and writing of the manuscript were executed by the author together with the co-authors.

Publication 7 – "Characterization of UHF RFID Tags Fabricated Directly on Convex Surfaces by Pad Printing" is contributed by the author together with the co-authors. The author fabricated the prototypes and selected the materials for them. Simulation was carried out by T. Björninen. The measurement setup was planned and the measurements were performed by the author and T. Björninen. The results were analyzed and the manuscript was written by the author with help of the co-authors.

Publication 8 – "Analysis of Electrically Conductive Silver Ink on Stretchable Substrates under Tensile Load" is contributed by the author together with the co-authors. The author fabricated the prototypes and selected materials for them. The measurement set up was planned and the measurements were performed by the author. The results were analyzed and the manuscript was written by the author with the help of the co-authors.

Publication 9 – "Embedded Wireless Strain Sensors Based on Printed RFID Tag" is contributed by the author together with the co-authors. The author fabricated the prototypes and selected materials for them. The measurement setup was planned by the author. The measurements were performed by the author and T. Björninen. The results were analyzed and the manuscript was written by the author with the help of the co-authors.

List of abbreviations and symbols

Abbreviations

3D	Three-dimensional
Al	Aluminum
AC	Alternating current
Class1Gen 1	UHF Air Interface Protocol Standard (old)
Class1Gen 2	UHF Air Interface Protocol Standard
Cu	Copper
DC	Direct current
E-plane	Plane which contains $\overline{E}$ vector and direction of maximum radiation
EIRP	Effective isotropic radiated power
EM	Electromagnetic
EMT	Effective medium theory
EPC	Electronic product code
ERP	Effective radiated power
FCC	Federal Communications Commission
FEM	Finite element method
FR-4	Flame retardant-4, a PCB laminate
GID-96	General identifier, 96 bit
H-plane	Plane which contains $\overline{H}$ vector and direction of maximum radiation
HF	High frequency
HFSS	High frequency structural simulator (from Ansoft)
IEEE	Institute of Electrical and Electronics Engineers
IC	Integrated circuit
IL	Insertion loss
IR	Infrared
LF	Low frequency
MSL	Micro strip line
PCB	Printed circuit board
PET	Polyethylene terephthalate
PI	Polyimide
PLF	Polarization loss factor
PLM	Product life cycle management
PRC	Power reflection coefficient
PTF	Polymer thick film
PVC	Polyvinyl chloride
RCS	Radar cross section
RF	Radio frequency
RFID	Radio frequency identification

SCM	Supply chain management
SEM	Scanning electron microscope
SI	The International System of Units
SMA	RF connector type (Subminiature Type A)
UHF	Ulta high frequency
VNA	Vector network analyser

Symbols

a	Eq. (5-12): Conductivity exponent
A_e	Effective aperture (area) of an antenna (m^2)
$A_{e,receiver}$	Effective aperture of a receiving reader antenna (m^2)
$A_{e,tag}$	Effective aperture of a tag (m^2)
α	1) Attenuation constant (Np/m, where 1 Np = $20\log_{10}e \approx 8.69$ dB [Chen_93]) 2) Eq. (3-15): Coefficient which depends on specific modulation details of IC
$\overline{B}$	Magnetic flux density (T)
β	Phase constant (rad/m)
$\overline{D}$	Electric flux density (C/m^2)
D	Directivity
$D(\theta,\phi)$	Directivity in direction (θ,ϕ)
dl	Infinitesimal length (m)
δ	Skin depth (m)
ΔRCS	Vector differential radar cross section (m^2)
$\overline{E}$	Electric field strength (V/m)
E_0	Amplitude of electric field strength (V/m), see Eq. (2-7)
E_a	Electric field strength amplitude (of an antenna (V/m), see Eq. (3-9))
$\overline{E}_i$	Electric field of an incoming wave (V/m)
E_i	Electric field strength amplitude of an incoming wave (V/m), see Eq. (3-8)
E_θ	Electric field strength θ-component (V/m)
e	Euler's number (≈ 2.71828 [Spie_99])
$\hat{e}_r$	Unit vector, see Fig. 2.2
$\hat{e}_\phi$	Unit vector, see Fig. 2.2
$\hat{e}_\theta$	Unit vector see Fig. 2.2
$\hat{e}_x$	Unit vector in x direction, see Fig. 2.1

e_0	Total antenna efficiency
e_c	Conduction efficiency
e_d	Dielectric efficiency
e_{cd}	Radiation efficiency
e_r	Reflection (mismatch) efficiency
ε	Permittivity (F/m)
ε_0	Permittivity of free space ($\approx 8.85419 \cdot 10^{-12}$ F/m [Youn_00])
ε_c	Complex permittivity (F/m)
ε_r	Relative permittivity
ε'	Real part of complex permittivity (F/m)
ε''	Imaginary part of complex permittivity (F/m)
f	1) Frequency (Hz) 2) Volume fraction of conductive filler material in a composite, see Eqs. (5-11), (5-12) and Eq. (5-13)
f^*	Critical conductor volume fraction (f at percolation threshold)
G	Gain of an antenna
$G(\theta,\phi)$	Gain in direction (θ,ϕ)
G_i	Gain of an isotropic emitter
G_r	Gain of a receiver antenna
G_t	Gain of a reader transmit antenna
G_{tag}	Gain of a tag antenna
$G_{\lambda/2}$	Gain of a half-wave dipole antenna
G_s	Sheet conductance (S□), see Eq.(5-25)
Γ_{tag}	Power reflection coefficient of a tag antenna
γ	Propagation constant (m^{-1})
$\overline{H}$	Magnetic field strength (A/m)
$\overline{H}^*$	Complex conjugate of magnetic field strength (A/m)
H_ϕ	Magnetic field strength ϕ-component (A/m)
h	Thickness (m), see Fig. 5.2
I	Current (A)
I_{rms}	Root-mean-square value of current (A)
IL_{dB}	Insertion loss of a transmission line (dB), see Eq. (5-29)
$\overline{J}$	Electric current density (A/m^2)
j	Imaginary unit
k	Wave number (rad/m)
k_c	Complex wave number (rad/m)
k'	Real part of complex wave number (rad/m)
k''	Imaginary part of complex wave number (rad/m)

l	Length (m), see Fig. 5.2
L_{mod}	Modulation loss factor
λ	Wave length (m)
μ	Permeability (Vs/Am)
μ_0	Permeability of free space ($4\pi \cdot 10^{-7}$ Vs/Am [Youn_00])
μ_r	Relative permeability
η_0	Characteristic impedance of vacuum (≈ 377 Ω [Wadell_91; Bala_05])
ω	Angular frequency (rad/s)
P_{chip}	Power delivered to IC (W)
P_L	Loss power (W), see Eq. (3-4)
P_{loss}	Approximation of power loss (W) of structure in Fig. 5.2, see Eq. (5-21)
P_r	Radiated power (W)
$P_{received,\ signal}$	Power of modulated tag signal received by a reader (W)
$P_{scattered}$	Power scattered from a tag (W)
P_{tag}	Power which is captured by a tag (W) when transmitting $P_{transmitted}$, see Eq. (3-18)
$P_{transmitted}$	Transmitted power by a reader (W)
ψ_p	Angle between two unit vectors (polarization vectors), see Eq. (3-10)
q	Charge (C)
R	Resistance (Ω)
R_a	Antenna resistance (Ω)
R_L	Loss resistance (Ω)
R_l	Sheet resistance of lower layer of a conductor (Ω/□), see Eq. (5-27)
R_r	Radiation resistance (Ω)
R_s	Sheet resistance (Ω/□), see Eq. (5-26)
R_u	Sheet resistance of upper layer of a conductor (Ω/□), see Eq. (5-27)
r	Distance (m)
$\hat{r}$	Unit vector which points from a source point to a field point, see Eq. (2-1)
R_a	Surface roughness value, which is arithmetical average of deviations of average line and absolute measured value (m)
R_z	Surface roughness value, which is average of five highest points and five lowest points of a surface (m)
ρ	Resistivity (Ωm)
$\hat{\rho}_a$	Unit electric field vector (polarization vector) of an antenna
$\hat{\rho}_{tag}$	Unit electric field vector of a tag antenna
$\hat{\rho}_t$	Unit electric field vector of a transmitting antenna
$\hat{\rho}_w$	Unit electric field vector of an incoming wave

ρ_1	Power wave reflection coefficient of a tag in matched chip impedance state, see Eq. (3-15)
ρ_2	Power wave reflection coefficient of a tag in mismatched chip impedance state, see Eq. (3-15)
$\rho_{antenna}$	Power wave reflection coefficient of an antenna
$\lvert\rho_{antenna}\rvert^2$	Power reflection coefficient of an antenna
ρ_{tag}	Power wave reflection coefficient of a tag antenna
ρ_v	Electric charge density (C/m^3)
$\overline{S}$	Poynting vector (W/m^2)
S_{av}	Time-average Poynting vector (W/m^2)
$S_{incident}$	Incident power density (W/m^2)
S_{rad}	Radiation density (W/m^2), see Eq. (3-5)
$S_{scattered}$	Scattered power density (W/m^2)
S_t	Power density (W/m^2), see Eq. (3-16)
S_{21}	Transmission coefficient from port 1 to port 2, see Eq. (5-29)
S_{11}	Reflection coefficient of port 1, see Eq. (5-29)
S_{22}	Reflection coefficient of port 2, see Eq. (5-29)
σ	Electrical conductivity (S/m)
σ_c	Conductivity of a composite (S/m)
σ_f	Conductivity of filler (S/m)
σ_m	Conductivity of insulator phase (matrix) (S/m)
σ_r	Radar cross section (m^2)
σ_{ant}	Radar cross section related to antenna mode scattering (m^2)
σ_{struct}	Radar cross section related to structural mode scattering (m^2)
t	Time (s)
$\tan\delta$	Loss tangent
θ	Angle (rad) between dipole axis (z) and unit vector $\hat{e}_r$, see Fig. 2.2
U	Radiation intensity (W/solid unit angle)
$U(\theta,\phi)$	Radiation intensity in direction (θ,ϕ)
U_0	Radiation intensity of an isotropic radiator
vol%	Volume percent
V_{rms}	Root-mean-square value of voltage (V)
$\overline{v}$	Velocity (m/s)
v_p	Phase velocity (m/s) in (2-8)
w	Width (m), see Fig. 5.2
wt%	Weight percent
X_a	Antenna reactance (Ω)

Z_0	Characteristic impedance of transmission line or associated equipment (Ω)
Z_a	Antenna impedance (Ω)
Z_a^*	Complex conjugate of antenna impedance (Ω)
Z_{IC}	Chip impedance (Ω)
Z_{IC}^*	Complex conjugate of chip impedance (Ω)
Z_{in}	Input impedance (Ω)
Z_{tag}	Tag antenna impedance (Ω)
Z_{tag}^*	Complex conjugate of tag antenna impedance (Ω)

Table of contents

Abstract
Acknowledgements
List of publications
Author's contribution
List of abbreviations and symbols
Table of contents

1. Introduction 1
1.1 Radio frequency identification systems 2
1.1.1 Manufacturing methods of passive RFID tag antennas 3
1.2 Research challenges and the scope of the thesis 4
1.3 Structure of the thesis 5
2. Fundamentals of electromagnetics 7
2.1 Fundamental equations of electromagnetics 7
2.1.1 Maxwell's equations 7
2.1.2 Plane wave 9
2.1.3 Power density 10
2.1.4 The elemental electric dipole 10
3. Passive UHF RFID system 13
3.1 The structure and the operational principle of the passive UHF RFID system 13
3.2 Parameters for antennas 16
3.3 Power transfer between the reader and the tag 25
3.4. Measured quantities in evaluating tag performance 28
4. Printable tags – fabrication and materials 31
4.1 Printing methods and curing process 31
4.1.1 Screen printing method 32
4.1.2 Other printing methods 33
4.1.3 Curing process 34
4.2 Materials used in this study 35
4.2.1 Substrate materials 35
4.2.2 Electrically conductive polymer thick film inks 36
4.2.2.1 Composition of the ink 36
4.2.2.2. Morphology of the printed films 39
5. Challenges of printed passive UHF RFID polymer thick film tag antennas 47
5.1. Electrical performance of the substrates 47
5.1.1 Electrical properties of the substrates 48
5.2 Electrical performance of the polymer thick films 55
5.2.1 Electrical performance and ink composition 55
5.2.2 Electrical performance and morphology of the films 58
5.2.3 Electrical performance and curing 63
5.3 Electrical performance of samples in publications P2, P4-P7 64
5.3.1 Electrical performance of PTF structures with direct current 64
5.3.2 Electrical performance of PTF structures as a function of frequency 68
5.4 The effect of printing process and materials on the performance of passive UHF RFID tags 74

6. Applications of printed passive UHF RFID polymer thick film tag antennas – case studies 88
6.1 Printed passive UHF RFID tags in paper reel identification 88
6.2 Embedded passive UHF RFID tags 90
6.3 Tag-based sensing – wireless strain sensor 95
7. Final remarks and conclusions 104
References 107

Appendix: Publications P1-P9

1. Introduction

In recent years automatic identification procedures have become very popular in many service industries, purchasing and distribution logistics, manufacturing companies and material flow systems [Fink_03]. Radio frequency identification is an automatic identification technology with full benefits to be emerged in several years to all industries worldwide. RFID technology has potential, for example, in improving supply chain efficiency and hence to enhance the profitability level of the organization. Many leading organizations, the world largest retailers Wal-Mart and Mark & Spencer, as well as United States Department of Defense, for example, have become major supporters of this technology. Research activities have also recently increased [Mehr_08; Mehr_09].

The first known use of RFID was in World War Two to identify aircrafts. The technology was gradually taken into further use and nowadays it is utilized in applications such as access control and security, airline baggage handling, vehicle immobilizers, inventory management and smart cards. Much work is now being done to improve the systems and to lower their costs. A lot of effort is also being done to evolve standards for RFID and to improve privacy issues and reliability of RFID tag reading. A future goal is to lower the costs of the tags so they can be used in item level tracking and thus making them as ubiquitous as barcodes. More research is needed to create cost effective manufacturing processes and to find cheaper materials. Another way of increasing the benefit of RFID is to use it in new applications and this is the major research interest of present thesis. Printing the tags directly onto items would help in tagging the objects and also in product life cycle management (PLM) and brand protection. An important future trend is also to further exploit the RFID systems for other purposes, such as tag based sensing [Ukko_06; Side_07; Dobk_08; Mehr_08; Swed_10].

One vision considering the future of RFID is called “The Internet of Things” in which billions of unique tags would be attached to objects in different industries and applications. Manufacturing costs, implementation and maintenance of the tags are important factors in such applications. Passive tags, which are of main focus in this study, have the advantage of being easy to manufacture and they are also maintenance free. Currently the high frequency and ultra high frequency RFID inlay market is dominated by market segments that are strongly business to business oriented while the consumer market potential remains almost untapped. The greatest market potential is considered to be in applications that relate to the needs of consumers such as the use of wearable, embedded and “intelligent” tags [Dobk_08; Mehr_08; Numm_10; Virt_10].

1.1 Radio frequency identification systems

RFID systems consist of a reader, tags and a data processing system. The tags are located on objects which are identified and they typically consist of a coupling element and a microchip. The data processing system is connected to the reader in order to process the data and to provide additional information on the identified object. The communication and coupling between the reader and the tags in RFID systems are based on radio frequency electromagnetic (EM) fields and waves and this has many advantages over other identification systems. Many items can be remotely identified simultaneously, no visual contact is needed, reading through certain materials is possible, the tags can be made durable and the reading distance is longer. The tag memory capacity and data security are also better compared to visual identifiers. Despite the benefits of RFID, reliable reading requires knowledge about the interaction of surrounding materials and the EM fields and waves [Fink_03; Numm_10].

There are many different types of RFID system. Depending on the method of powering up the RFID tag, RFID systems can be categorized as active, semi-active or passive systems. Active RFID tags have an internal energy source (battery) to support microchip operation and transmit data to the reader and thus the tags can be classified as transmitting devices. The active tags have longer reading distances than passive systems, but they are more expensive. The semi-active RFID tags, called battery-assisted tags, also have an on-board power source. Semi-active tags provide a local battery to power the tag circuitry but use the power emitted from the reader to transmit their data. In passive RFID systems, the RFID tag has no on-board power source and it uses the power emitted from the reader to energize itself and transmit its data. Compared to active or semi-active tags, passive tags have shorter reading distances, they require higher-power readers and they are constrained in their capacity to store data. However, passive tags are simpler in structure, lighter in weight, less expensive, generally more resistant to harsh environmental conditions, and offer virtually unlimited operational lifetime. This thesis concentrates on passive systems because of the future potential for item level tracking which might lead to explosive growth in the use of passive RFID tags. In addition, the passive technology shows promise in embedded applications since passive tags require very little maintenance [Fink_03; Ukko_06; Chen_07; Numm_10].

Another common way to classify RFID systems is according to the operation frequency and coupling of the systems. The following frequency ranges are typically used: LF (low frequency, 30 - 300 kHz), HF (high frequency, 3 - 30 MHz) and UHF (ultra high frequency, 300 MHz - 3 GHz). Microwave frequency systems also exist (5.8 GHz, for example) [Dobk_08].

LF and HF systems typically use inductive coupling based on magnetic fields, and the coupling elements of these systems are coils. The systems work in the near field and

thus their reading distances are limited (1 cm for LF and about 1 m for HF). LF and HF systems like 125 kHz and 13.56 MHz are already used in many RFID applications such as access control, cattle tracking and smart cards. LF systems are reaching the end of their development cycle and new applications are unlikely to emerge. Systems which work at UHF frequencies are under research and development and their use is emerging. UHF systems have potential in applications such as supply chain management (SCM) and product life cycle management. UHF systems communicate using electromagnetic waves in far field and thus longer reading distances are achieved. With UHF systems the identification is fast and many objects can be "simultaneously" identified. It is also possible to identify moving objects. This thesis focuses on the passive UHF RFID system and this is discussed in greater detail in Chapter 3 [Fink_03; Ukko_06; Dobk_08; Mehr_08].

1.1.1 Manufacturing methods of passive RFID tag antennas

RFID tags are manufactured by the same manufacturing processes as printed circuit boards (PCB). Etching is commonly used in tag manufacturing to produce the conductive antenna pattern. The initial material is typically Cu or Al film on plastic substrate. Etching is a mature, robust process, and produces films with excellent conductivity. However, the etching process is subtractive, involves numerous process phases and uses many different chemicals, which is not environmentally friendly and which adds costs. Substrate must also tolerate the process chemicals. One recent trend is to embed electronics into other structures such as packaging, machines and clothing. In the case of RFID tags, it would be convenient to use the item which is to be identified as the substrate. This would eliminate the need for additional substrate material and create cost savings as well as offering the opportunity to develop new applications. For these reasons additive processes are gaining interest.

Printing methods are the most common additive methods applied in RFID tag antenna fabrication and they are nowadays being widely researched. Printing is a simple and fast method which also enables mass production and roll to roll manufacturing. The printing process involves only two process steps - printing and curing. The material loss and the use of different chemicals are considerably reduced compared with etching and thus there is also significantly less waste. Printing methods also enable the use of various substrates including plastics, papers and fabrics. This creates an opportunity to develop novel light-weight, flexible applications such as large area sensors. In addition, it enables embedding electronics into other structures. The term "printed tag" refers (also in this thesis) to a tag whose antenna is fabricated by printing instead of etching. Printing could also be used in the RFID microchip manufacturing although printed chips are not available in the market due to challenges related to semiconductor inks. Though, it is worth noticing that promising results have recently been published also considering the

semiconductor inks. The capability of fabricating entirely printed tag would dramatically increase the use of printed tags [P8; P9; Kovi_11].

1.2 Research challenges and the scope of the thesis

A common challenge in RFID tag manufacturing is to maintain feasible electrical performance of the tags while achieving savings of cost. The printing process is cost effective but the ink materials tend to be expensive. Thus, in tag antenna printing, it is important to reduce the use of ink and also to find applications that would benefit most from the use of printed tags as opposed to their etched counterparts. The aim of this thesis is to apply polymeric silver inks and challenging substrates in passive UHF RFID tag antenna manufacturing and, ultimately, develop new applications and assist integration of electronics on other structures [P4; P5; Dobk_08].

The tag antenna's performance is dependent on the selected printing method as well as on the tag's materials. The materials are considerably different from those typically used in electronics manufacturing. Polymer thick film (PTF) conductive ink which consists of insulating polymer matrix, conductive fillers, solvents and additives, is typically used as the conductive medium. Modern conductive silver inks achieve sheet resistance of around 12 mΩ/□ – 20 mΩ/□, which is about 10 times higher than solid copper [Dobk_08]. A common substrate is flexible plastic foil, but in the case of embedded applications the substrate could equally be paper, fabric or other material. Information on the characteristics of such materials is limited, especially on RF frequencies. In addition, printed films are uneven, in contrast to the relatively smooth copper films. For these reasons, this study also examines the effect of printing methods, PTF inks and non-traditional substrates on the performance of passive UHF RFID tags. The goal is to determine how the materials and the new manufacturing method affect tag operation and how these can be utilized in different applications. This is realized by determining the interaction of electromagnetic waves and the novel materials used in printed tags and applying the information in RFID.

The main focus of this thesis is screen printed polymer thick film antennas, though direct gravure printing and pad printing are also discussed as reference methods for screen printing. Comparisons are also made between traditional etched copper structures and printed structures. Other printing techniques, microchip printing and semiconductor inks, thin films, long term reliability, chip attachment and active applications lie beyond the scope of the study.

1.3 Structure of the thesis

This thesis consists of 9 publications and 7 chapters which include the theoretical background and the major objectives of this study. The structure of the thesis is presented in Fig. 1.1.

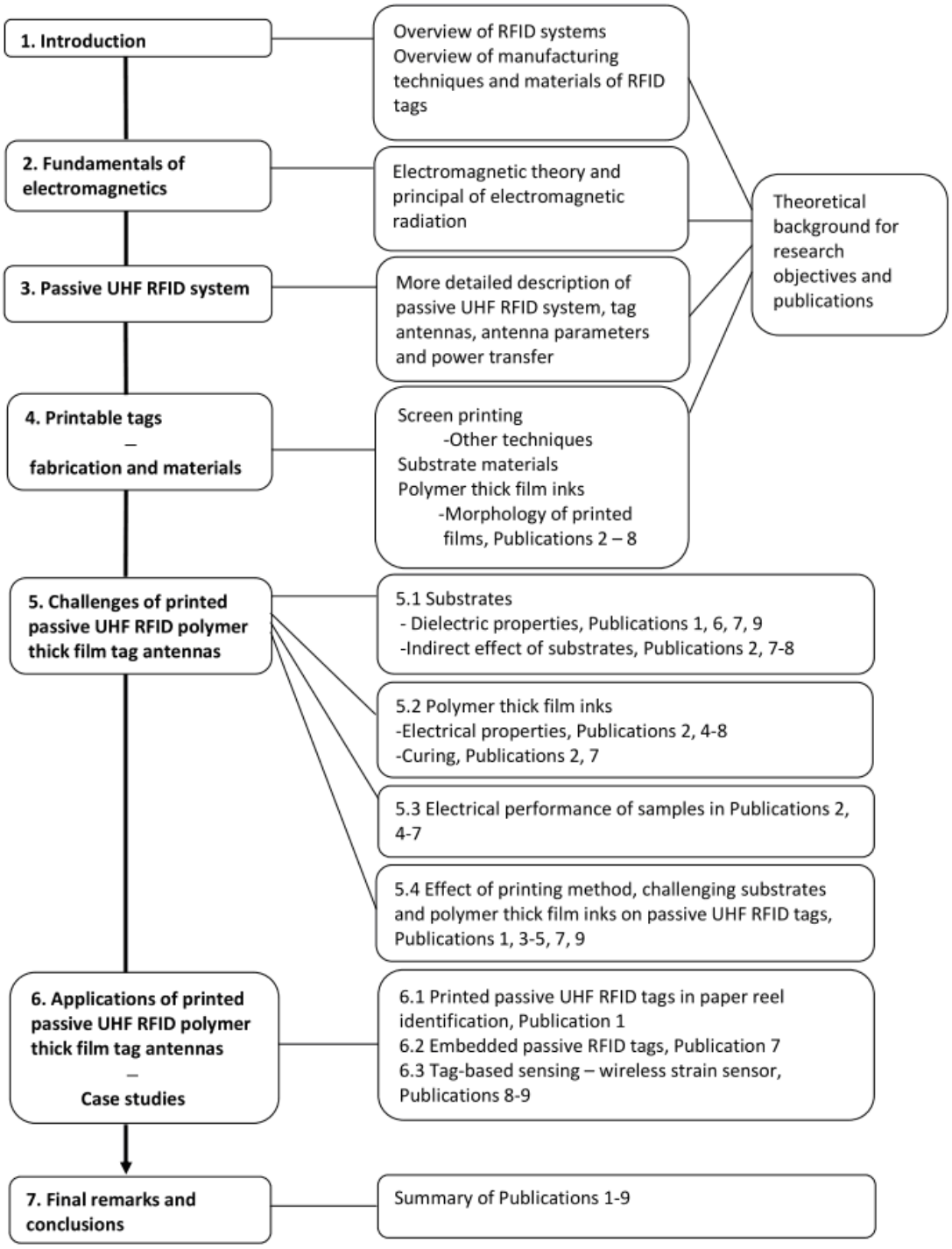

Figure 1.1 Structure of the thesis.

Because the operation of the RFID system is based on electromagnetic fields and waves, the basics of electromagnetic theory are first introduced in Chapter 2. The passive UHF RFID system is then discussed in Chapter 3 since the thesis deals mainly with this type of RFID system. The focus is on tag antennas and thus basic antenna parameters are introduced in order to analyze tag performance. Power transfer between the reader and the tag is discussed so as to link the properties of the tag to the performance of the entire RFID system. Printing of the tag antennas is discussed in Chapter 4. The principle of screen printing, gravure printing and pad printing are presented. In addition, the typical conductive polymer thick film ink, the substrate materials and the effect of the substrate on the printed film morphology are discussed. The challenges arising from the printing of passive UHF RFID antennas with PTF inks on non-traditional substrates are considered in Chapter 5. The electrical performance of the substrates is investigated and the indirect effects of substrates are discussed. The conductor losses of printed polymer thick films are also analysed. The effect of the composition, morphology and curing are examined. Finally, the effects of all the above factors on UHF RFID tag performance are introduced at the end of Chapter 5. They are implemented and utilized in various applications in Chapter 6 (case studies). Chapter 7 contains some final remarks and presents the conclusions of the study. Publications [P2; P4 - P8] deal with the performance of the printed films and the substrates. Publications [P1; P3 - P5; P7; P9] present the effect of the materials on passive UHF RFID tag operation. Case studies of the opportunities offered by the use of printed passive UHF RFID tags are presented in publications [P1; P7; P9]. In publication [P9] the effect of materials on the tag antenna operation is applied in a novel application, wireless strain sensor.

2. Fundamentals of electromagnetics

The operation of the UHF RFID system is based on signal transmission. Electromagnetic waves and their ability to carry energy form the basis of the technology. Because of this it is important to understand the basic theoretical principles of electromagnetics. These are discussed below.

2.1 Fundamental equations of electromagnetics

A point charge creates an electric field around it. The electric field strength $\overline{E}$ (V/m) depends (in free space) on the charge q (C) and distance r (m) from the charge by the equation

$$\overline{E} = \frac{1}{4\pi\varepsilon_0}\frac{q}{r^2}\hat{r}, \tag{2-1}$$

where ε_0 is permittivity of free space ($\approx 8.85419 \cdot 10^{-12}$ F/m [Youn_00]), $\hat{r}$ is unit vector which points from the source point to the field point. A moving charge (or current) creates a magnetic field in the surroundings in addition to the electric field. When considering a point charge with constant velocity $\overline{v}$ (m/s), the magnetic flux density $\overline{B}$ (T) can be expressed as

$$\overline{B} = \frac{\mu_0}{4\pi}\frac{q\overline{v}\times\hat{r}}{r^2}, \tag{2-2}$$

where μ_0 is the permeability of the free space ($4\pi \cdot 10^{-7}$ Vs/Am [Youn_00]). The magnetic field is always perpendicular to the velocity and vector $\hat{r}$. If these fields do not vary with time (as in the case of a charge at rest and at constant velocity described above), electric and magnetic fields can be analyzed independently. When the fields vary with time, they are no longer independent. This is the case, for example, when the point charge is moving with accelerating velocity. In such a case the accelerating charge creates electromagnetic waves. Interaction between the electric and magnetic fields is summarized in Maxwell's equations [Youn_00].

2.1.1 Maxwell's equations

The theoretical concepts of electromagnetics are described by a set of basic laws formulated by Faraday, Ampere, Gauss, Lenz, Coulomb, Volta and others. The laws were

combined into a standard set of vector equations by James Clerk Maxwell in 1864 [Bala_89]. In engineering the sinusoidal time dependence makes the handling of equations easier. In practice, most generators produce voltage and currents and hence electric and magnetic fields vary sinusoidally with time [Chen_93].

Field vectors that vary with space and are sinusoidal functions of time t (s) can be presented by vector phasors which depend on the space coordinates *(x, y, z)* but not on time. Time harmonic $\overline{E}$ referring to cos ωt can be expressed as: $\overline{E}(x, y, z, t) = \mathrm{Re}\left[\overline{E}(x, y, z)e^{j\omega t}\right]$, where angular frequency $\omega = 2\pi f$ (rad/s), f is frequency (Hz) and $\overline{E}(x, y, z)$ is a vector phasor that contains information on the direction, magnitude and phase of the field. By using phasor expressions $\frac{\partial}{\partial t}$ can be replaced by multiplying by $j\omega$ and time harmonic Maxwell's equations are presented as

$$\nabla \times \overline{E} = -j\omega\mu\overline{B} \tag{2-3}$$

$$\nabla \times \overline{H} = \overline{J} + j\omega\varepsilon\overline{D} \tag{2-4}$$

$$\nabla \cdot \overline{D} = \rho_v \tag{2-5}$$

$$\nabla \cdot \overline{B} = 0 \tag{2-6}$$

where j is the imaginary unit, $\overline{D}$ is the electric flux density (C/m^2), $\overline{J}$ is the electric current density (A/m^2), $\overline{H}$ is the magnetic field strength (A/m), $\mu = \mu_0\mu_r$ is the permeability (Vs/Am) (μ_r is the relative permeability of a medium), $\varepsilon = \varepsilon_0\varepsilon_r$ is the permittivity (F/m) (ε_r is the relative permittivity of a medium) and ρ_v is the electric charge density (C/m^3). In a linear and isotropic medium $\overline{D} = \varepsilon\overline{E}$ and $\overline{B} = \mu\overline{H}$ (see Eq. (5-1) and (5-2)) [Chen_93; Bala_89].

Faraday's law (Eq. (2-3)) shows that a time-varying magnetic field gives rise to an electric field (electromagnetic induction). In a conductive medium (in this thesis, in antennas) this creates a voltage and a current. Ampere's law (Eq. (2-4)), including Maxwell's displacement current density $j\omega\varepsilon\overline{D}$, shows that both conduction current and time-varying electric flux density act as sources of a magnetic field. In addition to the laws of Ampere and Faraday, Gauss's law and Gauss's law for magnetism include Maxwell's equations. Gauss's law (Eq. (2-5)) states that the total electric flux through any closed surface (Gaussian surface) is proportional to the net electric charge inside the surface. Gauss's law for magnetism (Eq. (2-6)) shows that magnetic flux through any closed surface is always zero (there are no isolated magnetic charges) [Bala_89; Chen_93; Youn_00].

2.1.2 Plane wave

A uniform plane wave is one particular solution for Maxwell's equations. In this case $\overline{E}$ has the same direction, same magnitude and phase in all planes perpendicular to the propagation direction, and similarly for $\overline{H}$. The electric field is mainly discussed, but similar examination can be made with the magnetic field. A uniform plane wave does not exist in practice, but far enough away from the source of the wave, which is the case in the UHF RFID systems discussed in this thesis, the surface of constant phase (wave front) becomes spherical. When considering a very small portion of a large spherical surface, it may be considered almost a plane [Chen_93].

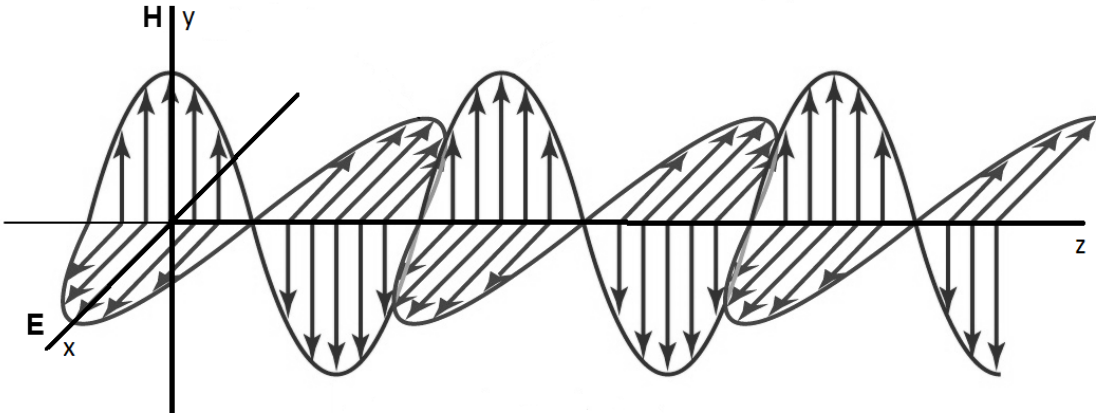

Figure 2.1 A plane wave propagating in z direction [Meri_06].

The plane wave, where the fields vary sinusoidally, propagating in z direction in Fig. 2.1 can be represented by the equation

$$\overline{E}(z,t) = \hat{e}_x E_0 \cos(\omega t - kz) = \mathrm{Re}\left\{\hat{e}_x E_0 e^{j\omega t} e^{-jkz}\right\}, \tag{2-7}$$

where $\hat{e}_x$ is unit vector in x direction, E_0 is amplitude and $k = \frac{2\pi}{\lambda}$ (rad/m) is wave number (λ is wave length (m)). Wave number in a lossless medium with permeability μ and permittivity ε can be expressed as

$$k = \omega\sqrt{\mu\varepsilon} = \frac{\omega}{v_p}, \tag{2-8}$$

where v_p is phase velocity (m/s). As can be seen from the above expression, a medium has an effect on the propagating wave through material parameters μ and ε. The effect of materials on wave propagation and losses is discussed further in Chapter 4 [Chen_93].

2.1.3 Power density

In wireless communication systems (such as UHF RFID system) electromagnetic waves are used to transfer energy and, as a consequence, also information. The Poynting vector $\overline{S}$ is a power density vector which represents the energy flux (in W/m^2) of an electromagnetic field. The equation for the Poynting vector is

$$\overline{S} = \overline{E} \times \overline{H} . \tag{2-9}$$

The Poynting vector has the same direction as the direction of the wave's propagation.

The Poynting vector at a point is equivalent to the power density of the wave at that point. In regard to power transfer, its average value is more a significant quantity than the instantaneous value. The time-average Poynting vector (Eq. (2-10)) can be computed from the instantaneous Poynting vector (Eq. (2-9)). If the fields are time harmonic and the vectors are of phasor form, the time average power density can be written as

$$S_{av} = \tfrac{1}{2} \mathrm{Re}\{\overline{E} \times \overline{H}^{*}\}, \tag{2-10}$$

where $\overline{H}^{*}$ is a complex conjugate of the magnetic field strength [Bala_89; Chen_93].

2.1.4 The elemental electric dipole

As explained earlier, electromagnetic waves originate from sources, which in electromagnetic terms are time-varying (accelerating) charges and currents. Antennas are structures which are designed to transmit and receive electromagnetic energy efficiently in a prescribed way [Chen_93]. When current flows in an antenna (for example, when an antenna is fed), according to Amperes law (Eq. (2-4)), conduction current and time-varying electric flux density act as sources of a magnetic field. According to Faraday's law (Eq. (2-3)) a time-varying magnetic field induces an electric field. Time varying electric flux density acts as a source of a magnetic field and so on. As a result of this, electromagnetic waves are radiated from the antenna.

In UHF RFID systems the tag antennas are typically dipoles. The elemental electric dipole is an infinitesimal conductor, also called a current element. It can be considered as an ideal dipole since the conductor is electrically very small (<< wavelength) and this way the current is uniform in both magnitude and phase in the radiating element (and the current and the electric field are not place-dependent). Though such a structure does not exist, it describes the functioning of a dipole. More complex structures can be constructed from elemental dipoles [Ukko_06].

The expression of an electric and magnetic field of an ideal dipole can be derived from Maxwell's equations. In UHF RFID systems the tags typically operate in the far field region, where the angular field distribution is assumed independent of the distance from the antenna. The electric and magnetic field of an oscillating ideal dipole of length *dl* in time harmonic case in spherical coordinates (Fig. 2.2) can be written as

$$\overline{H} = \hat{e}_\phi j \frac{Id\ell}{4\pi}\left(\frac{e^{-jkr}}{r}\right)k\sin\theta \tag{2-11}$$

$$\overline{E} = \hat{e}_\theta j \frac{Id\ell}{4\pi}\left(\frac{e^{-jkr}}{r}\right)\eta_0 k\sin\theta \tag{2-12}$$

where $\hat{e}_\phi$ and $\hat{e}_\theta$ are unit vectors, r is the distance from the ideal dipole and θ (rad) is the angle between the dipole axis (z) and the unit vector $\hat{e}_r$ (see Fig. 2.2), I (A) is current and $\eta_0 = \sqrt{\frac{\mu_0}{\varepsilon_0}}$ is the characteristic impedance of vacuum (≈ 377 Ω [Wadell_91; Bala_05]). It is seen from Eqs. (2-11) and (2-12) that $E_\theta = \eta_0 H_\phi$, where E_θ is the electric field strength θ-component and H_ϕ is the magnetic field strength ϕ-component [Bala_05; Ukko_06].

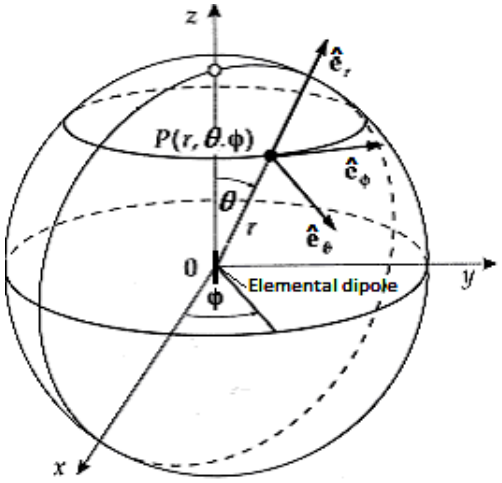

Figure 2.2 Ideal dipole and spherical coordinates which relate to Eqs. (2-11) and (2-12) [Meri_06].

It can be seen that in the far field, electric and magnetic fields are in phase and orthogonal to each other. It is also noted that they are mutually dependent and the fields decay as 1/*r*. In addition, if the expression of power density is examined, it would indicate power transfer through a spherical surface. The fields, therefore, form an electromagnetic wave [Bala_05; Ukko_06].

In real finite antennas the current and electric field vary along in the antenna (unlike in the case of an ideal infinitesimal dipole). A simple antenna that is commonly used is the half wave dipole. A standing wave occurs in the dipole when it is at its resonant frequency. In a half wave (λ/2) dipole at base frequency, the current changes most powerfully in the middle of the dipole and is zero at the ends. The electric field changes most powerfully at the ends of the dipole and is zero at its middle. Thus, λ/2 antennas are resonant antennas, which means that the input impedance at resonance frequency is real (reactance = 0). UHF RFID tag antennas are usually constructed to achieve half-wavelength resonance, but the size and geometry of the tag is typically modified [Yang_06]. This is discussed in greater detail in the next chapter [Carr_01; Yang_06].

3. Passive UHF RFID system

This chapter presents the passive UHF RFID system and also takes a closer look at tag antennas which are the main topics of this thesis. The operational principle of passive UHF RFID system is first described and then typical antenna parameters are introduced. These help in the evaluation of tag antenna performance. Next there is a description of power transfer between the reader and the tag in order to link the properties of the tag to the performance of the entire system. Finally, typical measurement quantities of the RFID tags used in publications [P1; P3 - P5; P7; P9] are discussed.

The performance of the passive UHF RFID system depends on the properties of the tag as well as the reader. In addition, other matters such as sources of interference from the environment (other equipment and materials), placement of the tag and the reader antennas, and also the tag population and movement have an effect on tag performance. The focus in this thesis is on tag antenna properties.

3.1 The structure and the operational principle of the passive UHF RFID system

As discussed in the introduction, there is variety of different RFID systems. RFID tags at lower frequencies (LF and HF) function over short distances. Such systems are known as close coupling systems (read range 0 - 1 cm) and remote coupling systems (read range up to approximately 1 m). However, longer reading distances are needed in many applications. Passive UHF spectrum RFID systems achieve read ranges of over one meter, and are thus termed long range systems. The commonly encountered UHF band is 860 MHz - 960 MHz. The UHF centre frequencies are: 866 MHz in Europe, 915 MHz in the Americas and 950 MHz in Asia and Australia. There are also microwave frequency systems. These systems work at frequencies of 2.4 GHz - 2.45 GHz and 5.8 GHz. The UHF band formally ends at 3 GHz, but in order to make a convenient distinction between systems operating at ≈ 900 MHz and 2.4 GHz systems, the 2.4 GHz systems are known as microwave systems. The UHF and microwave frequencies have relatively short wavelengths, which allow construction of antennas with smaller dimensions and greater efficiency that would be possible using frequency ranges below 30 MHz [P1; Rao_99; Fink_03; Dobk_08].

The space surrounding an antenna is usually subdivided into three regions: 1. reactive near field (defined by C.A. Balanis [Bala_05] as “that portion of the near field region immediately surrounding the antenna wherein the reactive field predominates”), 2. radi-

ating near field (defined by C.A. Balanis [Bala_05] as “that region of the field of an antenna between the reactive near field region and the far field region wherein radiation fields predominate and wherein the angular field distribution is dependent upon the distance from the antenna”) and 3. far field regions. Long range systems (UHF and microwave) work in the antenna’s far field. The far field region is defined by C.A. Balanis [Bala_05] as “that region of the field of an antenna where the angular field distribution is essentially independent of the distance from the antenna”. In this study it is assumed that the tag antennas are in the far field region and their properties in other field regions are not further discussed [Bala_05].

In long range systems, the interaction between the reader and the tags is based on electromagnetic wave propagation. Radio waves reflect from objects which are larger than $\lambda/2$. Reflection from smaller objects is called scattering, or in the case of a transmitter and a receiver, the term used is backscattering. Backscattering means that the transmitted wave which is then received by the receiver is reflected from an object at the same frequency (transmitted frequency). The passive UHF RFID system is thus based on backscattering. The system consists of the data processing system, the reader and the tags, which are attached to the objects to be identified. In publications [P3 - P5, P7 and P9] the RFID system supports EPCglobal UHF Class 1 Gen 2 standard (Electronic Product Code Class 1 Generation 2) and in publication [P1] Class 1 Gen 1 standard (Electronic Product Code Class 1 Generation 1). Gen 2 standards were ratified at the end of 2004 in response to the limitations of the Gen 1 standards. In addition to other improvements, Gen 2 standard is specially designed to take account of global telecommunication regulations. The EPCglobal organisation publishes an update online report of UHF regulations worldwide through their website. The RFID protocols are not discussed in detail in this thesis, but some principles of the communication between the reader and the tags in passive UHF RFID systems are discussed below [Fink_03; Ukko_07; Zebr_07; Numm_10; Zebr_10].

In passive UHF RFID systems which support the EPC Class 1 Gen 2 standard, communication begins with the reader which emits a continuous wave (power) to activate the tag. The continuous wave is followed by a command, typically a query command. After the command, the reader starts to send a continuous wave which is then modulated and backscattered by the tag, according to its identification code. The modulation is executed by changing the scattered field from the tag. The communication between the reader and the tag is half duplex, which means that when the reader “talks”, the tag “listens” and vice versa. The tag is allowed to talk when it has been given a command by a reader (reader talks first). The principle of passive UHF RFID system, which is also used in the measurements in this thesis, is illustrated in Fig. 3.1 [Fink_03; Ukko_07; EPC_08; Loo2_08; Numm_10].

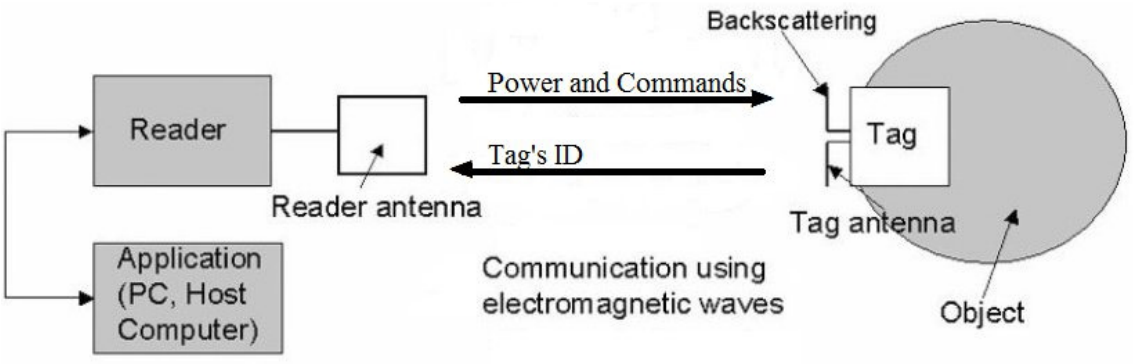

Figure 3.1. Principle of passive UHF RFID system [Ukko_07].

The tags are antennas loaded with a microchip in which all the electronics that the tag needs are integrated. In passive RFID systems the tag receives all its operation power from the electromagnetic wave sent by the reader. Supply voltages for the electronics such as modulator/demodulator, logic and memory are provided by voltage rectifier from the wave. Each chip has memory which contains at least a unique identification number, but also other data can be added to the memory depending on the type of chip. One potential form of RFID tag data content is electronic product code, EPC, which is a globally unique serial number. When the number is read, it can be associated with data stored in a database. The general and most simple type of EPC is called a general identifier, 96 bit, GID-96 [P1; P3; P7; P9; Auto_02; Numm_10].

The antenna's function in the tag is to receive and backscatter the electromagnetic wave which is transmitted by the reader. The wave is led through the tag antenna to the microchip and backscattered to the reader according to modulation. In backscattering systems the modulation of the scattering from the tag is realized by switching the input impedance of the chip between two different values. Typically the chip has a matched impedance state and a mismatched impedance state (although use of other impedance states has also been reported). In the case of poor matching (commonly chip impedance $Z_{IC} \approx 0$ or $Z_{IC} \approx \infty$) almost all power is backscattered to the reader. In the well-matched state the power is transferred from the tag antenna to the chip and a fraction of the transmitted power is backscattered. In addition to the amplitude of the backscattering wave, also the phase may be changed (depending on the chip impedance states). These changes in the backscattering wave can be interpreted as bits 1 and 0 [Fink_03; Dobk_08].

Since the tags' antenna transfers power to the chip, their impedances must be well matched to maximize the power transfer. Typically antennas are designed to match either 50 Ω or 75 Ω loads. However, the RF front end of passive RFID chips often incorporates Schottky diodes, which give the chip input impedance far from the common impedances of other RF systems. The input impedance of the chip typically has a relative-

ly low real part and a capacitive imaginary part of some hundred Ohms. The maximal power is transferred when the impedance of the antenna is a complex conjugate of the chip. Chip manufacturers usually provide "optimal" design impedance, to which the antenna impedance is matched. This chip impedance is 1200 – *j*145 Ω in article [P1], 40 – *j*95 Ω in article [P3] and 17 – *j*137 in articles [P4; P5; P7 and P9], for example. To provide the inductive imaginary part of the antenna, tuning circuits (see t-match in article [Marr_08], for example) are used in the tag geometry. Antenna impedance and chip impedance are also both functions of frequency. In addition, chip impedance is a function of power absorbed. This is why complex conjugate matching only occurs at a single frequency. If wide band antennas are required, other matching techniques are more suitable [P3; P4; P9; Pill_06; Stor_06; Ukko_06 Yang_06; Side_07; Loo1_08; Loo2_08; Loo3_08].

The UHF RFID tag antenna is usually built to achieve half wavelength resonance for efficiency optimization. In the UHF band, a half-wave dipole antenna is ≈ 16 cm in length in free space. For the purpose of reducing tag sizes, modifications (i.e. meander line structure and folded arms) are typically made to downsize the tag. Because of the tuning and size reduction, the structure of the tag antenna is complex and simulations are typically used in the design process. The antenna design issues lie outside the scope of the thesis but various antenna structures are presented in the attached publications [P1; P3 - P5; P7; P9; Yang_06].

3.2 Parameters for antennas

The focus of this thesis is printed tag antennas and their performance. Definitions of antenna parameters are needed to describe the performance and typical parameters are presented below.

Input impedance of an antenna is defined as "the impedance presented by an antenna at its terminals" [Bala_05]. The ratio of voltage to current at these terminals, with no load attached, defines the impedance of the antenna as

$$Z_a = R_a + jX_a, \tag{3-1}$$

where Z_a is antenna impedance (Ω), R_a is antenna resistance (Ω) and X_a is antenna reactance (Ω). In Eq. (3-1) the antenna is assumed to be isolated from the surroundings.

Since the input impedance of an antenna is generally a function of frequency, the antenna will be matched to the interconnecting transmission line or associated equipment (in the case of RFID tags, tag antenna to IC) only within a bandwidth. In addition, the input impedance of the antenna depends on many factors such as its geometry and surrounding objects. Only a limited number of practical antennas have been investigated analyti-

cally. For many others, the input impedance has to be determined experimentally [P1; P3 - P5; Bala_05; Loo1_08; Loo2_08].

In general the resistive part of the antenna impedance (see Eq. (3-1)) consists of two components: radiation resistance R_r and loss resistance R_L as follows*

$$R_a = R_r + R_L . \tag{3-2}$$

Part of the power that is delivered to the antenna is radiated through the mechanism provided by the radiation resistance. Another part of the power is dissipated as heat, which affects the efficiency of the antenna (see Eq. (3-4)) [Bala_05; Ukko_06].

* Loss resistance cannot in all antennas be represented in series with radiation resistance.

The **total antenna efficiency e_0** (dimensionless) is used to take account of losses at the input terminals and within the structure of the antenna. These losses include dielectric losses, conductor losses and reflections caused by the mismatch between antenna and the transmission line or other associated equipment. Overall antenna efficiency can be presented as

$$e_0 = e_r e_c e_d , \tag{3-3}$$

where e_c is conduction efficiency, e_d is dielectric efficiency and e_r represents reflection (mismatch) efficiency. As discussed, in RFID tags both IC and tag antenna have complex impedance. The power reflection coefficient $\left|\rho_{antenna}\right|^2$ is a quantity that describes the quality of the power transfer between two complex impedances. The reflection efficiency can be given with the power reflection coefficient as: $e_r = (1-\left|\rho_{antenna}\right|^2)$, where $\left|\rho_{antenna}\right|^2 = \left|(Z_{in} - Z_0^*)/(Z_{in} + Z_0)\right|^2$, $\rho_{antenna}$ is the power wave reflection coefficient, Z_0 is characteristic impedance of transmission line or associated equipment, Z_0^* is its complex conjugate and Z_{in} is the input impedance of the antenna. Power reflection coefficient is related to the concept of power waves, which are not travelling waves like voltage waves. If Z_0 is real, $\rho_{antenna}$ represents the voltage reflection coefficient [P9; Kuro_65; Stut_98; Niki2_05; Loo2_08].

Conductor and dielectric losses are very difficult to compute, but they can be experimentally evaluated. Even then, however, they cannot be separated and it is convenient to use $e_{cd} = e_c\ e_d$ and refer to it as **radiation efficiency**. The radiation efficiency e_{cd} describes the fraction of power that is radiated from the total power received by the antenna structure.

It can thus be derived from radiated and loss power values or from radiation resistance and loss resistance (Eq. (3-2)) as

$$e_{cd} = \frac{P_r}{P_L + P_r} = \frac{R_r}{R_L + R_r} \tag{3-4}$$

where the subscript *L* refers to the combined conductor and dielectric loss power and the corresponding loss resistance [Bala_05].

In addition to losses of the antenna, it important to consider how the antenna radiates in different directions. According to C.A Balanis, **radiation pattern** is "a mathematical function or graphical representation of the radiation properties of the antenna as a function of space coordinates" (not a function of distance). The radiation pattern is usually presented in far field region. The radiation properties include radiation intensity, field strength, flux density, directivity (gain) and polarization. The most typical radiation property is the spatial distribution of radiated energy as a function of the observer's position along a path or surface of constant radius [Bala_05].

Radiation patterns are often normalized with respect to their maximum value and thus often given in decibels (dB). Radiation patterns can be presented three dimensionally and also in a series of two-dimensional patterns. Two planes which are often used in the case of linearly polarized antennas (polarization is discussed later in this chapter) are E-plane (which contains the $\overline{E}$ vector and direction of maximum radiation) and H-plane (which contains the $\overline{H}$ vector and direction of maximum radiation). Fig. 3.2 shows the E-plane and H-plane radiation patterns of an elemental electric dipole described in Section 2.1.4. Fig. 3.3 illustrates the same radiation pattern three-dimensionally. The three-dimensional radiation pattern (Fig. 3.3) contains one H-plane and infinity E-planes [Bala_05].

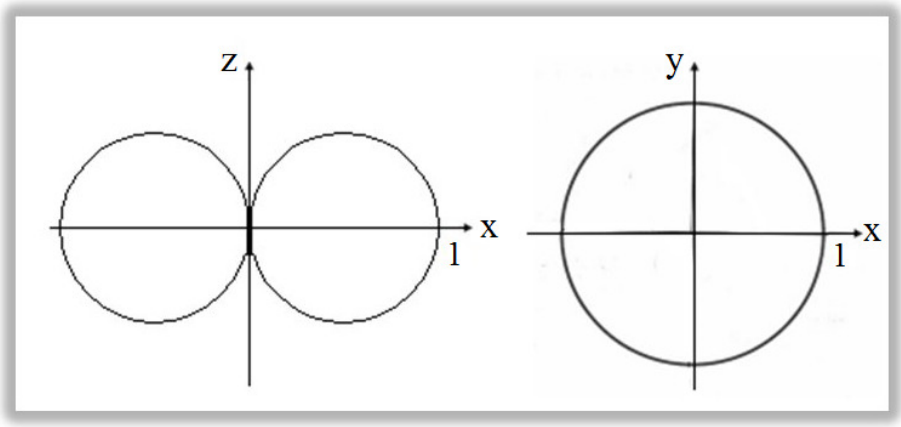

Figure 3.2 Normalized E (left) and H (right) plane cuts of the radiation pattern of the infinitesimal dipole.

In RFID applications an omnidirectional radiation pattern is usually desired. An omnidirectional radiation pattern is defined as one having an essentially nondirectional pattern in a given plane and a directional pattern in any orthogonal plane (see Fig. 3.3.). In RFID tags an omnidirectional radiation pattern means that in a nondirectional plane the identification is possible around the tag (Fig. 3.2 in H plane). An isotropic radiator is defined as "a hypothetical lossless antenna having equal radiation in all directions". Although isotropic antennas do not exist in reality, it is often used as a reference for expressing the directive properties of actual antennas. Although the SI unit for power is W, the power in that case is typically expressed in dBi, where i stands for the reference level from an isotropic antenna. Directional radiation means that the antenna radiates more efficiently in some directions than in others. The segments of the directive radiation patterns are called lobes or beams. The main lobe contains the direction of maximum radiation. Since the thesis does not deal with strongly directive antennas, the lobes are not discussed further, though parameters such as directivity and gain are considered in more detail [Bala_05].

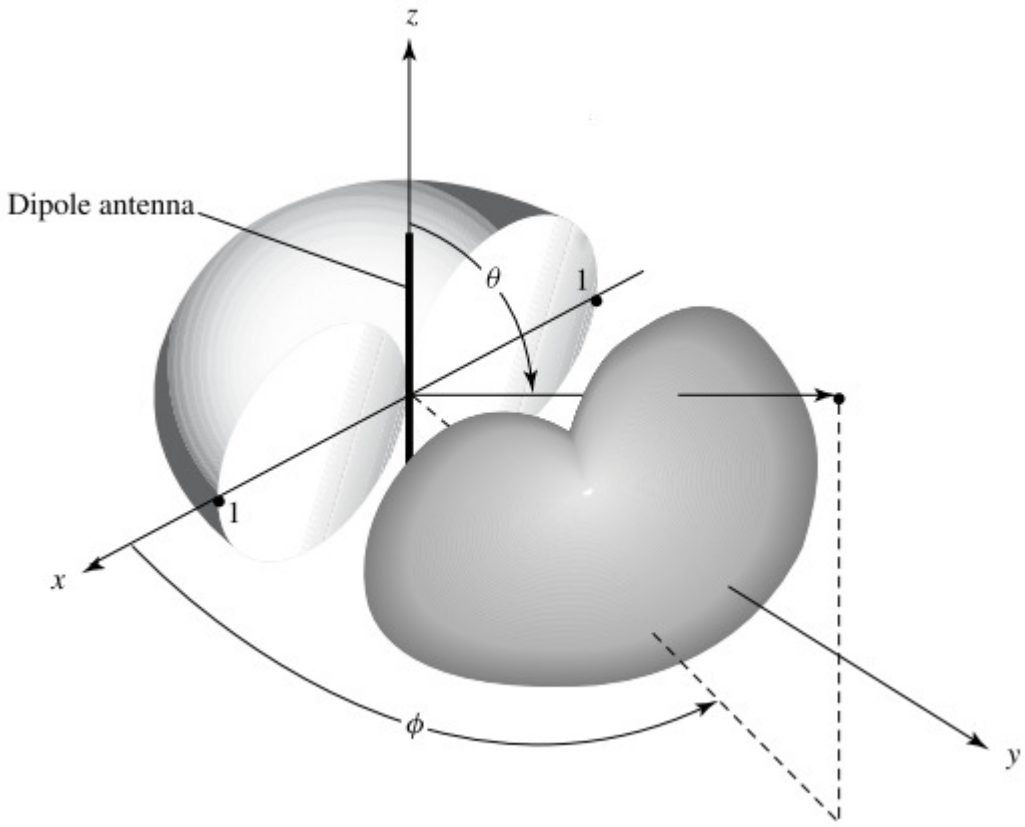

Figure 3.3 Three-dimensional radiation pattern of infinitesimal dipole [Bala_05].

Radiation intensity *U* is a far field parameter which needs to be introduced before the directivity is determined. In a given direction it is defined as "the power radiated from an antenna per unit solid angle" [Bala_05]. The power density (see $\overline{S}$ in Chapter 2) associated with the electromagnetic fields of an antenna in its far field region is predominately real and is thus referred to as radiation density S_{rad} (W/m^2). The radiation intensi-

ty is obtained by multiplying the radiation density by the square of the distance. In equation form this is

$$U = r^2 S_{rad}, \tag{3-5}$$

where U is radiation intensity (W/solid unit angle) and r is distance (m) from the radiator.

Directivity *D* of an antenna is defined as "the ratio of the radiation intensity in a given direction from an antenna to the radiation intensity averaged over all directions" or, in other words, it is the radiation intensity in a given direction divided by the radiation intensity of an isotropic radiator which (in all directions) is $U_0=P_r/4\pi$, where P_r is the radiated power. Directivity can thus be written

$$D(\theta,\phi) = \frac{U(\theta,\phi)}{U_0} = \frac{4\pi U(\theta,\phi)}{P_r} \tag{3-6}$$

where $U(\theta,\phi)$ is radiation intensity in direction (θ,ϕ). If no special direction is mentioned, maximum radiation intensity is implied. Directivity is dimensionless, but it is often expressed in decibels or in dBi.

Gain *G* of an antenna is closely related to directivity, but it also takes into account the conductor and dielectric losses (the radiation efficiency) of the antenna. Gain can be expressed with radiation efficiency (see Eq. (3-4)) and directivity (see Eq. (3-6)) as follows:

$$G(\theta,\phi) = e_{cd} D(\theta,\phi) \tag{3-7}$$

Gain can also be given in decibels and in dBi [Bala_05; Ukko_06].

Polarization is another important radiation property of an antenna. Polarization of an electromagnetic wave is defined as "the property describing the time-varying direction and relative magnitude of the electric-field vector; specifically, the figure traced as a function of time by the extremity of the vector at a fixed location in space, and the sense in which it is traced, as observed along the direction of propagation" [Bala_05].

Polarization of an antenna is defined as the polarization of the wave transmitted by the antenna. Polarization is given in a specified direction. If the direction is not stated, the polarization is taken to be the polarization in the direction of maximum gain [Bala_05].

Polarization may be classified as linear, circular or elliptical polarization. If the electric field vector at a point in space as a function of time is always directed along a line, the field is said to be linearly polarized (see Fig. 3.4 a). If the electric field vector traces a

circle as a function of time, the field is said to be circularly polarized (see Fig. 3.4 b). However, the figure the electric field traces is usually an ellipse as a function of time and the field is said to be elliptically polarized. Linear and circular polarizations are actually special cases of elliptical polarization. If, looking away from the observer, the electric field vector rotates clockwise, the polarization is called right hand polarization and if counter clockwise, the polarization is called left hand polarization. These terms are unnecessary in the case of linear polarization [Flew_03; Bala_05].

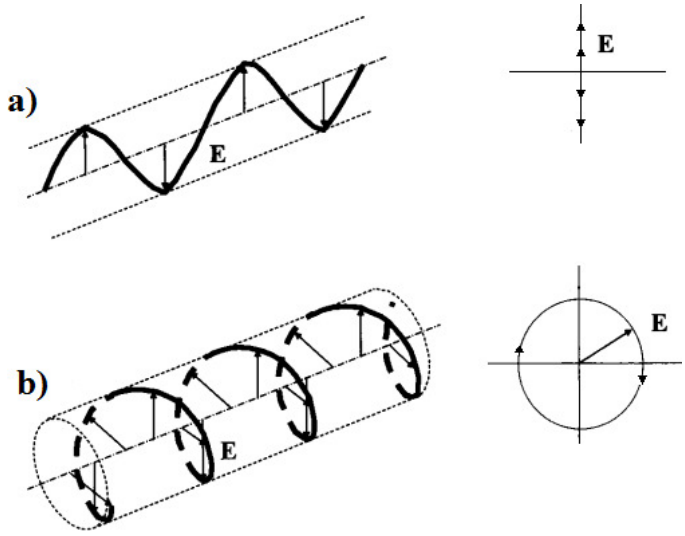

Figure 3.4 a) linear polarization and b) circular polarization [Viss_05].

In general, the polarization of the receiving antenna will not be the same as the polarization of the incoming (incident) wave. This is often the case in RFID systems as well. Linearly and circularly polarized antennas are used to transmit the electromagnetic waves in readers. Tag antennas are typically linearly polarized. If the polarization of the tag and the reader is not similar (type and direction), polarization mismatch and polarization loss occur [P1; Fink_03; Ukko_06].

The electric field of the incoming wave $\overline{E}_i$ can be written

$$\overline{E}_i = \hat{\rho}_w E_i \tag{3-8}$$

where $\hat{\rho}_w$ is the unit electric field vector of the wave and E_i is the electric field strength amplitude of the wave. The electric field of the receiving antenna can be written

$$\overline{E}_a = \hat{\rho}_a E_a \tag{3-9}$$

where $\hat{\rho}_a$ unit electric field vector (polarization vector) of the receiving antenna and E_a is the electric field strength amplitude of the receiving antenna. By assuming Eq. (3-8)

and Eq. (3-9), the polarization loss can be taken into account by **polarization loss factor, *PLF*** (dimensionless). It is defined on the basis of the polarization of the antenna in its transmitting mode as

$$PLF = \left|\hat{\rho}_w \cdot \hat{\rho}_a\right|^2 = \left|\cos\psi_p\right|^2 \tag{3-10}$$

where ψ_p is the angle between the two unit vectors [Bala_05]. If the antenna is polarization matched, *PLF* will be unity ($\psi_p = 0$) and the antenna will extract maximum power (which depends on other parameters of the antenna) from the incoming wave. If linear polarisation is considered, the largest amount of energy is transferred from one antenna to another when the antennas have the same polarization direction. The read range of a linearly polarized tag with a linearly polarized reader antenna is thus heavily dependent of the antenna orientation and the tag should, therefore, be aligned with the reader antenna polarization plane. When using a circularly polarized reader antenna, the read range is not dependent on the tag position because the polarization plane rotates with the electric field vectors. The disadvantage of circular polarization is the 3 dB power loss which appears as a result of polarization mismatch when the tag antenna is linearly polarized. This power loss shortens the reading range (in theory by factor $1/\sqrt{2}$ but in practice even more according to publications [P1], [Scha_05] and [Ukko_06]) [P1; Flew_03; Bala_05; Ukko_06].

In addition to the above parameters, receiving antennas, which tag antennas can also be considered, are mainly associated with their capturing characteristics. If a wave impinges on a receiving antenna, its ability to capture power can be derived by a number of equivalent areas. **The effective aperture** A_e (also known as effective area) (m^2) is one of the most common quantities. It is the relation of power available at the receiving antenna terminals and power density of the incident wave. If the wave polarization is matched to the antenna, the effective aperture A_e is

$$A_e = \frac{\lambda^2}{4\pi} e_{cd} D\,. \tag{3-11}$$

The effective aperture is, strictly speaking, a direction-dependent quantity, but, if no direction is specified (as in the above equation) the direction is assumed to be that of maximum directivity [Viss_05; Saha_06].

Because passive UHF RFID systems are based on backscattering, it is important to evaluate the reflection and scattering characteristics of a tag as well. **The radar cross section, RCS**, σ_r, is a far field parameter, which is used to characterize the scattering

properties of a radar target. The RCS describes the relation of scattered power density and incident power density [Knot_04].

The IEEE dictionary of electrical and electronics terms defines RCS as a measure of the reflective strength of a target defined as 4π times the ratio of the power per unit solid angle scattered in a specified direction to the power per unit area in a plane wave incident on the scatterer from a specified direction. More precisely, it is the limit of that ratio as the distance from the scatterer to the point where the scattered power is measured approaches infinity

$$\sigma_r = \lim_{r\to\infty}\left[4\pi r^2 \frac{\left|S_{scattered}\right|^2}{\left|S_{incident}\right|^2} \right] \tag{3-12}$$

where r is distance from the target, $S_{scattered}$ is scattered power density and $S_{incident}$ is the incident power density at the scattering object. Eq. (3-12) can be used to derive the RCS of any antenna [Knot_04; Bala_05; Ukko_06].

In general, the RCS of a target is a function of the position of the transmitter relative to the target, position of the receiver relative to target, target geometry and material, angular orientation of target relative to transmitter and receiver, frequency of operation, transmitter polarization and receiver polarization. Backscatter cross section is commonly the topic of interest when the transmitter and the receiver are collocated, as in UHF RFID systems. Most experimental results are of backscatter cross section. The units of RCS are meters squared (m^2) or, for normalized values, decibels relative to a square meter (dBsm). Sometimes the RCS is also given in decibels relative to a squared wavelength (λ^2). Although the radar cross section is area, it does not necessarily relate to the physical size of the target. Nevertheless, larger targets typically have a larger radar cross section. It should be noted that the RCS can only be precisely calculated for simple structures. Analytical derivation of the RCS of an antenna with an arbitrary structure is difficult [Knot_04; Bala_05; Chen_07].

Antennas are generally regarded as having two modes of scattering. The first is structural mode, the scattering which occurs because the antenna has a given shape, size, and material and which is independent of the fact that the antenna is specially designed to transmit or receive EM waves. The second scattering mode is antenna mode, the scattering that has to do directly with the fact that the antenna is designed to radiate or receive RF energy and has a specific radiation pattern. The antenna-mode scattered field depends on the antenna termination and its spatial distribution is completely determined by the antenna radiation characteristics [Bala_05].

The RCS of an antenna σ_r can conceptually be defined as

$$\sigma_r = \sigma_{struct} + \sigma_{ant}, \tag{3-13}$$

where σ_{struct} is the radar cross section related to structural mode scattering and σ_{ant} is the radar cross section related to antenna mode scattering. Although the concept of dividing the antenna RCS into two components is simple and easily grasped, it should be noted that there is no formal definition of these scattering modes [Chen_07].

According to publication [Bala_05] the structural scattered field is completely determined by diffraction of the incident wave from a conjugate-matched antenna. Its spatial distribution cannot be predicted on the basis of the antenna radiation characteristics. Other references than conjugate-matched antenna can also be used. This leads to a different but equally valid definition of the structural and antenna mode scattering [Knot_04].

As discussed earlier, in passive UHF RFID systems the IC modulates the tag's response, the scattered field, by switching its input impedance between two states. At both impedance states the tag presents a complex radar cross section with certain magnitude and phase. The difference between these two complex RCS values is called **vector differential radar cross section**, ***ΔRCS***. It should be noted that the power of the modulated backscattered signal received by the RFID reader thus depends not only on the scalar difference between the radar cross-sections defined by the two states of tag chip input impedance, but also on the relative phases of the reflected field components [Niki_06; Loo2_08].

ΔRCS is an important parameter to characterize the strength of the backscattering from an RFID tag. It maps the incident carrier power at the tag's location to the signal power density at the receiver antenna. According to Nikitin et al., in a monostatic RFID system, where the same antenna is used for transmission and reception, the *ΔRCS* can be expressed as

$$\Delta RCS = \frac{P_{received,signal}(4\pi)^3 r^4}{P_{transmitted} G_t^2 \lambda^2} \tag{3-14}$$

where $P_{received,signal}$ is the power of the modulated tag signal at the reader, $P_{transmitted}$ is the transmitted power by the reader and G_t is the gain of the reader transmit/receive antenna. In the case of the bistatic reader in Eq. (3-14), G_t^2 would read G_tG_r, where G_r would refer to the gain of the receiver antenna. The polarization mismatch is not included in the definition of the *ΔRCS* and it does not appear in Eq. (3-14) [Niki_07].

Eq. (3-14) is of practical value since it can be used to measure the *ΔRCS* of an RFID tag through the transmitted and received power. However, it is interesting to relate *ΔRCS* to the properties of the tag. Differential RCS of a tag can be defined as shown in articles [Niki_08; Purs_08]:

$$\Delta RCS = \frac{\lambda^2 G_{tag}^2}{4\pi} \alpha \left| \rho_1 - \rho_2 \right|^2 = \frac{\lambda^2 G_{tag}^2}{4\pi} L_{mod} \tag{3-15}$$

where ρ_1 and ρ_2 (dimensionless) are the power wave reflection coefficients of the tag in matched and mismatched chip impedance states respectively, G_{tag} is the gain of the tag antenna, α (dimensionless) is a coefficient which depends on the specific modulation details and L_{mod} (dimensionless) denotes the modulation loss factor determined by the impedance matching between the antenna and the chip in matched and mismatched chip impedance states [P9; Niki_08; Meri_10].

3.3 Power transfer between the reader and the tag

In the previous section, important antenna parameters were introduced. By using these parameters, this section describes how the signal is sent from a tag to a reader and how the power is transferred. Communication between reader and tag begins with a command from the reader. This stage is excluded from further examination. After the command, the reader sends a carrier wave which is modulated and backscattered by the tag. These phases are now investigated further.

The investigation begins with the reader sending power (carrier wave) to the tag. At distance *r* from a transmitting antenna, the power density S_t equals the power density of an isotropic radiator multiplied by the gain of the transmitting antenna

$$S_t = \frac{P_{transmitted} G_t}{4\pi r^2}. \tag{3-16}$$

$P_{transmitted} G_t$ is called the reader transmitted Effective Isotropic Radiated Power (EIRP), which is limited by national radio communication regulations. Generally EIRP is the measure of the radiated power which an isotropic emitter (G_i = 1 or 0 dB) will need to supply in order to generate a defined radiation power at the reception location. Another power, given in power regulations, is Effective Radiated Power, ERP. This is the product of the power supplied to the antenna and its gain relative to a half-wave dipole antenna ($G_{\lambda/2}$ = 1.64 = 2.15 dB) in a given direction, usually in the direction of maximum gain. For example, in Europe between frequencies 865.6MHz - 867.6 MHz radio frequency regulations limit the transmit power by the reader antenna ($P_{transmitted} G_t$) to 2 W

ERP = 3.28 W EIRP ≈ 35 dBm. When power is given in dBm, reference power of 1 mW is used. The measured powers in publications [P3 - P5; P7; P9], for example, are given in dBm [P9; Fink_03; Chen_07; Meye_07; Loo2_08].

The available power for an RFID tag antenna from an incident power density is determined by its effective aperture ($A_{e,tag}$) in the direction of the incoming wave and it is related to the gain of the tag antenna through Eq. (3-7) and Eq. (3-11)

$$A_{e,tag} = \frac{\lambda^2}{4\pi} G_{tag}, \tag{3-17}$$

where G_{tag} is the tag antenna gain. In Eq. (3-17) it is assumed that the polarization is matched. If the polarisations are not matched, additional power loss may be introduced through polarization mismatch between the incident wave and the tag antenna, as discussed earlier. The magnitude of this loss depends ultimately on the tag antenna geometry and its alignment with respect to the incident field, which determine the induced current density on the antenna structure. It is important, therefore, to include the polarization mismatch in the link calculations. By definition, the tag antenna gain includes the directivity and radiation efficiency of the tag antenna, but excludes the polarization loss (see Eq. (3-7)). By taking the polarisation loss into account and combining Eqs. (3-10), (3-16) and (3-17), the power received by the tag antenna P_{tag} can be expressed as

$$P_{tag} = S_t A_{e,tag} PLF = P_{transmitted} G_t G_{tag} \left(\frac{\lambda}{4\pi r} \right)^2 \left| \hat{\rho}_t \cdot \hat{\rho}_{tag} \right|^2 \tag{3-18}$$

where $\hat{\rho}_t$ and $\hat{\rho}_{tag}$ are unit electric field vectors of the transmitting antenna and tag antenna, respectively [P9; Loo2_08].

The received power by the tag antenna, given in Eq. (3-18), is the available power for the on tag microchip, but the delivered power to the chip depends on the impedance matching between the tag antenna and the chip. The quality of the power matching between a tag antenna and the IC can be evaluated in terms of the power reflection coefficient of the tag

$$\Gamma_{tag} = \left| \rho_{tag} \right|^2 = \left| \frac{Z_{ic} - Z_{tag}^*}{Z_{ic} + Z_{tag}} \right|^2 \tag{3-19}$$

where the impedance ratio denoted by ρ_{tag} is the power wave reflection coefficient of the tag [Kuro_65]. In terms of power, Γ_{tag} is the ratio of the available power from the

tag antenna to the reflected power from the antenna-IC interface, due to impedance mismatch. Thus, combining Eqs. (3-18) and (3-19), the power delivered to the IC is

$$P_{chip} = (1-\Gamma_{tag})P_{tag} = (1-\Gamma_{tag})P_{transmitted}G_t G_{tag}\left(\frac{\lambda}{4\pi r}\right)^2 \left|\hat{\rho}_t \cdot \hat{\rho}_{tag}\right|^2 \qquad (3\text{-}20)$$

Obviously, P_{chip} in Eq. (3-20) is maximized by minimizing Γ_{tag}, for example, by tuning the tag antennas impedance so that $Z_{tag} = Z_{IC}^*$ [P9; Loo1_08; Loo2_08; Loo3_08].

When the chip has enough power to operate, it still has to successfully modulate its data to the carrier wave, and the tag must reflect the modulated wave back to the reader. As discussed earlier, when the IC modulates the tag's response, two RCS values are generated and two distinct received powers will be picked up by the receiving reader antenna. The backscattered signal power, the time average power of the modulated tag signal received by the reader, can be calculated in a similar way to P_{tag} in the case of forward link (Eq. (3-18)) by noting these two different RCS values (the ΔRCS). By using Eqs. (3-14) and (3-15), the received backscattered signal power can be expressed as

$$\begin{aligned} P_{received,signal} &= \frac{P_{scattered}G_{tag}A_{e,receiver}}{4\pi r^2} = P_{tag}G_{tag}G_t\left(\frac{\lambda}{4\pi r}\right)^2 L_{\text{mod}} \\ &= P_{transmitted}G_{tag}^2 G_t^2\left(\frac{\lambda}{4\pi r}\right)^4 \alpha\left|\rho_1 - \rho_2\right|^2 \end{aligned} \qquad (3\text{-}21)$$

where $P_{scattered}$ is the power which is scattered from the tag, $A_{e,receiver}$ is the effective aperture of the receiving reader antenna and it is calculated in a similar way to the tag in Eq. (3-17). The polarization loss is excluded from Eq. (3-21).

From the above discussion it can be seen that the performance of the RFID system is dependent on both forward (reader to tag) and return link (tag to reader). When the tag has received sufficient power to turn on, it might fail to reflect enough power to be detectable by the reader. The minimum detectable variation of the received power is called the sensitivity of the reader [Dobk_08; Loo2_08].

Theoretical read range (m) of a tag can be calculated for the forward link from Eq. (3-20) by replacing P_{chip} with IC chip threshold power, and for reverse link from Eq. (3-21) by replacing $P_{received,signal}$ with reader sensitivity, and solving r. However, the sensitivity of the reader receiving system is always very high (−70 dBm to −90 dBm) while the threshold power of the UHF chip (IC chip sensitivity) is about −10 dBm. Assuming the tag antenna is matched properly to the chip, the sensitivity of the reader is typically not

a constraint and the forward link is more critical. Though it should also be noted that the sensitivity of the ICs has improved significantly lately (almost −20 dBm sensitivity has recently been reported [Impi_11]) and the return link may be the limiting factor instead, unless the readers will be further improved as well [Loo2_08; Bhat_09].

3.4. Measured quantities in evaluating tag performance

Many of the antenna parameters discussed above can be difficult to measure for RFID tags since the tag antenna impedance is not matched to the typical impedance of RF measurement equipment (50 Ω or 75 Ω). Measured quantities in publications [P1; P3 - P5; P7; P9] are chosen to evaluate the overall performance of the tags and they are dependent on the antenna parameters described above. The measured quantities in publications [P1; P3 - P5; P7; P9] are described below.

The read range is a critical parameter of RFID tags. In publication [P1] **Maximum Reliable Read Range (MRRR)** (m) is the parameter which is used to evaluate the practical reading distance of a tag. MRRR is the reading distance at which the tag can be continuously identified for at least one minute. Alien Technology monostatic reader unit was used in MRRR measurements in article [P1] and the reader unit supported EPC Class 1 Gen 1 standard. Linearly polarized and circularly polarized reader antennas were used in these measurements. The centre frequency used in article [P1] was 915 MHz and the RFID system was compliant with Federal Communications Commission (FCC) regulations.

In publications [P3; P9] **the transmitted threshold power** (dBm) was used to describe tag performance. The transmitted threshold power is the minimum sufficient power required from the reader to activate the IC-chip (in matched state). Threshold measurement is performed by increasing the transmitted power until the tag can respond to the query command of the reader.

Power on tag (dBm) is defined as the power that would be acquired at the location of the tag with a power matched 0 dBi antenna (Eq. (3-18) when G_{tag} = 1 = 0 dBi). Power on tag is equal to Eq. (3-20) when the realized gain of the tag ($(1-\Gamma_{tag})G_{tag}$) is 1 = 0 dBi. It can thus be interpreted as the power which would be absorbed by the RFID chip if it was connected to a perfectly matched 0 dBi tag antenna [Niki 09]. The lower the measured power on tag, the higher the realized gain of the tag antenna.

The measured transmitted threshold power can be used to derive the power on tag. Power on tag is the transmitted threshold power normalized by the power loss factor (path loss) from the output port of the generator to the antenna port of a 0 dBi antenna. This means that power on tag is the threshold power multiplied by the power loss factor. It is the minimum power necessary to activate the chip, assuming 0 dBi tag antenna gain

and perfect matching. The normalization of the transmitted threshold power makes it possible to remove the effect of multipath propagation from the results and thus compare the tag antennas consistently. Power on tag was measured in publications [P4; P5; P7]. This parameter is termed **tag sensitivity** in publication [P7].

Radiation pattern was measured in publication [P7]. Measuring the radiation patterns was based on the tag sensitivity. The measurement was carried out at constant frequency by rotating the tag by 15° steps and measuring the tag sensitivity at each orientation. Since the tag sensitivity is inversely proportional to the tag antenna gain pattern, the normalized pattern can be obtained by observing the difference of the tag sensitivity over the rotation angles. The reference power used is the lowest measured tag sensitivity.

Publications [P4; P5; P9] measured **the backscattered signal power** (dBm). The backscattered signal power is the time-average power detected from tag response at the receiver. This was measured as a function of frequency in publication [P9] with the threshold power as the reader transmitted power. In publications [P4; P5] it was measured as a function of transmitted power. The backscattered signal power is described by Eq. (3-21).

Voyantic Tagformance™ Lite measurement system was used to measure transmitted threshold power, power on tag (tag sensitivity) and backscattered signal power. Voyantic Tagformance™ Lite is a complete measurement solution for evaluating the functionality and performance of EPC Class 1 Gen 2 tags. The device is essentially a vector network analyzer with RFID capabilities. All measurements made with Voyantic Tagformance were performed in an anechoic chamber. A calibration process was also used in the measurements to eliminate the effect of multipath propagation on the measurement results. In the calibration procedure, the path loss is approximated by using a calibration tag with known properties. The calibration tag is provided by the manufacturer of the measurement device as part of the measurement system. The measured path loss includes: cable losses, transmit/receive antenna gains and path loss between transmit/receive antenna to tag [P4; P5; Voya_10].

A bistatic reader was used in publications [P3 - P5; P7; P9]. The gain of the transmitting and receiving antenna as well as their distance from the tag is same for each measurement. In articles [P3] and [P7] the distance was 1 m and G = 9.5 dBi, in article [P4] distance was 1.5 m and G = 9.5 dBi, in article [P5] distance was 1 m and G = 9.5 dBi and in article [P9] distance was 1.5 m and G = 8.5 dBi. In publications [P1; P3 - P5; P7; P9] linearly polarized reader antennas were used.

Because many of the parameters of a tag can be difficult to measure due to complex antenna impedance, certain parameters were evaluated by Ansoft High Frequency Structure Simulator (HFSS). This is a commercially available finite element method (FEM) -based full-wave electromagnetic simulator. HFSS was also used in antenna design process. Simulations were also carried out to support the measurement results.

4. Printable tags – fabrication and materials

This chapter discusses tag antenna manufacturing by printing. A passive UHF RFID tag consists of substrate material, a tag antenna pattern and a microchip. The chips are commercially available ASICs (application-specific integrated circuit) and the antenna pattern is designed for a certain chip. The tag antenna pattern can be produced by various methods, but etching and printing are considered the most suitable due to the manufacturing speed and throughput. Most commonly the antenna pattern is manufactured by chemically etching copper or aluminium which is on PET foil. Chemical etching is an established technology in the electronics industry. However, in electronics, the printing methods are adopted from the graphics industry. Printing is an additive, simple and fast process, and creates less material waste than chemical etching. It also allows the development of new lightweight applications which can be printed on various substrate materials and embedded into other structures. Many printing methods can be used to print RFID tag antennas, but since each process has different characteristics, some are more suitable than others. In passive UHF RFID tag manufacturing, the resolution is very seldom a limiting factor when selecting the printing process. Printed film thickness, however, is a critical parameter since it affects the electrical performance of the film. Printing methods, curing process and materials used in the printed conductive structures of this study are introduced in this chapter [P1 - P9; Lehp_07].

4.1 Printing methods and curing process

In general, the potential of different printing techniques in electronics manufacturing is well understood. For example, conductors, sensors, passive components, and passive microwave circuits have been made using a variety of printing methods such as screen printing, gravure printing, pad printing, flexography, offset-lithography and inkjet. In this thesis screen printing, gravure printing and pad printing are used and they are now discussed in greater detail. Screen printing is the most useful printing technique when thick films are needed. If very high throughput is required, however, gravure printing is more suitable. Pad printing provides interesting opportunities because it is suitable in printing on 3D objects. After printing, the ink films are cured and this process is also discussed later in this section [P1; P2; P4; P5; Golo_96; Evans_97; Evans2_97; Side_05; Radi_06; Tudo_07; Mänt_09].

4.1.1 Screen printing method

Screen printing is a versatile technique which is already widely used in the electronics industry to print thick film structures like conductors, dielectrics and passive components, membrane touch switches and also to print coatings such as solder masks and resists. The technique is thus familiar to electronics manufacturers [P1; P8; P9; Prud_94].

In screen printing the ink is pressed through a screen, a fabric mesh of threads, onto the substrate with a squeegee (blade). Non-image areas of the screen mesh are blocked out with a stencil, often an emulsion, and in the image areas the screen is left open. A schematic diagram of flatbed screen printing used in this thesis is presented in Fig. 4.1. Before printing, the ink is stirred and poured onto the screen. After this the squeegee is applied and drawn over the screen, forcing the ink through it. In flatbed screen printing the screen is stretched onto a frame and the screen is separated from the substrate by a small gap (snap-off gap). The squeegee pushes the screen down toward the substrate and the screen rises behind the squeegee after the squeegee has passed over it. The substrate is held in position by either a vacuum table or by a special jig. The squeegee is typically made of rubber (Shore hardness of 40 to 90) or stainless steel. Various blade profiles are available. The angle between the squeegee and the direction of the normal of the screen plane (attack angle) is typically about 45° [Prud_94; Hoff_97; Kipp_01].

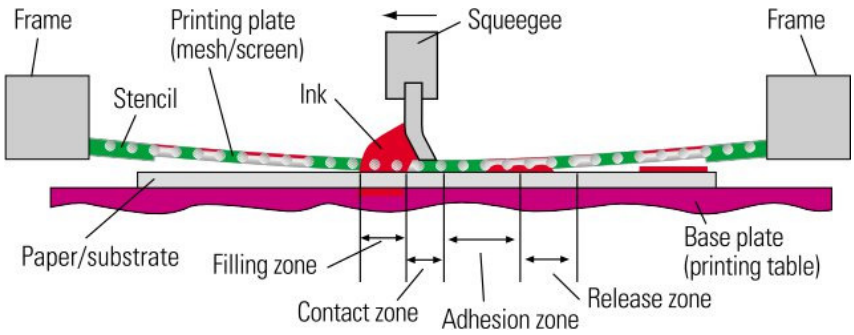

Figure 4.1. The principal of flatbed screen printing [Kipp_01].

The screen is usually made of polyester because of its dimensional stability and flexibility but steel screens are also available. Screens are available in different mesh counts given in threads per inch or cm (10 to 200 threads per cm are available), in different thread structure (monofilament, multifilament), in different thread diameters and also in different weave structures (simple, single twill, double twill). The screen parameters are selected according the printed application. The correct screen tension is also an important factor in achieving good print quality. The screen mesh is typically aligned at angles of 22.5°, 45° or 90°. A 45° mesh provides the maximum flexibility for the screen, but may produce serrated edges on the conductor lines which are aligned in parallel or at 90° to the direction of squeegee. A 90° mesh may cause a fine line conductor

to disappear if a thread is placed on the area of the line. A 22.5° mesh is a compromise and this was selected for the screens used in this study [Prud_94; Hoff_97; Kipp_01].

Screen printing allows printing of films of thickness from 0.02 µm to 100 µm. The thickness is determined by several factors such as screen, stencil, ink composition, printing parameters (print speed and pressure, squeegee angle, gap between the screen and the substrate, curing etc.) and substrate material. The typical resolution for screen printing is reported to be 50 lines per cm. There is also rotary screen printing which is a faster process and can be used in reel to reel manufacturing lines [Land_94; Kipp_01; Blay_05; Cost_05; Cagl_10].

4.1.2 Other printing methods

Gravure printing is a technique that uses an engraved cylinder, gravure cylinder, to transfer the figure onto the substrate. The figure on the gravure cylinder consists of gravure cells which hold the ink while transferring the figure. The substrate is pressed between the gravure cylinder and an impression cylinder which transfers the ink from the gravure cells onto the substrate. Gravure printing is a fast technique, it enables mass production and it is typically used for long runs. The thickness of the printed figure depends on the engravings on the gravure cylinder but process parameters such as printing speed and pressure also have an effect on the figure. In addition, the ink and the substrate affect the thickness. In article [Puda_05] 20 µm – 60 µm gravure cells produced a 4 µm - 7 µm thick film, which is rather a typical thickness of gravure printed films. In gravure printing, the substrate must be flexible because of the pressure which is needed in the figure transfer. The resolution that can be achieved with gravure printing is 100 lines per cm. Offset gravure is a technique similar to traditional direct gravure printing but the figure is first transferred onto a rubber cylinder and from there onto the substrate. This widens the substrate selection but a figure printed with offset gravure is thinner than one printed with the direct gravure method [P1; Kipp_01; Blay_05; Puda_05].

Pad printing is an indirect gravure printing process. Instead of a gravure cylinder, an engraved printing plate (cliché) is used. The pattern is transferred from the printing plate to the substrate with a silicon rubber pad. After the cliché is filled with ink and the excess ink is wiped off, the pad raises the ink from the engravings and transfers it onto the substrate. The technique is based on the tackiness of the ink. The ink becomes tacky when the surface of the ink dries. First the tacky ink sticks onto the pad when the pad is pushed toward the cliché and then the ink sticks to the substrate when the pad is pushed towards it. Multiple sequential print presses can be performed to increase film thickness. Three and five print presses were used in this thesis [Kipp_01].

Pad printing is used especially in printing on three-dimensional objects and it is also suitable for printing fine line circuits. It is economically more competitive in printing small series than direct gravure printing. In pad printing there are typically limitations to the size of pattern that can be printed. If large areas are printed, gravure offset printing is more convenient because a much larger pattern fits on the gravure cylinder. Pads are available with different hardness, shape and size for different applications. Clichés of different cell depth, material and accuracy are also available [P7; Hoff_97; Love_97; Laht_99; Hahn_01].

In addition to screen printing, gravure printing and pad printing, RFID tags can be printed with flexography, offset lithography and inkjet techniques. Flexography is suitable in similar applications to gravure printing but inkjet and offset lithography are typically used for printing other applications than RFID tags. Further discussion of these methods lies outside the scope of this thesis [P1; P4; P5; P7; Kipp_01; Blay_05; Ujii_06; Side2_07].

4.1.3 Curing process

Once printing is complete, the ink needs time to dry and the time this takes depends on the ink type. Dryers speed the drying process and the dryer selection is thus important in terms of productivity. The speeding of the drying can be done by the application of air, heat or both. This is usually performed by an automatic conveyorized drying system [Hoff_97].

Radiation is used for heat transfer, for example, in infrared (IR) heating devices. A radiant heat source can generate high levels of heat energy in a short time. Radiant heat is ideal for use with thermal setting inks. Ultraviolet (UV) radiation is used with special UV inks that are formulated with an initiator or catalyst to trigger a polymerization reaction that causes the ink to cure or harden. The reaction is instantaneous and thus curing is rapid [Hoff_97].

Several oven and dryer designs use convection as a means to heat the ink on the substrate. Curing of the samples in this study was performed in a convection oven at temperatures between 100 °C and 180 °C. During curing, the solvents of the PTF inks evaporate and the conductive silver particles come closer to each other and more conductive paths occur to allow the electrons to move from particle to particle. The resin in the inks polymerizes and a solid film is produced. The curing temperature is an essential parameter in achieving sufficient electrical performance of the printed films. The curing parameters are further discussed in Chapter 5 [P2; Hoff_97; Worz_07].

4.2 Materials used in this study

4.2.1 Substrate materials

Substrates mainly provide the mechanical support and electrical insulation for electrical circuits, but the properties of the substrate can affect both the processes and the final characteristics of the devices. Typical passive UHF RFID tag antenna substrates are flexible plastic foils. Many plastic materials are available as films. Most are strong, have good electrical properties and good resistance to moisture. Some also have limitations at operating temperature. The most common substrate material used in passive UHF RFID tags is PET. If the antennas are fabricated by printing PTF ink, the choice of substrate is considerably large and paper, fabric and other unusual electronics substrate materials can be used. This is important if conductive patterns like antennas are integrated directly on other structures such as packaging or clothes. The substrate materials that are used in publications [P1-P9] are discussed below [Prud_94; Hoff_97; Laug_03].

Polyethylene terephthalate (PET) is one of the materials used in flexible printed circuits. PET is a versatile material and has many good properties such as excellent electrical insulation, fair heat resistance and it is resistant to most industrial chemicals and abrasion. This makes it suitable in product identification applications. PET, which is used by the screen printing industry, is produced in two forms: non oriented and oriented. Most uses for PET require the material's molecular structure to be oriented because it is stronger and more dimensionally stable. Oriented PET was also used in this study. One disadvantage of PET is that it does not tolerate typical soldering temperatures and is stable only to temperatures of 135 °C – 150 °C [Hoff_97; Cous_01; Vacc_02; Camp_08].

Polyimides (PI) are promising substrate materials in printed electronics applications. For organic material, PI retains electrical, mechanical, and physical properties over exceptionally wide temperature ranges (down to -195 °C and up to 400 °C). The chemical resistance of PIs at elevated temperatures makes them ideal for use in extreme environments. In addition to thermal stability, PIs have excellent electrical properties. The biggest disadvantage of polyimide film is its higher cost compared to other common plastic films. If high temperatures are used in tag manufacturing, PI is a suitable substrate material but otherwise it is an expensive choice. Another possible drawback of PI is its relatively high water absorption [Prud_94; Coom_01; Pard_04; Camp_08].

Polyvinyl chloride (PVC) is a strong, low cost thermoplastic polymer with excellent characteristics. It has good chemical and electrical insulating properties, low water absorption as well as fair resistance to heat and abrasion. PVC is available in flexible or rigid form depending on the amount of plasticizer. Rigid PVC films are used in applications such as smart cards. The films are good for printing without the need for pre-

treatment. In addition to packaging, flexible PVC films are used in a very wide range of applications. The elastic PVC foil used in this study is intended for screen printing. It contains an adhesive layer and it is meant to be pressed to clothes with heat and pressure. PVC melts at approximately 240 °C and processing is normally in the range of 170 °C - 200 °C [P9; Hoff_97; Cous_01; Laug_03; Pard_04; Meri_10].

Fabrics can be used as substrates for printed tags when the tags are embedded into clothing, for example [P2; P3; P8; P9]. The temperature tolerance is dependent on the fabric type but most fabrics tolerate PTF ink curing temperatures. A vast range of different fabrics are available. Fabrics are produced by weaving, knitting, braiding or netting from natural or synthetic fibres. Cotton is a common natural fibre while PET, nylon, rayon and acetates are common synthetic fibres. The compatibility of different textiles with the ink should be considered before application. The characteristics of the fabrics, such as ink absorption and surface morphology, affect the printed film quality that is achieved. Some ink types remain on the surface of the fibres and bond with these, while others soak into fibres. The morphology of the printed films on certain fabrics is discussed later in this chapter [Hoff_97; Vacc_02].

Paper is used in the packaging and graphics industries which makes it an interesting substrate material for RFID tags. Paper also tolerates the curing temperatures of PTF inks and it has a wide range of properties based on its composition; it can be flexible or rigid, soft or coarse and it may absorb or repel water. Papers are also available with textured surfaces. The properties of paper are controlled by the type and size of the fibre, the manufacturing process and the treatments applied after the paper has been produced. As with fabrics, paper and its characteristics affect the printed film morphology. This is discussed further later in this chapter [Hoff_97; Vacc_02].

4.2.2 Electrically conductive polymer thick film inks

4.2.2.1 Composition of the ink

The conductive inks, excluding inkjet inks, are polymer thick film composites. Conductive PTF ink consists of metallic filler, binder material (polymer matrix), solvents and additives. The ingredients, as well as their relative amounts, are selected according to the printing method. This chapter deals mainly with screen printable silver inks, though the ink composition used in other printing methods (excluding inkjet) is similar. The compositions of particular inks are well guarded business secrets, but some typical ingredients are briefly introduced in this section [Gooc_97; Roth_03; Ujii_06].

The **filler** of the ink is metal powder, commonly silver, which is also used in this study. Silver and its oxides are good conductors and cheaper than many other precious metals. Thick film inks with other particles are also commercially available, but due to their in-

appropriate characteristics (such as conductivity, process compatibility and price), the use of these materials is not common in PTF inks which are meant for applications like tag antennas. The selected printing technique and the line width of the conductive pattern set demands on the particle size. Typically, the particle size (the median of the particle size distribution [Whee_99]) in screen printable silver inks is a few microns. The particles are usually in flake form and the size distribution is relatively large. Fig. 4.2 illustrates a typical screen printed conductive polymer thick film [P2; Prud_94; Hoff_97].

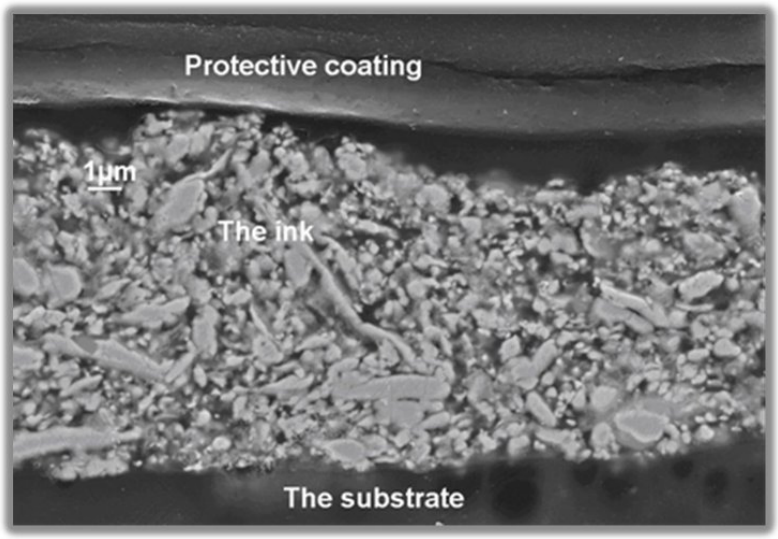

Figure 4.2 Scanning electron microscope (SEM) micrograph of screen printed conductive PTF cross section [P2].

The particles are suspended in **vehicle** for printing use. The vehicle normally consists of a non-volatile and a volatile portion which will evaporate during curing. **Solvents** form the volatile part of the vehicle and they are normally used to impart the desired characteristics of flow, viscosity and ink density. The non-volatile portion of the vehicle is called **binder**. Binder is needed to hold the particles together once the ink is transferred onto a substrate, to affix them to the surface and to protect the film from being damaged. Binder materials in screen printing inks are **resins**. The types of resins are acrylic, alkyd, epoxy, polyester, urethane and vinyl resins. Resins are selected according to substrate type and desired ink characteristics [P2; Gooc_97; Hoff_97; Whee_99; Ujii_06].

A **modifier** or **additive** ingredients are used to affect the characteristics of the ink. Additives are used to improve printability, durability, adhesion or stability and to change viscosity, flow out, dry or other characteristics. Additives include rheology modifiers and surfactants [Hoff_97; Ujii_06].

Rheology modifiers are used to control the rheology profile of the ink, which includes yield stress and viscosity at different shear modes and rates. In screen printing, the requirements for ink are different in different printing stages. When the ink is being

forced through the screen, a low viscosity is needed. On completion of printing, the film must retain its printed geometry and so high viscosity is required. Thus lower ink viscosity is required as applied pressure (shear rate) increases. The classification for fluids of this type is termed pseudo-plastic. Fig. 4.3 shows the viscosity of a typical screen printable ink during the printing cycle [Prud_94; Ujii_06].

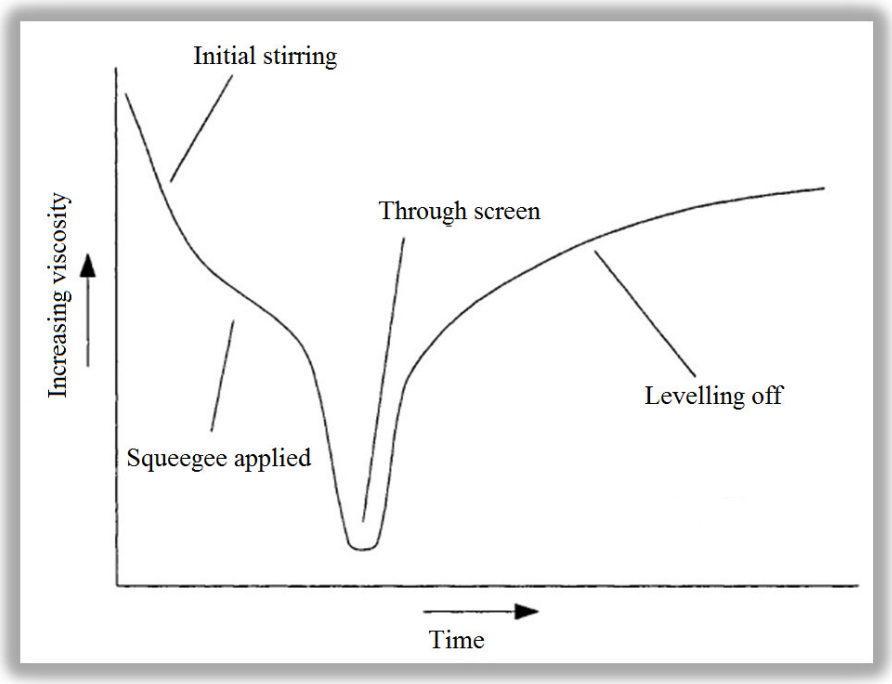

Figure 4.3. The viscosity of the ink during a screen printing cycle [Prud_94].

A thinner is used to dilute the ink solution to the desired consistency. A fast drying thinner speeds drying and a slow drying thinner helps to keep the ink open and wet in the screen. However, a slow thinner has less effect than a **retarder**. In addition to slowing the drying of the ink, a retarder also lowers ink viscosity. **Flow promoter** changes the surface tension of the ink and increases the flow of the ink [Hoff_97].

Surfactants are used to modify the surface energies of the ingredients of the ink. Surfactants include **dispersants** and **coupling agents**. Dispersants are used to prevent the interparticle interaction (particle agglomeration) and coupling agents are used to improve the adhesion between the particles and the matrix and thereby prevent reagglomeration of dispersed particles [Roth_03].

Other additives can also be introduced into the ink solution, for example, to control the penetration and to prevent spoilage (reducing agents). The choice of additives is dependent on the type of printing method and also on the other ingredients in the ink solution (compatibility). It is preferable to keep the formulation simple and to use one ingredient to serve multiple functions. It should be noted that climate conditions and the age of the ink affect the ink composition and properties [Gooc_97; Hoff_97; Ujii_06].

Certain characteristics of the PTF inks used in this thesis are presented in Table 4.1. The data is provided by the ink suppliers.

Table 4.1 The characteristics of the inks [P2 - P9].

Ink	Manufacturer's description	Curing conditions (°C, min)	Viscosity (Pa·s)	Conductivity (MS/m)
(A)	Polymeric ink consisting of silver particles, vinyl chloride based copolymer resin and <1 % epoxy resin. The solid content is 70 % and the silver content is 2.2 g/cm^3. Particle sizes are mainly ≤ 5 µm.	120, 30	3 - 5	1.7
(B)	One component silver ink consisting of polyester resin and silver particles. Silver content is 60 - 65 wt% and polyester resin content is 11-14 wt%. Particle sizes are mainly in the range from 3 to15 µm.	150, 20	20 - 30	1.25
"A"	Silver pigment in vinyl chloride based copolymer resin for flexographic or rotogravure printing techniques. Silver content is 72 wt%. The particles are flake form. Particle size: 10 % less than 1.5 µm, 50 % less than 5.5 µm, 90 % less than 18 µm.	120, 15	400	3.8
"B"	Silver pigmented conductive paint on PVC-copolymer base, designed for metallization of plastic by pad printing process. Silver content is 52 wt%. The particles are flake form. The maximum length of the silver-flakes is between 10µm and 20 µm.	100, 10 (room temperature, 60)	80 - 120	0.7

Inks (A) and (B) are intended for screen printing methods and inks "A" and "B" are intended for gravure printing methods.

4.2.2.2. Morphology of the printed films

Morphology of a printed film is dependent on the printing method, substrate and composition of the ink. Thickness and surface roughness of printed films are discussed in this section since these parameters affect the electrical performance of films printed with conductive inks (see Section 5.2.2). Screen printed films are the main focus of interest, but films printed with gravure printing and pad printing are also considered.

In terms of print quality, the relevant substrate properties include ink absorption, smoothness, porosity, thickness consistency, static effect and surface chemistry. The surface energies of the ink and the substrate are important factors. The surface energy of the ink must be lower than the surface energy of the substrate in order to wet the substrate surface and prevent the ink from beading. In addition to substrate, the binder of

the ink should provide good adhesion and wetting to filler. Good wetting prevents trapped air bubbles and aids adhesion. Good adhesion of binder to filler and of ink to the substrate is required to achieve the required mechanical properties. Instead of mechanical properties, this thesis deals mainly with the electrical performance of the ink [Hoff_97; Busc_01; Roth_03].

The behaviour of the ink on the substrate is also dependent on **the absorbency of the substrate**. The ink may soak into the substrate or it may remain on the substrate surface. If the ink is absorbed into the substrate, it may spread as typically happens on porous substrates such as paper and fabrics. Printed film is also affected by the substrate **surface consistency,** the degree of difference in surface structure. A smooth surface will have complete and even contact with the screen during printing. This makes it possible for the stencil (emulsion) to seal with the substrate to keep the ink within the desired image area. It also prevents ink from spreading. Textured or irregular surfaces are more complicated because there are many levels to print. It is easy to print on the raised areas but the transfer of the ink onto recessed areas is difficult [Hoff_97].

Printing equipment and printing parameters also have an impact on print quality. In screen printing, the screen plays an important role. The mesh count of the screen, thickness of the thread, wave type and material of the screen and thickness of the emulsion, for example, determine the amount of the ink that is transferred through the screen. Squeegee pressure, angle, hardness, speed and blade profile as well as snap-off gap are parameters which also affect the deposited ink [Hoff_97].

Even when the printing equipment and the process parameters have been correctly adjusted and the substrate is non-absorbent and smooth, waving of the film is a common with screen printed films. The film is thinner from the areas where the threads of the screen are during printing. A typical screen printed film is illustrated in Figs. 4.4 and 4.5, which show cross section micrographs of the PTFs on PET substrate.

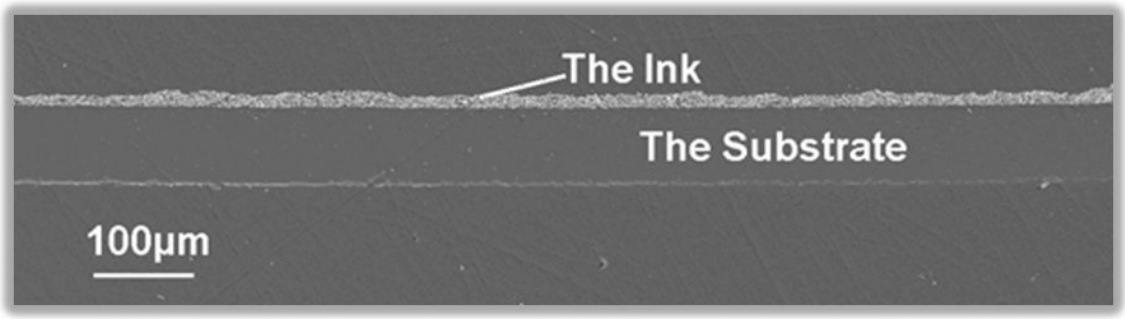

Figure 4.4. SEM micrograph of Sample 1 in article [P5], average thickness 13.9 µm.

Figure 4.5. SEM micrograph of Sample 2 in article [P5], average thickness 21.5 µm.

Due to waving, it is impossible to determine the thickness of the printed film precisely. Nevertheless, the thickness of the film is a crucial parameter in determining the performance of printed PTF tag antennas. Instead of absolute thickness, average thickness values can be measured and compared. In publication [P2] average **thickness** of printed film on five different substrates was measured using optical microscopy of the cross sections. Two PTF inks were used: ink (A) and ink (B) (see Table 4.1). The average thickness of the printed films on different substrate materials is illustrated in Fig. 4.6. The measurements were taken at random points on the cross section.

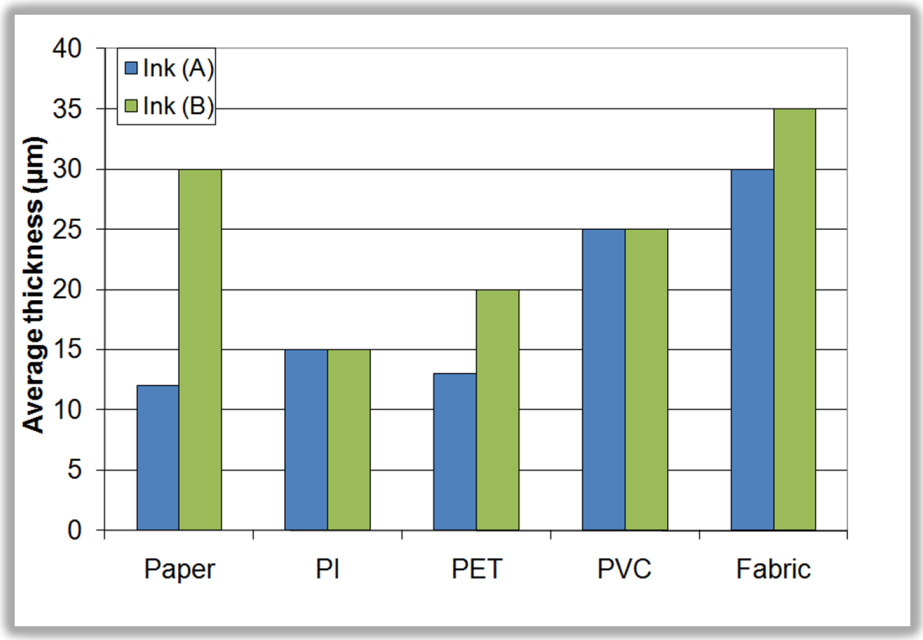

Figure 4.6. Average thickness of the screen printed conductive patterns on different substrate materials with inks (A) and (B) [P2].

It is seen that average thickness of the printed film is different on different substrates. On porous substrates (paper and fabric), the ink is partially absorbed into the substrate. The absorption is higher on fabric and lower on paper. The ink has partially penetrated between the fabric fibres but the fibres have not absorbed the ink. Similar behaviour is shown in Figs. 4.7 and 4.8 (in the case of ink “A”). Absorption increases the average

thickness of the film since it was measured at random points of the cross section figures of the printed films [P2].

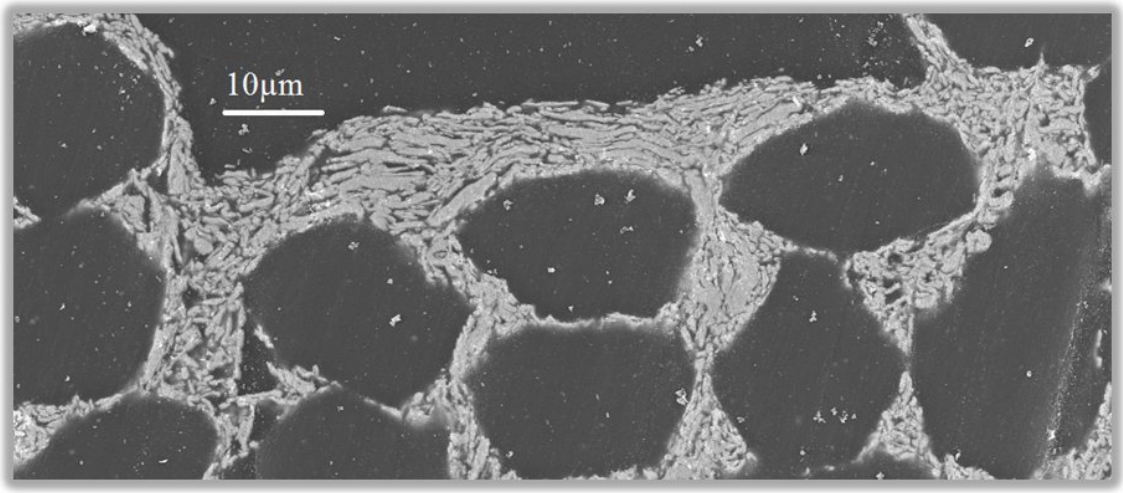

Figure 4.7. SEM micrograph of ink "A" on fabric substrate (sample from article [P3]) printed with screen printing.

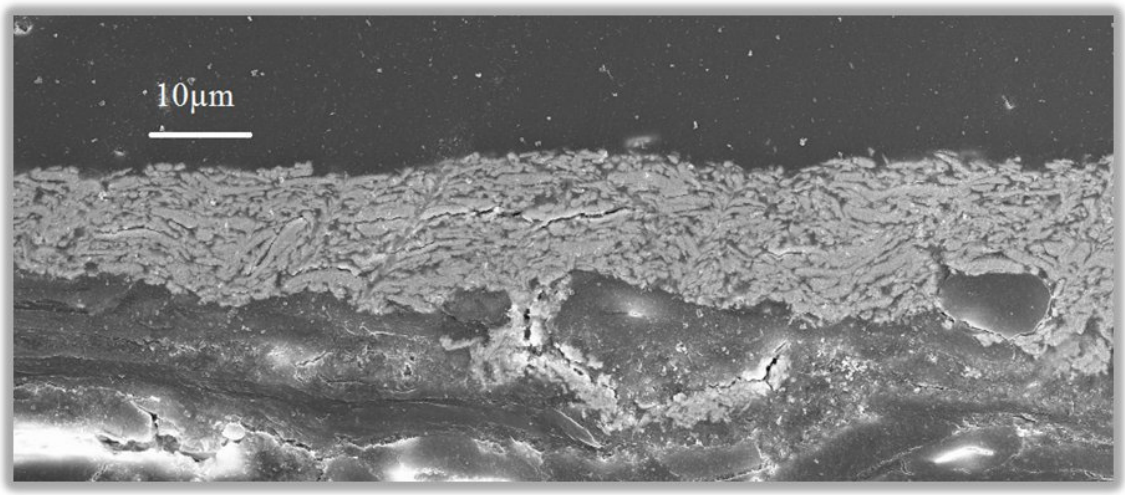

Figure 4.8. SEM micrograph of ink "A" on paper substrate (sample from article [P3]) printed with screen printing.

Fig. 4.6 shows that, in addition to the substrate material, the average film thickness is dependent on the ink. From the results it can be seen that ink (B) gives a typically thicker film. The viscosity of ink (B) is higher than the viscosity of ink (A) which indicates that ink (A) contains more solvents. During curing more solvents are evaporated from ink (A), reducing the film thickness. Nevertheless, it can be concluded that the thickness of the film is more heavily dependent on the substrate material than on the screen printable ink used in the study. Only with the paper substrate is there any appreciable difference in the thickness between inks (A) and (B) [P2].

Publications [P3 - P8] evaluate the thickness of the films printed with screen printing, gravure printing and pad printing. The measurements, **average thickness, standard de-**

viation, minimum and maximum values, of the film thickness were made with a measurement software connected to an optical microscope. The results are presented in Tables 4.2 and 4.3 [P3 - P8].

Table 4.2. The thickness measurement statistics of samples in articles[P3 - P6; P8]. Ink (B) is used with screen printed samples except the samples in article [P3]. Ink "A" is used in other samples.

Substrate	Printing method	Average thickness (µm)	Min (µm)	Max (µm)	Standard deviation (µm)	Notification
FR-4	Screen printing	14.6	12.6	17.2	1.3	[P6]
PET	Screen printing	13.9	10.9	18.5	1.8	"Thin" film [P5]
PET	Screen printing	21.5	16.8	26.0	2.5	"Mid" film [P5]
PET	Screen printing	50.5	39.5	58.8	6.4	"Thick" film [P5]
PET	Screen printing	7.0	5.9	8.4	0.9	[P3]
PI	Screen printing	7.6	5.9	9.3	1.2	[P3]
Paper	Screen printing	14.1	10.1	17.4	2.9	[P3]
Fabric	Screen printing	34.4	16.6	68.4	16.5	[P3]
PET	Gravure printing	4.5	2.5	6.4	0.9	[P3]
PI	Gravure printing	5.2	3.0	8.0	1.2	[P3]
Paper	Gravure printing	5.8	2.4	12.9	2.7	[P3]
PVC	Screen printing	27.3	20.1	31.4	2.4	[P8]
Fabric 1	Screen printing	82	25	156	48	[P8]
Fabric 2	Screen printing	53	11	143	46	Fabric in article [P9]
Fabric 3	Screen printing	267	104	342	51	"Fabric 2" in article [P8]
PET	Screen printing	21.5	16.8	26.0	2.5	[P4]
PET	Gravure printing	3.8	1.6	5.4	0.8	[P4]

The effect of the screen on the printed film thickness is seen in Table 4.2 in screen printed samples from publication [P5]. Different average thickness was achieved with different screen choice and the screen affected the surface profile (the waving) of the film. Different screens were also used in the samples from different publications and thus the absolute values in Table 4.2 cannot be compared. Certain common trends, however, can be seen and the table gives a good idea of the printed film morphology. More information on the equipment can be found in the attached publications [P3 - P6; P8].

The measurement results in Table 4.2 support the findings in Fig. 4.6. It is seen that the average thickness of the printed film depends on the substrate material. The thickness variation seems to occur on smooth non-absorbent substrates (plastics), but the variation is most obvious on porous and rough substrates (paper and fabrics). Different fabrics absorb different amounts of ink due to differences in woven structure and surface finish which also affects the morphology of the printed film [P3 - P8; Hoff_97].

As the results in Fig. 4.6 showed, in addition to the substrate characteristics, the amount of the transferred ink is dependent on the properties of the ink. Properties such as composition, viscosity, flow, drying rate and the amount of evaporating solvents have an effect on the printed film. Ink “A” (see Table 4.1) is intended for gravure printing and thus contains significantly more solvents than inks which are intended for screen printing. This difference affects the achieved cured film thickness. From Figs. 4.7 and 4.8 it can be seen that, although the gravure ink contains more solvents, the cured ink (ink “A”) is of the same kind as the ink which is intended for screen printing (see ink (B) in Fig. 4.5). In general, the film printed with gravure printing is thinner than that printed with screen printing. Although the amount of the solvent affects the thickness, the reduced thickness is mostly due to the gravure printing method itself [P3 - P8; Hoff_97].

As was discussed, pad printing is an indirect gravure method. Table 4.3 contains thickness measurements of the samples fabricated by pad printing on both flat and convex surfaces. The average thickness of 20 measurements was taken at three different points on the samples. More information on the measurement point is found in publication [P7].

Samples printed with pad printing (Table 4.3) also show an irregular film surface. Although the surface of the film is uneven, no clear relation or trend between the measurement point and the thickness can be seen. However, it can be seen from the standard deviation values that the printed film shows greater variation on convex surfaces.

The solvent in ink “A” is N-prophyl acetate and the solvents of ink “B” are ethyl acetate and N-prophyl acetate. During the printing process, ethyl acetate evaporates faster which affects the process parameters and thus may also affect print quality (for example, thickness; see Table 4.3). Both solvents evaporate rapidly during the printing process and this may also cause differences between the samples printed at different times [P7].

Table 4.3. The thickness measurement statistics of samples printed with pad printing on flat substrates and on convex objects. Ink "A" and ink "B" (see Table 4.1) was used in the samples [P7].

Sample	Print presses	Measuring point	Average thickness (µm)	min (µm)	max (µm)	Standard deviation (µm)
Ink "A" on Paper	3	Inner	**6.6**	3.3	10.0	2.2
Ink "A" on Paper	3	Middle	**5.6**	3.2	7.9	1.2
Ink "A" on Paper	3	Outer	**6.0**	3.3	10.1	1.8
Ink "A" on PET	3	Inner	**6.9**	4.2	10.2	1.5
Ink "A" on PET	3	Middle	**5.9**	3.3	8.0	1.4
Ink "A" on PET	3	Outer	**6.7**	3.3	9.2	1.5
Ink "B" on Paper	3	Inner	**6.9**	5.0	9.4	1.3
Ink "B" on Paper	3	Middle	**6.5**	3.8	10.2	1.9
Ink "B" on Paper	3	Outer	**6.4**	3.8	10.0	1.8
Ink "B" on PET	3	Inner	**7.1**	5.1	9.2	1.1
Ink "B" on PET	3	Middle	**6.5**	4.2	9.7	1.3
Ink "B" on PET	3	Outer	**6.8**	5.2	9.6	1.2
Ink "A" on Paper	5	Inner	**10.6**	7.2	13.1	1.4
Ink "A" on Paper	5	Middle	**11.4**	6.3	18.2	3.2
Ink "A" on Paper	5	Outer	**10.9**	4.6	19.7	3.4
Ink "A" on PET	5	Inner	**11.8**	9.2	13.9	1.4
Ink "A" on PET	5	Middle	**10.5**	7.9	13.4	1.8
Ink "A" on PET	5	Outer	**11.5**	17.1	18.8	2.3
Ink "A" on bottle, horizontally*	5	Inner	**28.0**	21.8	31.5	2.9
Ink "A" on bottle, horizontally*	5	Middle	**25.2**	20.5	29.3	2.6
Ink "A" on bottle, horizontally*	5	Outer	**19.3**	7.5	22.4	4.0
Ink "A" on bottle, vertically*	5	Inner	**11.1**	6.9	14.4	2.1
Ink "A" on bottle, vertically*	5	Middle	**20.7**	12.7	25.1	3.7
Ink "A" on bottle, vertically*	5	Outer	**22.9**	20.1	27.2	2.2
Ink "A" on cardboard reel, vertically*	5	Inner	**13.1**	8.4	19.7	4.1
Ink "A" on cardboard reel, vertically*	5	Middle	**11.9**	7.1	15.1	2.0
Ink "A" on cardboard reel, vertically*	5	Outer	**11.0**	7.5	21.3	3.2

* Horizontally/vertically indicates the positioning of the printed tag. "Vertically" means that the tag's length is placed in direction of the cylindrical object's axis. "Horizontally" means that the tag's length is placed in direction perpendicular to the cylindrical object's axis.

In addition to the standard deviation of the thickness measurements and microscopic examination, **the surface roughness** values R_a and R_z can be used to evaluate the fluctuations of the ink surface. The surface roughness value R_a is the arithmetical average of the deviations of average line and absolute measured value. The surface roughness value R_z is the average of the five highest points and the five lowest points of the surface. R_a and the standard deviation of film thickness give an indication of the average amplitude of the wavy surface. The minimum and maximum thickness values and R_z give information about the extreme values. Table 4.4 presents the surface roughness values

of certain substrates and screen printed films on them. The values are measured using a profilometer [P8].

Table 4.4 Surface roughness values of some substrates and of printed films on them.

Material	Screen (mesh / thickness of the thread in µm)	R_a (µm)	R_z (µm)
Ink on PVC	63/63	2	8
PVC	-	1	6
Ink on Fabric 1	63/63	21	96
Fabric 1	-	21	80
Ink on Fabric 2	63/63	28	126
Fabric 2	-	23	129
Ink on Fabric 3	63/63	34	151
Fabric 3	-	37	111

Fabric substrates are rough, but the surface of the PVC substrate is not completely smooth either. As with the previous results, the effect of the substrates on the printed film thickness variation is clearly seen in the results shown in Table 4.4. The large surface roughness of the printed film on fabrics is due mainly to the rough substrate surfaces. However, as can be seen from the measurements from the PVC sample, the printing method also affects the printed film surface roughness. In the case of samples on PVC, the surface of the substrate is not completely smooth, though it is still smoother than the printed film surface on it. The amount and the characteristics of the particles (such as size and formation of aggregates) also have an impact on the printed film surface. However, these factors are considered insignificant in comparison with the effect of the printing process and the substrate on the film surface [P8].

In printed UHF RFID tags, the surface roughness of the printed film is an important parameter since, at UHF frequencies, most of the electrical current flows in a layer a few microns thick near the surface of the film [Dobk_08]. It is concluded that film thickness variation occur in samples printed with screen printing (Table 4.2) gravure printing (Table 4.2) and with pad printing (Table 4.3). In article [Hay_07] it was shown that the higher the vehicle content of the ink, the more uneven is the film surface printed with the offset lithography method. The uneven film surface is also noted in publication [Side2_07] in samples which were printed with the flexography method. Uneven films are thus common to all of these printing methods. It should be noted that as well as the printing method, the thickness and morphology of the printed film is dependent on the ink, the substrate and the process parameters. Careful choice of the printing equipment is crucial in achieving good print quality and effective operation of tags.

5. Challenges of printed passive UHF RFID polymer thick film tag antennas

This chapter deals with the electrical properties of novel substrate materials and printed PTF structures. Their effect on the performance of passive UHF RFID tags is also discussed. Despite the benefits of printing processes, printed electronics faces several challenges. The printing process itself affects the properties of the fabricated structure. The materials also differ significantly from those traditionally used in electronics manufacturing and relatively little is known about their electrical properties or their effect on the final printed product. In addition, the materials have a crucial role in applications such as printed tag antennas. There is a need, therefore, for more research into such materials and printed structures and their performance in practical applications also needs further investigation.

5.1. Electrical performance of the substrates

The substrates are dielectric materials whose main function is to insulate the conductors from each other and from the ground. There are many important parameters which affect substrate performance in electronics applications. In addition to the required electrical insulation properties, factors such as thermal properties, mechanical properties and process compatibility are important [Camp_08].

Coefficient of thermal expansion (CTE) is a major factor in determining the compatibility between the substrate and the added components. The effect of poorly matched CTEs on the added components, including the thick films (such as silver ink) may be catastrophic over lifetime and in the presence of thermal excursions. Manufacturing issues include costs and the capacity of the substrate to withstand manufacturing processes. A good substrate surface finish and material compatibility are required. The substrate must also tolerate the environmental conditions during manufacture and during the lifetime of the tags. Substrates must also be mechanically robust enough to resist abrasion, vibration shocks and mechanical forces in order to maintain the electrical performance of the electronics product [Prud_94; Camp_08].

All of the above mentioned properties need to be considered when selecting the substrate material for antennas since they have at least an indirect effect on the electrical performance of the final product. One example of the indirect effect of the substrate material is its effect on the achieved printed film morphology which, in turn, affects the electrical performance of the film. This is discussed further in Section 5.2.2. Instead of

indirect effects, the present section deals mainly with the electrical performance (insulating properties) of the substrate materials themselves.

5.1.1 Electrical properties of the substrates

Almost all thermoplastic substrates have very good insulation properties. Plastic dielectrics typically have a weak interaction with EM fields because of their non-polar molecular structure. The challenge of fabric, paper and other unconventional substrate materials is that their electrical properties are relatively unknown. There is also large variation of fabrics and papers whose properties may differ greatly from each other. Most fibrous materials, such as wood and paper, are organic cellulose-based substances. In these materials the interaction with EM fields may be stronger than in plastics, especially in a humid environment. In general, the electrical properties of the substrates are dependent on the surrounding conditions such as alternating current (AC) frequency, temperature and moisture. The most important insulation characteristics of dielectrics are permittivity, loss tangent, resistivity and dielectric strength. These are discussed in this section [Busc_01; Coom_01; Fore_01; Simp_02; Chan_05; Mena_07; Camp_08].

Permittivity

When an insulating material is subjected to an electric field, a limited displacement of charge takes place at the atomic, molecular and bulk material levels. This charge displacement is known as polarization. In an atom the electrons are very light and they respond rapidly to the action of an applied electric field. The displacement of electrons relative to the nucleus is called electronic polarization. In a molecule, the ionic bond is deformed when an electric field is applied, resulting in increase of the dipole moment of the lattice. This is called molecular polarization. Molecular polarization can be simple ionic where a simple separation of the centre takes place (positive and negative ions move relative to each other) or distorted ionic when large ions are distorted by other close ions in addition to the simple ionic polarization. In liquids and gases, whole molecules move/orientate in accordance with the acting electric field. In solids, interfacial polarization occurs when charge carriers accumulate in materials' internal interfaces, such as at crystallite interfaces. In the presence of an interface with materials of different electrical properties (permittivity and conductivity), space charge polarization occurs [P7; Laug_03].

The relative permittivity ε_r is a parameter that indicates the relative charge (energy) storage capabilities of the dielectric material. The relative permittivity determines the amount of potential electric energy, in the form of induced polarization that is stored in a material when that material is placed in an electric field. Relative permittivity is expressed as the ratio of the dielectric permittivity of the material ε to that of a vacu-

um ε_0. In a linear, isotropic, homogenous medium the following equations for electric flux density and magnetic flux density can be used

$$\overline{D} = \varepsilon \overline{E} \tag{5-1}$$

$$\overline{B} = \mu \overline{H} \tag{5-2}$$

Eq. (5-1) indicates that the larger the permittivity, the larger is the electric flux density experienced by applying an electric field (similar to *B,* μ and *H* in Eq. (5-2)) [P7; Chen_93; Busc_01; Fore_01].

When applying a reversing electric field, reversed polarisation will occur. In non-ideal dielectrics it does not follow the reversing field exactly because polarization takes a finite time. Generally, interfacial polarizations are the slowest of the polarization mechanisms and they have the longest response time (time constant). Molecular and dipole polarizations are intermediate, ionic polarization is fast, and electronic polarization, due to the shift of electron orbitals, is the most rapid. This variation of the time constant governs the influence of frequency on dielectric properties. The ion displacement and the displacement of electrons relative to the nucleus have resonant frequency so there might be regions in frequency response where the relative permittivity is increasing. With increasing frequency, the factors producing slower polarization diminish. This is why the relative permittivity usually decreases when the frequency increases. When frequency increases to high enough values, neither of these mechanisms can be in phase with the changing field [P7; Busc_01; Fore_01].

An ideal dielectric releases all stored energy when the electric field is removed, but in practice dielectrics dissipate some of the energy as heat. Non-ideal dielectric materials contain free charge carriers that cause ohmic losses when an electric field is applied. In addition to this, dielectric losses occur. In an electromagnetic wave the direction of the electric (and magnetic) field vector changes, which causes the dipole molecules of the dielectric medium to rotate and charged particles to displace according to the applied field vector. As the frequency increases (shorter field reversal), the inertia of the charged particles tends to prevent the particle displacements from keeping in phase with the field changes, leading to a frictional damping mechanism that causes power loss (dielectric losses) since work must be done to overcome the damping forces [P7; Busc_01; Fore_01].

Complex permittivity is a parameter which can be used to model the losses in dielectrics. If only ohmic losses are taken into account, the complex permittivity ε_c can be written as [P7; Bala_89; Chen_93]:

$$\varepsilon_c = \varepsilon - j\frac{\sigma}{\omega} \tag{5-3}$$

in which the imaginary part presents the ohmic losses. As is seen, the imaginary part is also frequency dependent. The frequency dependency is derived from Eq. (2-4) and Ohm's law ($\overline{J} = \sigma\overline{E}$). If both ohmic and dielectric losses are taken into account, the complex permittivity can be written as:

$$\varepsilon_c = \varepsilon' - j\varepsilon'' \tag{5-4}$$

where ε' is the real permittivity and ε'' is the imaginary permittivity which presents all losses (ohmic and dielectric). It should be noted that in this case the frequency dependence of the imaginary part is more complicated than inverse proportionality.

If the medium in which an EM wave propagates is lossy, it attenuates the propagation of the wave. In this case complex permittivity is used instead of dielectric permittivity of the medium. In Chapter 2 the EM plane wave propagating in z direction (see Fig. 2.1) was introduced. When replacing the dielectric permittivity with the complex permittivity in Eq. (2-8), the wave number becomes complex and it can be written as $k_c = \omega\sqrt{\mu(\varepsilon' - j\varepsilon'')} = k' - jk''$. It is found that by using Eq. (2-7) the propagating wave can be expressed as

$$\overline{E}(z,t) = \mathrm{Re}\left\{\hat{e}_x E_0 e^{j\omega t} e^{-jk_c z}\right\} = \mathrm{Re}\left\{\hat{e}_x E_0 e^{j\omega t} e^{-j(k'-jk'')z}\right\} = \mathrm{Re}\left\{\hat{e}_x E_0 e^{j\omega t} e^{-jk'z} e^{-k''z}\right\} \tag{5-5}$$

As can be seen from (5-5), when z increases, the term $e^{-k''z}$ decreases, causing the wave damping.

Propagation constant γ (m^{-1}) is a parameter which is typically used in transmission line theory. The relation between propagation constant and the complex wave number is

$$\gamma = jk_c = j\omega\sqrt{\mu\varepsilon_c} \tag{5-6}$$

The propagation constant can thus be expressed as

$$\gamma = \alpha + j\beta = jk' + k'' \tag{5-7}$$

and the propagating wave can then be expressed as:

$$\overline{E}(z,t) = \mathrm{Re}\left\{\hat{e}_x E_0 e^{j\omega t} e^{-jk'z} e^{-k''z}\right\} = \mathrm{Re}\left\{\hat{e}_x E_0 e^{j\omega t} e^{-j\beta z} e^{-\alpha z}\right\} \tag{5-8}$$

where α and β are positive quantities. The factor $e^{-\alpha z}$ decreases when z increases and it is thus an attenuation factor. The symbol α is called an attenuation constant (Np/m). The second factor $e^{-j\beta z}$ is a phase factor and β is called a phase constant (rad/m), which expresses the amount of phase shift that occurs as the wave propagates [Chen_93].

It is generally desirable to have relative permittivity of the substrate as small as possible because the capacitance effects are directly proportional to relative permittivity and they decrease the signals' speed and increase the power needed for their propagation. In the case of passive UHF RFID tags, the higher relative permittivity might sometimes be desirable because the tag would be less affected by the object to which it is attached. In addition it might offer possibilities in antenna miniaturization [Prud_94; Camp_08].

It should be noted that the reported values of measured relative permittivity at high frequencies can vary according to the specific test method used. Furthermore, the relative permittivity is not a constant and it will vary, in addition to frequency, with temperature and humidity [Coom_01].

Loss tangent

The loss tangent is another quantity which is used to describe the losses of dielectric materials. The loss tangent is a measure of the conversion of the reactive power to the real power, expressed as heat. Thus a low loss tangent indicates low power losses and a more efficient insulator. The loss tangent of a material can be expressed with the aid of the complex permittivity (Eq. (5-4)) as [Bala_89]

$$\tan\delta = \frac{\varepsilon''}{\varepsilon'} \tag{5-9}$$

Commercial antenna substrate manufacturers typically provide the relative permittivity and the loss tangent in their data sheets. When selecting insulating materials for high frequency equipment used at higher voltage, in addition to low relative permittivity, low loss tangent is required. The dielectric properties, especially the loss tangent of a thermoplastic material, are closely related to the molecular structure of the material. The smaller the dipole moment (or polarity), the smaller is the value of the loss tangent of the material. Loss tangent typically increases with frequency. In addition, the loss tangent is affected by temperature, humidity and other environmental conditions. The major electrical effect of humidity on an insulating material is to greatly increase the magnitude of its interfacial polarization, increasing conductivity and losses [P7; Prud_94; Busc_01; Coom_01; Laug_03; Camp_08].

Electrical resistivity

Electrical resistivity describes the degree to which electrical charges can be conducted through a material to which an electrical potential or voltage differential is applied. Volume resistivity and surface resistivity refer to the insulation properties through the thickness and the surface, respectively [Fors_54; Mena_07; Camp_08].

Volume resistivity is the ratio between the material's potential gradient parallel to the current to the current density. It is numerically equal to the volume resistance in ohms between opposite faces of a cubic meter of the material [Fors_54; Camp_08].

Surface resistivity is the ratio of the potential gradient parallel to the current along its surface to the current per unit width of the surface. It is numerically equal to the surface resistance between two electrodes forming opposite sides of a square. Surface resistance is the ratio of the direct voltage applied to the current obtained from two electrodes placed on the surface of a material [Camp_08].

The higher the resistivity values are, the better the dielectric material is. In other words, the lower the resistance of the insulator is, the more conduction losses occur. The resistivity also depends on several factors, including temperature and moisture. Surface resistance changes rapidly with humidity, but volume resistance or conductance changes slowly, although the final change may eventually be greater [Coom_01; Camp_08].

Dielectric Strength

In addition to the parameters discussed above, dielectric strength is an important quantity in electronics applications. Dielectric strength determines the voltage breakdown properties of the substrate. Dielectric strength (V/m) is the maximum electric field strength that the material can withstand without dielectric breakdown. A fundamental requirement for the insulation in electrical applications is that it should withstand the voltage imposed on it in service. In the case of RFID tags, the dielectric strength is assumed not to be a constraint and it is left out of further discussion. Other electrical properties of some dielectric materials are presented in Table 5.1. Some of the dielectrics in Table 5.1 are used as substrate materials in this thesis and others are included in the table to provide reference points. The properties are measured at room temperature if no other information is given. The values give some idea of their magnitude, although there are differences in the values given in different references [Prud_94; Coom_01; Camp_08].

Table 5.1. Electrical properties of some dielectric materials.

Material	Relative permittivity	Loss tangent	Volume resistivity (Ω·m)	Notes
Air	1.0006 [Laug_03]	0* [Laug_03]		* @ kHz
PET	3.5 *[Camp_08] 3.2 **[Laug_03]	0.005*[Camp_08] 0.005**[Laug_03]	10^{13} *[Camp_08]	* 30 % glass reinforcement, @ 10^2 Hz ** @ kHz
PI	3* [Prud_94] 3.6**[Camp_08] 3.5***[Laug_03] 4.3 *[Coom_01] 3.7 ****[Coom_01]	0.003*[Prud_94] 0.002**[Camp_08] 0.003**[Laug_03] 0.013*[Coom_01] 0.007****[Coom_01]	10^{16} *[Prud_94] $5 \cdot 10^{12}$ **[Camp_08] 10^{11} (*) [Coom_01]	* @ 1 MHz ** @ 10^2 Hz *** @ kHz ****@ GHz (*) see text under this table
PVC	3.3* [Camp_08] 3 - 7**[Laug_03]	0.009* [Camp_08] 0.01 - 0.02**[Laug_03]	$9 \cdot 10^{11}$*[Camp_08]	* for rigid PVC [Camp_08] ** @ kHz
Paper	1.9 - 2.9 [Laug_03] 3.5 [Frad_04]	0.005*[Laug_03] 0.007**[Laug_03]	10^{16} [Laug_03]	*@ 50Hz ** @ kHz
Wood (dry)	1.4 - 4 [Busc_01] 2 - 5 [Fore_01]		10^{14} - 10^{16}*[Fore_01]	* for oven-dry wood [Fore_01]
Cotton	5*[Laug_03] 3.2***[Mena_07] 3.0****[Mena_07]	0.2*[Laug_03] 0.15**[Laug_03]		* Cloth, varnished cotton @ 50Hz ** Cloth, varnished cotton @ kHz *** 0 % relative humidity @ kHz **** 0 % relative humidity @ 100 kHz.
Wool (dry)	1.5 [Simp_02]			
Nylon 6.6	3.5 – 6 [Laug_03]	0.02 - 0.06* [Laug_03]	10^{13} [Laug_03]	* @ Mhz

(*) Sample subjected to 90 % relative humidity, 35 °C for 96 h (96/35/90) [Coom_01].

In addition to the dielectric strength which was assumed not to cause problem in RFID tags, the challenges caused by the substrate resistivity and loss tangent are assumed minor in this study because the substrates are considered as low loss dielectrics. According to the literature, the relative permittivity of the substrates is low and the difference between the materials is relatively small. The relative permittivity was also measured with Agilent vector network analyser VNA E8358A, using the Agilent 85070E Di-electric probe kit. The effect of frequency on the relative permittivity was examined and it was found to be insignificant in the UHF RFID frequency range. The measured relative permittivity of the substrates is presented below, in Table 5.2.

Table 5.2. The measured relative permittivity of some substrate materials.

Substrate	The relative permittivity at UHF
PET	1.8 [P7]
PI	2.5
PVC	2.8 [P9]
Paper	1.8 [P7]
Cardboard	2.6 [P7]
Fabric 2	1.5 [P9]
PET, soft drink bottle	1.6 [P7]

There are minor differences between the measured relative permittivity values (Table 5.2) and the values reported in the literature (Table 5.1). The values in Table 5.2 are measured at higher frequency than most of the values in Table 5.1. The measured permittivity values show even smaller difference between the substrates [P7; P9].

The significance of the substrates' parameters and their effect on the electronics applications increases by increasing their volume. This means that the significance of small changes in the electrical parameters also increases. In Section 5.2.2, power loss of conductive material is examined with the structure in Fig. 5.2. The power loss of the structure is approximated with Eq. (5-24) which can also be applied to approximate power loss in good dielectrics (in which $\left(\frac{\sigma}{\omega\varepsilon}\right)^2 << 1$ and $\varepsilon'' << \varepsilon'$). In this case, skin depth δ (m), which is discussed further in Section 5.2, is approximated with

$$\delta \cong \frac{2}{\sigma}\sqrt{\frac{\varepsilon}{\mu}} \tag{5-10}$$

By using Eq. (5-10) to define the skin depth, Eq. (5-24) describes the approximated losses of a dielectric structure with similar geometry to that illustrated in Fig. 5.2. It is seen from Eq. (5-24) that the thicker the dielectric layer is, the larger is the power loss [P7; Bala_89].

The losses caused by the substrate material can be found in experimental results. These are discussed further in Sections 5.3 and 5.4.

5.2 Electrical performance of the polymer thick films

In this section the effects of composition, morphology and curing on the electrical performance of the printed conductive PTFs are discussed. Generally the conductivity σ (S/m) of silver inks is lower than that of pure metals, such as copper or aluminium. Typical conductivity of PTF silver ink is a few mega siemens per meter whereas, for example, the conductivity of copper is 58 MS/m. Instead of conductivity, sheet resistance (Ω/□) is typically given in the ink suppliers' data sheets, though this is more a guideline. The electrical performance of the final printed product is dependent on its composition and morphology. Curing also affects electrical performance through its effect on the ink composition [Chen_93; Dobk_08].

5.2.1 Electrical performance and ink composition

The conductivity of polymer thick film composites, such as silver ink, is a complicated phenomenon and there are several different mechanisms which control the total conductivity. The electrical conductivity of composites similar to silver ink used in this study is discussed, for example, in articles [P2; P8; Hay_07; Hu_08; Kure_08; Sevk_08].

In a typical conductive PTF composite, a large quantity of irregular conductive particles is suspended in insulating polymer. In order to describe the electromagnetic properties of such composite materials, it is necessary to solve the Maxwell equations applied to these systems. Although they enable the electromagnetic behaviour to be fully described, their solutions are far from being solved exactly. Only in the case of an isolated metal particle inside an insulator ceramic matrix, with a simple geometry (spheres, ellipsoids and infinity cylinders), can the Maxwell's equations be solved exactly. Even in these specific cases, the huge difference in electric properties between the filler and matrix and the cumbersome formulation of these solutions make the task of finding an accurate solution very difficult. In addition, in the case of real inks (irregular shapes and large concentrations of conductive particles) the Maxwell equations cannot be solved analytically [Moya_07].

However, the electrical conductivity of composites similar to the PTF silver ink has been analyzed using different models. Many models are created to describe the behaviour of polymer matrix composites with conductive fillers. The aim of this study is not to create a suitable model for the silver ink used, but some models are introduced to explain the factors affecting ink conductivity. In articles [Brom_97; Rims_04; Deep_09] the conductivity of the particle reinforced composites was noted as being dependent on the frequency in low particle content. However, in higher particle loadings (the case in this study) the conductivity was considered practically independent of the frequency. Direct current (DC) conductivity is discussed in the following sections to describe the effect of the ink composition on electrical performance [Brom_97; Rims_04; Deep_09].

The percolation problem can be applied to composite materials such as silver ink to describe the relation between the physicochemical properties and electrical properties. At a certain volume content the conductive particles of the composite form a conductive network. The percolation threshold is the critical volume fraction of conductive particles in the composite at which the conductive phase becomes connected and the effective conductivity changes dramatically. Below the percolation threshold, the composite is considered as an insulator and above the threshold a conductor. In other words, at the percolation threshold the resistivity ρ (Ωm) of the composite decreases rapidly when particle content is increased. The decrease finally becomes markedly slower as the filler volume content is further increased [P2; P8; Dzie_01; Dzie2_01; Jylh_07].

The dependence of experimental sheet resistance on conductive phase fraction (so called blending curve) is often used to analyze the electrical properties of composites. The schematic sketch of resistivity of a particle-reinforced composite as a function of conductive filler concentration for isotropic particles is introduced in Fig. 5.1 [P2; Kuls_02].

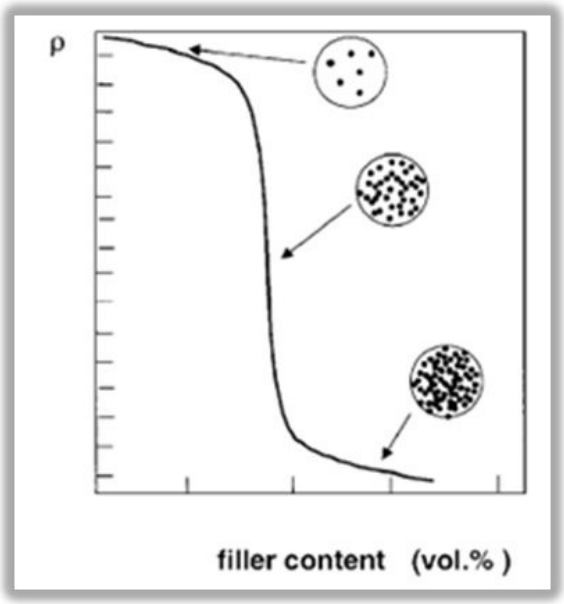

Figure 5.1 Resistivity of an insulating matrix/conductive filler composite as a function of filler concentration for isotropic particles [Kuls_02].

At concentrations of the conductive phase below the percolation threshold, two additional electrical transportation phenomena, hopping conductivity and quantum mechanical tunnelling, have been reported to occur. The effect of these conduction models decreases as the volume fraction of the filler particles increases. In the silver inks used in this study, the filler material content is high and the particles are assumed to form a conductive network. Thus, the effect of these phenomena on the total conductivity is assumed insignificant [Taya_98; Psar_06; Hu_08].

Effective medium theory, EMT, is used to predict the conductivity of conductive particles/insulating matrix composites at sufficiently high conductor loadings. According to article [Hick_80], EMT is semi quantitatively accurate at high loading and it treats conductive phase as single spheres. It does not take into account the clusters and chains. It is predicted that the conductivity of the composite asymptotically approaches the expression in Eq. (5-11) when the loading is increased.

$$\sigma_c / \sigma_f = \frac{3}{2}(f - \frac{1}{3}) \tag{5-11}$$

In Eq. (5-11) σ_c is conductivity of the composite (S/m), σ_f is conductivity of the conductive filler material (S/m) and f is the volume fraction of the conductive filler material in the composite. In article [P2] (silver content of the inks > 83 wt% of the solid contents) the formula gives the composite too high conductivity, but it does give an idea of the order of magnitude. There are also formulas that can be used closer to the threshold limit, but these contain empirical parameters and are more complex [P2; Hick_80].

Cohen et al. (1978) state that in the percolation model of a conductor–insulator composite, the effective conductivity of a composite σ_c can be expressed as

$$\sigma_c = \sigma_f (f - f^*)^a \ , \quad \text{for} f > f^* \tag{5-12}$$

where f^* is the critical conductor volume fraction (f at the percolation threshold), and a is an empirical conductivity exponent. Due to the power-law-type conductive behaviour, small changes in f or f^* can lead to large changes in the composite conductivity, especially close to the percolation threshold [P8; Taya_98].

An equation, which also takes account of the electrical properties of the matrix and does not involve any adjustable parameters, was introduced in article [Jylh_07]. According the article the volume fraction of the conductive filler can be expressed as

$$f = 1 + (f^* - 1)\frac{\sigma_f - \sigma_c}{\sigma_f - \sigma_m} - f^* \left(\frac{\sigma_f - \sigma_c}{\sigma_f - \sigma_m} \right)^{\frac{\sigma_f}{\sigma_m}} \tag{5-13}$$

where σ_m is the conductivity of the insulator matrix phase (S/m) [Jylh_07, Jylh_08]. The model predicts very flat effective conductivity below the percolation threshold, which is very typical behaviour for metal-filled polymers. The model is valid if the inclusions are well mixed [Jylh_07].

Eq. (5-13) shows that the conductivity of the matrix (polymer) also influences the effective conductivity of the composite (ink). However, the conductivity of polymer matrix material is typically insignificant. For example, polyester resin (polymer matrix of ink (B)) is investigated in article [Lear_69] where it is observed as having negligible conductivity.

If the following parameters are used for the silver ink: f^* = 30 vol% (assumed for spheres [Jylh_07]), f = 50 vol% (evaluated from SEM figures [P8]), $\sigma_m \approx 0$ S/m and σ_f = 63 MS/m (conductivity of silver), Eq. (5-13) gives an exaggerated value (a decade too high) of effective conductivity. Eq. (5-13) does not take into account the contact resistance of the adjacent silver particles and it assumes that the medium is perfectly isotropic, which it may not be (see Fig. 4.5, for example). In addition, the percolation threshold of the ink might not be 30 vol%. In article [Jing_00] it was found that particle size affects the percolation threshold. The smaller the particle size, the lower the percolation threshold [Jing_00]. In article [Jing_00] one model predicted about 30 vol% percolation thresholds for particles with diameter of about 10 nm. The average size of the particles of ink (B) is from 3 µm to 15 µm. Percolation threshold as high as 43 vol% is reported for some composites in article [Jing_00]. In addition to particle size, the percolation threshold is dependent on the shape, conductivity, orientation, distribution and size distribution of the particles and the properties of the matrix material which affects the tunnelling distance [P1; P8; Taya_98; Jing_00; Lin_04; Deep_09].

Advanced models that include the shape of the particles can also be found, for example, in article [Dzie2_01]. A model which would be valid from small to large filler content and which would take into account the frequency dependent behaviour of the substances would be useful, but in practice it is very challenging to develop [P2].

In summary, the conductivity of the PTF composite depends on many parameters such as the material, quantity, size, shape, distribution and orientation of the particles and particle-size distribution. Also the quality and quantity of the matrix material (polymer) and additives affect the performance of the PTF composite. In our case, the quantity of the conductive particles is high and the effect of tunnelling and hopping conductivity is assumed insignificant, as is the conductivity of the polymer matrix. Thus, the conductivity of the ink is assumed to be determined by the conductive particles. Experimental results of the electrical performance of different PTF inks are discussed further in Sections 5.3 and 5.4 [P2; P6; P8; Hay_07; Hu_08; Kure_08; Sevk_08].

5.2.2 Electrical performance and morphology of the films

Morphology of printed films was discussed in Chapter 4. This section deals with the effect of morphology on the electrical properties of the films. The cross section area of the conductive film is an important topic in this discussion. Both surface profile and

thickness of the film have an effect on the ink film cross section area. To minimize the use of costly silver, the printed patterns should be as thin as possible. However, the patterns must also be thick enough to guarantee low ohmic losses. This is critical, especially at higher frequency applications [P5; Side_05; Side2_07].

The conductive medium contains free charge carriers. In good conductors they move freely according to the applied electric field and they cancel the electric field inside the conductor. In real conductors, losses are introduced due to collision of charge carriers in atoms (friction). When the frequency is increased, the charge carriers do not have time to move in phase with the electric field and the electric field penetrates slightly inside the conductor. Consequently, the current density is packed into the region near the surface of a good conductor. This is called the skin effect. Skin depth, or penetration depth, is defined as the depth below the surface of the conductor at which the amplitude of an incident electric field has decreased by factor 1/e ≈ 0.37. The skin effect has an impact on the ohmic losses by decreasing the effective conductor cross-section area. When the frequency is high enough, every material becomes an insulator since the wave "does not see" the matter anymore. This is because the charge carriers do not have time to move in phase with the frequency (for example X-rays). In this case, the electromagnetic wave also penetrates and propagates in conductors. Inside the conductor, high frequency waves, such as X-rays, are partially absorbed because they excite electrons from the inner energy levels of atoms. Our research is mainly focused on the lower frequency regime (RF) where skin effect and ohmic losses play an important role [P5; P7; Bala_89; Chen_93].

An approximate expression for the skin depth can be found by considering the normal incidence of a plane wave into a good conductor ($\left(\frac{\sigma}{\omega\varepsilon}\right)^2 >> 1$). Suppose that the electric field oscillates along x-axis and the wave propagates in the positive *z*-direction. Then the incident field is defined by the expression

$$\overline{E}(z;t) = \hat{e}_x E(z) e^{j\omega t} \tag{5-14}$$

In a lossy medium, characterized by constitutive parameters ε, μ and σ, the phasor of the incident field is

$$E(z) = E(0) e^{-\gamma z} \tag{5-15}$$

where $E(0)$ is the amplitude of the wave at the surface of the medium. When Eq. (5-3) is used to derive ε_c, the propagation constant (Eq. (5-6)) can be expressed as

$$\gamma = \sqrt{j\omega\mu(\sigma + j\omega\varepsilon)} \tag{5-16}$$

In a good conductor the attenuation constant (see Eq. (5-7)) which models the attenuation of the wave, can be approximated by

$$\alpha = \mathrm{Re}(\gamma) \approx \sqrt{\frac{\omega\mu\sigma}{2}} \tag{5-17}$$

Then, applying the definition of the skin depth one can write

$$e^{-1}E(0) = \left|E(\delta)\right| = \left|E(0)\right|\left|e^{-\gamma\delta}\right|, \tag{5-18}$$

where δ denotes the skin depth and then solve

$$\delta = \frac{1}{\alpha} = \frac{1}{\sqrt{\pi f\mu\sigma}}. \tag{5-19}$$

The magnitude of current density in the conductor at depth z, due to the incident field is now

$$J(z) = \left|\sigma E(z)\right| = \sigma E(0)e^{-\alpha z} = \sigma E(0)e^{-z/\delta} \tag{5-20}$$

According to Eq. (5-19) the skin depth is inversely proportional to the frequency and so the conductive (ink) film does not have to be very thick in UHF applications. With different printing techniques it is possible to produce films having a thickness of the same order of magnitude as the skin depth and hence the resistance of the film remains low. It should be noted that the lower the conductivity of the ink, the thicker the printed film that is needed to minimize the losses. Therefore, in practical applications, it is important to ensure that the performance of the conductors is sufficient through the desired frequency range, regardless of the fabrication method and the materials used [P1; P5; P6; Bala_89; Blay_05; Puda_05; Side_05; Mole_06].

If the thickness of the printed film is reduced, the ohmic losses increase because the structure starts to disturb the current flow. The effect of the characteristics of the conductor material on losses can be evaluated as follows. Consider the rectangular conductor shown in Fig. 5.2.

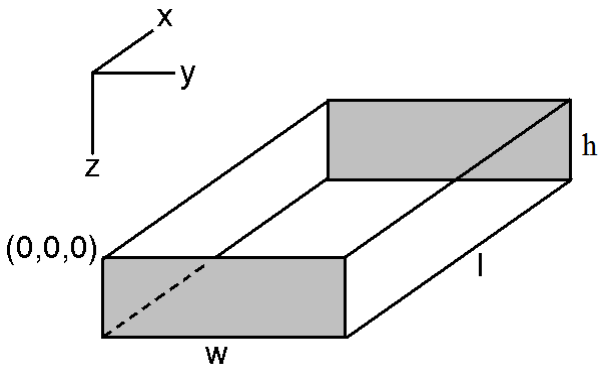

Figure 5.2. Rectangular conducting structure in Cartesian coordinates.

The power loss in the structure P_{loss} can be approximated using Joule's law as [Chen_93]

$$P_{loss} = \int \overline{J} \cdot \overline{E} dv \tag{5-21}$$

The expression for the electric field strength inside the conductor is given in Eq. (5-15) and its value at the surface of the conductor is, in this case

$$E(0) = \frac{V_{rms}}{l} \tag{5-22}$$

where V_{rms} is the root-mean-square value of the voltage (V) and l is the length in Fig. 5.2. Current flows in all surfaces of the structure (Fig. 5.2), but if $h << w$ the only significant contribution comes from the faces at $z = 0$ and $z = h$. Then the power loss can be approximated as

$$P_{loss} = 2 \int_0^{h/2} \int_0^w \int_0^l \frac{\sigma V_{rms}^2}{l^2} e^{-2\frac{1}{\delta}z} dx dy dz \tag{5-23}$$

Recalling that conductivity is the inverse of resistivity ($\sigma = \rho^{-1}$), the expression for loss power becomes

$$P_{loss} = \frac{V_{rms}^2 w \delta}{\rho l} (1 - e^{-h/\delta}) \tag{5-24}$$

Considering Eq. (5-20), the sheet conductance G_s (S□) of a conductive layer of thickness h can be estimated as follows

$$G_s = \int_0^h dG_s = \int_0^h \sigma e^{-\alpha z} dz = \frac{\sigma}{\alpha} (1 - e^{-\alpha h}) \tag{5-25}$$

Recalling that the sheet resistance $R_s = G_s^{-1}$ and $\alpha = \delta^{-1}$, the sheet resistance of the conductive layer becomes

$$R_s = \frac{\alpha}{\sigma}(1 - e^{-\alpha h})^{-1} = \frac{\rho}{\delta}(1 - e^{-h/\delta})^{-1} \tag{5-26}$$

Since it was assumed that $h << w$ and the only significant faces are those at $z = 0$ and $z = h$, the resistance of the rectangular conductor in Fig. 5.2 can be regarded as a parallel resistance of the sheet resistance of the upper layer R_u (thickness $h/2$) and lower layer R_l (thickness $h/2$). The expression of the resistance can be then written as

$$R = \frac{l}{w}\left(\frac{1}{R_u} + \frac{1}{R_l}\right)^{-1} = \frac{l\rho}{2w\delta}(1 - e^{-h/2\delta})^{-1} \tag{5-27}$$

Considering Eq. (5-27) and Ohm's law, the expression for the loss power from Eq. (5-24) in terms of the effective current is

$$P_{loss} = \frac{I_{rms}^2 l\rho}{4w\delta}(1 - e^{-h/\delta})(1 - e^{-h/2\delta})^{-2} \tag{5-28}$$

where I_{rms} is the root-mean-square value of the current. Eq. (5-28) implies that as conductor thickness tends to zero, the power loss increases as the inverse of the thickness. When $h << \delta$, $(1 - e^{-h/\delta})(1 - e^{-h/2\delta})^{-2} \approx \frac{4\delta}{h}$ and $\lim P_{loss} = \frac{I_{rms}^2 l\rho}{wh}$ [P5].

On the whole, the presented formulation to model the losses is a rough estimate because the geometry is neglected. Nevertheless, it gives an idea of how the thickness of the conductor material affects the power loss. In publication [P5] the thickness dependency proposed by the Eq. (5-28) was verified by a simulation and this is further discussed in Section 5.3. The experimental results of the effect of printed film thickness on the performance of tag antennas are investigated in Section 5.4 [P5].

In addition to film thickness, it is important to consider the surface roughness of the film (and substrate). Additional conductor losses associated with the surface roughness of the conductor at high frequencies is well known. Morgan (1949) published the first quantitative analysis of the effect of surface roughness on conductor losses [Morg_49; Baye_04]. His analysis provides values for relative power dissipation (versus a smooth surface) for a number of well-defined surface geometries, including square, rectangular and triangular grooves. The grooves were oriented both parallel and perpendicular to the direction of current flow. The exact shape of the grooves was not considered to be critical. Instead, the increase in eddy current losses caused by grooves parallel to the current

is shown in a particular case to be only about one-third as great as the increase caused by transverse grooves of similar size [P6; Morg_49; Baye_04].

In our case the surface roughness appears in both directions (in parallel and in transversal directions), and the surface roughness is not as regular as in the article [Morg_49]. In addition, on a rough substrate surface, both the upper and lower surfaces of the printed film are irregular. In publication [P6] it was observed that when the substrate surface is rough compared to the desired film thickness, the current paths will elongate and variations in the deposited conductive layer thickness will occur, resulting in increased resistance. As noted in Chapter 4, in addition to ink and substrate properties, the printing process (the selected method, properties of the screen and other printing equipment, as well as the printing parameters) has a significant effect on the printed film morphology. Thus, in our case, Morgan's simplified model cannot be used to evaluate the losses caused by the surface roughness, but the model indicates that surface roughness has an impact on the conductivity of the conductive film and that this effect increases as the frequency increases because the skin depth decreases. Further examination of the effect of surface roughness on the electrical performance of printed film lies beyond the scope of this thesis. However, this remains an interesting field for future research [P6; P8; Morg_49; Baye_04].

5.2.3 Electrical performance and curing

In the case of electrically conductive inks, the curing process has an effect on the final printed film conductivity. The inks of this thesis are intended to be heat cured. The curing process affects the evaporation of the solvents in the ink and thus the solvents determine the required curing conditions. Too fast curing (short time, high temperature) makes the solvents evaporate too readily, causing the printed film to deteriorate. Too high curing temperatures also constrain the substrate material selection. Conversely, if the curing is too slow (long time, low temperature) residues may remain in the printed film. The inks dry at room temperature for the required period of time, but in this case the printed film conductivity remains low due to the residues. Fast curing is preferred in mass production. It is possible to compromise between the maximal film conductivity and the curing (time and temperature). Faster curing may deteriorate the conductivity but the process is more effective. This means that the curing conditions and the printed film conductivity must be considered in each particular case. The authors of article [Dzie_95] note that the curing temperature also affected the long term stability of the conductive films [P2; Dzie_95; Hahn_01].

In article [Hick_80] the effect of curing temperature was found to have a greater effect on the sheet resistance of polyvinyl acetate/Ag (70 wt%) composite than the curing time when curing temperatures were 70 °C and 95 °C. Only when the samples were cured at 50 °C did the curing time play a more important role [P2; Hick_80].

The physicochemical and electrical properties of carbon/polyesterimide thick film resistive composites were investigated in article [Dzie_07]. Irrespective of the filler used, the curing conditions (time and temperature) had a greater effect on the resistance of composites with smaller filler content. It was also found that the change in resistance was rapid after the curing temperature was raised and when kept at the same temperature, the change was smaller. Changes in resistance were attributed to an increase in conductive phase fraction [P2; Dzie_07].

Publication [Dzie_95] examined the effect of curing temperature on four different composites consisting of thermoplastic resin and about 90 wt% silver flakes. The effect of curing temperature on the same ink on three different substrates (alumina, phenyl laminate and polyester foil) was also examined. A decrease in resistance was detected for all samples though there were differences between individual inks. The substrate also appeared to influence the behaviour of the ink cured at different temperatures. The effect of the substrate on the drying of the ink is outside the scope of this thesis. However, experimental results for two inks (ink (A) and ink (B)) are given in Section 5.3.

5.3 Electrical performance of samples in publications P2, P4 - P7

In antenna applications radiation efficiency can be greatly affected by losses in the antenna structure [P4; P5; P7; P9; Side2_07]. As discussed in previous chapters, the electrical performance of the printed structures depends on the properties of both the conductor and the substrate. The electrical performance of the prototypes and test structures in publications [P2; P4 - P7] is presented and discussed below.

5.3.1 Electrical performance of PTF structures with direct current

In publication [P2] the sheet resistance values measured for the screen-printed conductive patterns on different substrates are presented in Fig. 5.3 for inks (A) and (B) (see Table 4.1). The sheet resistances of samples printed with both inks are reasonably low, which means they are suitable for many practical applications. The amount of ink is different on different substrate materials and this affects the resistance of the printed films. The average thickness of the samples is presented in Chapter 4 in Fig. 4.6. In addition, if the thickness variation is large, the amount of ink is partially small, which increases the resistance. As Fig. 5.3 shows, the sheet resistance of the conductive patterns prepared by using ink (A) is around 0.04 Ω /□ and this is lower than the sheet resistance of samples printed with ink (B). Nevertheless, the thickness of the films printed with ink (A) is smaller than that of films printed with ink (B). The reason for the lower sheet resistance is the higher silver content of ink (A). Minor differences in structure between inks (A) and (B) can also be seen in Fig. 7 and Fig. 8 in the article [P2]. An exception to this trend (ink (A) having lower sheet resistance) is the samples on PVC substrate,

where the sheet resistance of ink (A) is much higher than that of ink (B). Ink (A) contains two types of ketone solvents which may permeate the surface of the PVC and adversely affect the curing process of the ink [P2].

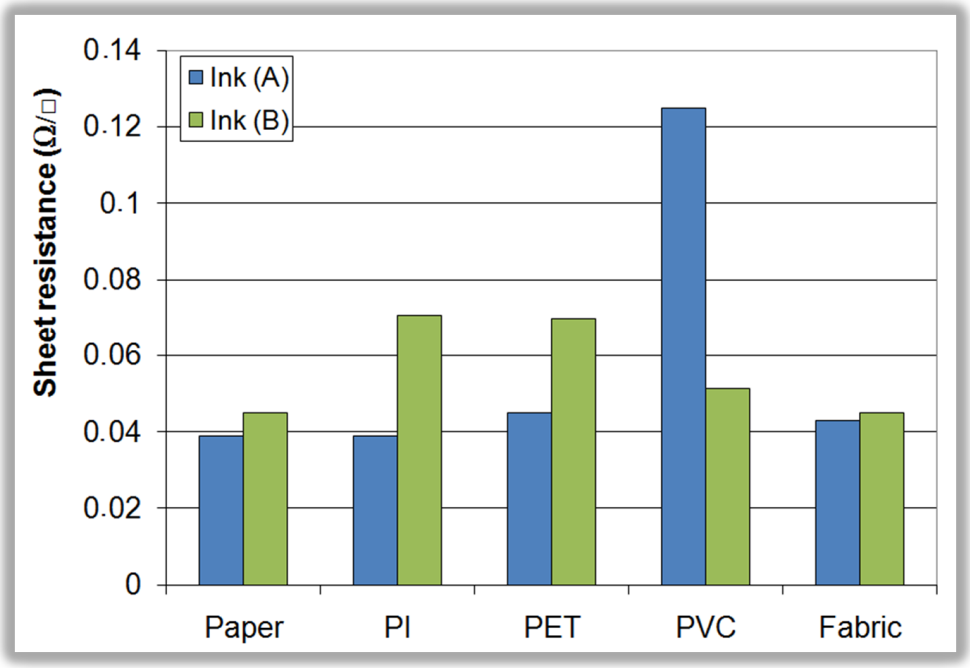

Figure 5.3. Sheet resistance of the conductive patterns with two different inks on different substrate materials [P2].

On fabric and paper substrates, the ink (including the silver particles) penetrates the substrate (see Figs. 4.7 and 4.8). This increases the amount of ink which is transferred to these substrates and may thus decrease the resistance of the printed film. However, the absorption causes large variations in the thickness of the films. The films are rather thick but this has no major effect on the average sheet resistances of the conductive patterns on these substrates compared with the other samples (see Fig. 4.6 and Fig. 5.3). This is assumed to be due to the poorer film quality on paper and fabric substrates [P2; Hick_80].

The effect of curing conditions on the electrical performance of the printed film is discussed in Section 5.2.3 and also in publication [P2]. Fig. 5.4 presents the changes in sheet resistance as a function of curing temperature for inks (A) and (B) on paper substrate.

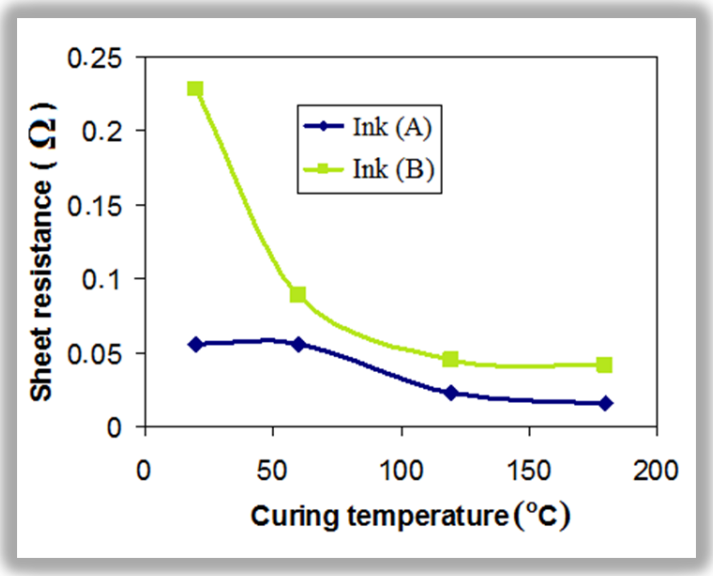

Figure 5.4. Effect of curing temperature on the sheet resistance of ink (A) and ink (B). Substrate material is paper [P2].

As can be seen, sheet resistance decreases up to a temperature of 120 ˚C and saturates at temperatures higher than this. The figure shows that the change in sheet resistance of ink (A) is less than that of ink (B). The main reason for the divergence of the chart lines is the different evaporation rates of the solvents in the low temperature area. The amount of evaporative solvents also affects the resistance change [P2].

The sheet resistances of the conductive patterns cured at 120 ˚C and 180 ˚C for different curing times are presented in Fig. 5.5 [P2].

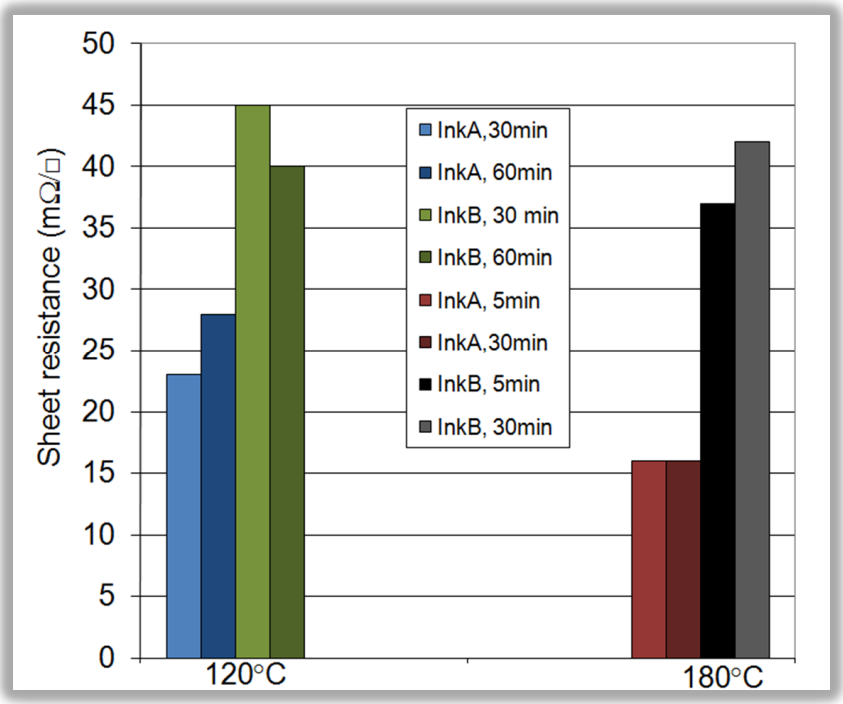

Figure 5.5. Sheet resistance of the samples printed with ink (A) and ink (B) at different curing temperatures and times. Substrate material is paper [P2].

No clear relationship between curing time and resistance was found. The sheet resistance remained nearly the same when ink (A) was cured at 180 ˚C for 5 minutes and for 30 minutes. The difference in sheet resistance was also very small when cured at 120 ˚C for 30 minutes and for 60 minutes. Similarly, only a small change was found with ink (B). These small changes lie within the error margin [P2].

The solvents evaporate effectively at about 120 ˚C and the silver particles come closer to each other. For this reason the curing temperature becomes a very important parameter while, on the other hand, the curing time seems to be less essential [P2].

In publication [P7] the DC resistance of films printed by pad printing with ink "A" and ink "B" was measured at two different points on printed prototype tags. The measurement results are presented in Table 5.3. There was no significant difference between the thickness of films printed with ink "A" and ink "B" (Table 4.3). Thus, the higher resistance of ink "B" is assumed to be due to the lower silver content. In addition, the particles in ink "A" are more uniformly distributed. Particle size and particle size distribution do not differ between the inks. With both inks the printed film is more uniform on PET than on paper, though still irregular. Microscopic examination even revealed pinholes in the printed conductive films [P7].

Table 5.3. The resistance measurement results for the different prototype tags [P7].

Sample	**Curing temperature (°C) and time (min)**	**1.Resistance (Ω)**	**2.Resistance (Ω)**
1. Ink "A" on Paper, 3 print presses	120, 15	0.9	0.4
2. Ink "A" on PET, 3 print presses	120, 15	0.7	0.3
3. Ink "A" on PET, 3 print presses	Room temperature	4.2	2.3
4. Ink "B" on Paper, 3 print presses	100, 10	1.3	0.7
5. Ink "B" on PET, 3 print presses	100, 10	1.7	0.7
6. Ink "A" on Paper, 5 print presses	120, 15	0.9	0.4
7. Ink "A" on PET, 5 print presses	120, 15	0.5	0.3
9. Ink "A" on soft drink bottle , 5 print presses, printed in horizontal position*	50, 20	1.6	1.2
10. Ink "A" on soft drink bottle , 5 print presses, printed in vertical position*	50, 20	1.6	0.6
11. Ink "A" on cardboard reel , 5 print presses, printed in vertical position*	120, 15	0.5	0.3

* "Horizontal position" means that the tag's length is placed in a direction perpendicular to the cylindrical object's axis. "Vertical position" means that the tag's length is placed parallel to the direction of the cylindrical object's axis.

Samples 3, 9 and 10 have higher resistance than the other samples. These samples were cured at lower temperatures and the higher resistance is assumed to be caused by the residues in the printed film [P7].

5.3.2 Electrical performance of PTF structures as a function of frequency

In transmission lines, couplers, circulators and passive RF-devices in general, the conductivity of the ink is related to the insertion loss (*IL*). In article [P6] performance of copper and silver ink micro strip lines (MSL) on FR-4 was evaluated by insertion loss per unit length (dB/cm). In the absence of coupling and discontinuities in the line, which would result to additional radiation loss, insertion loss is entirely due to dielectric and conductor losses. The losses were investigated by simulations and measurements at frequencies from 50 MHz to 5 GHz [P6; Denl_80].

HP8722D vector network analyzer (VNA) was used to extract the scattering matrix of the line and the insertion loss was determined from this data. To calculate the insertion loss from the measured scattering parameters (S parameters) the following equation was derived in publication [P6]

$$IL_{\mathrm{dB}} = -10\log_{10}\frac{\left|S_{21}\right|^2}{(1-\left|S_{11}\right|^2)(1-\left|S_{22}\right|^2)} \tag{5-29}$$

where IL_{dB} is the insertion loss of the transmission line in decibels, S_{21} is transmission coefficient from port 1 to port 2 (the amplitude of the reflected voltage wave from port 2, relative to the amplitude of the voltage wave incident on port 1, while the incident wave on port 2 is set to zero), S_{11} is the reflection coefficient of port 1 (the amplitude of the reflected voltage wave from port 1, relative to the amplitude of the voltage wave incident on port 1, while the incident wave on port 2 is set to zero) and S_{22} is the reflection coefficient of port 2 (similarly to S_{11} and port 1). The minus sign in Eq. (5-29) is added to obtain positive values. Insertion loss per unit length can be found from this by scaling the obtained result with the physical line length [P6; Will_03].

IL simulation for the MSLs were conducted with tan(δ) = 0.02 as constant approximation of the loss tangent of FR-4 laminate and, for comparison, with an approximation, where tan(δ) = 0.016 at 100 MHz and increases directly proportional to the frequency, to tan(δ) = 0.024 at 5 GHz. This approximate model was created according to the frequency dependent results for loss tangent of FR-4 in article [Djor_01]. FR-4 laminate thickness of 1.5 mm was used in simulations [P6].

Measured and simulated results for insertion loss of screen printed line with screen-printed ground plane on FR-4 substrate are presented in Fig. 5.6. Ink (B) was used as the conductive medium in the printed samples. The thickness of the printed film used in

simulations was set to measured mean value of 14.6 µm, but the thickness variations in the film may cause difference between simulated and measured results in case of printed samples [P6].

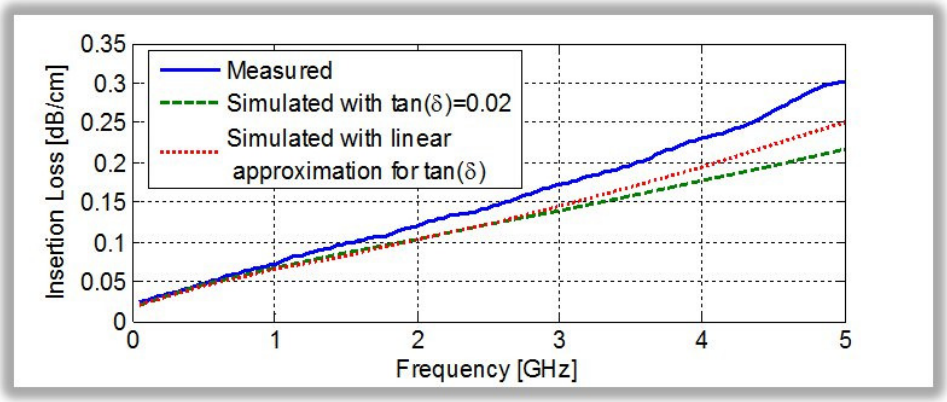

Figure 5.6. Insertion loss of the screen printed line [P6].

Based on the results presented for copper MSL in publication [P9] it is concluded that the substrate model in the simulations is sufficiently accurate to study the insertion losses of the lines. At frequencies below 2 GHz, both approximations agreed very well with the measurement result (see Fig. 6 in P9). In Fig. 5.6 increase in insertion loss of the screen printed line at highest frequencies is not predicted by the approximations for loss tangent. Thus there is an additional loss source, which is not included in the simulation model. This additional loss begins to occur after 1 GHz. Possible physical reasons for this include non-idealities in the connections to SMA connectors and imperfections in fabrication resulting to lower effective conductivity of the ink. In the conductive ink, the polyester resin surrounding the silver flakes is a dielectric, and this way it also affects the propagation of the signal. Still, the amount of polyester resin in the ink is relatively small. This suggests rather minor effect [P6].

The measured insertion loss of screen printed MSL compared with etched copper MSL line with copper ground plane on an FR-4 substrate are shown in Fig. 5.7. Thickness of the copper layer is 35 µm. Two different copper MSLs were fabricated, one with solder mask coating and one without it [P6].

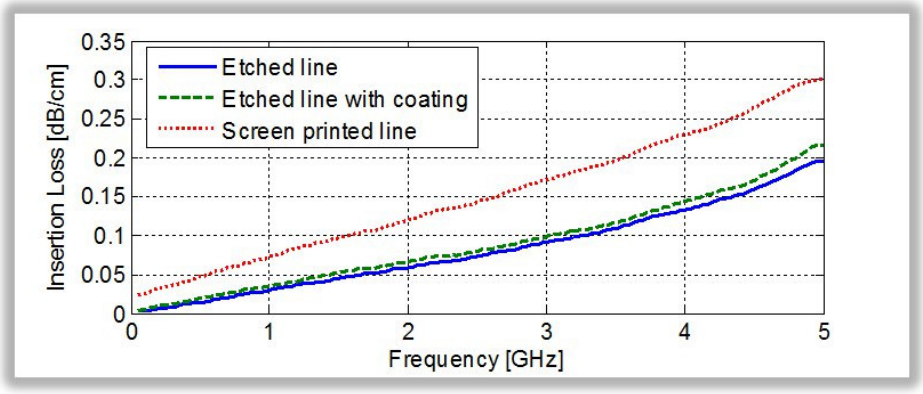

Figure 5.7. Measured insertion losses of the screen printed MSL compared with the etched copper MSLs [P6].

Firstly, from Fig. 5.7 it is seen that the effect of the protective coating does not significantly increase the losses of the line. This is to be expected since the coating material has approximately the same loss tangent as the substrate, though the thickness of the coating layer is very thin compared to that of the substrate. Therefore the contribution of the field distribution inside the substrate remains dominant. Secondly, due to the lower conductivity of the silver ink, the screen printed line has greater insertion loss than the etched lines. The insertion loss of the screen printed line is at maximum 0.1 dB/cm higher than the insertion loss of the etched line in the studied frequency range. This is low enough for many RF-circuit implementations. Maximum insertion loss occurs at the highest end of the frequency band and the difference between the results decreases towards the lower end of the band [P6].

The effect of gradually lowering the conductivity of the silver ink from the nominal value $\sigma_0 = 1.25$ MS/m down to $\sigma = 0.325\sigma_0$ was studied in the simulations to model possible imperfections in the fabrications process, which in practice might reflect as lower effective conductivity. The effect of lowering the conductivity of the silver ink while using the linear approximation of tan(δ) is illustrated in Fig. 5.8 [P6].

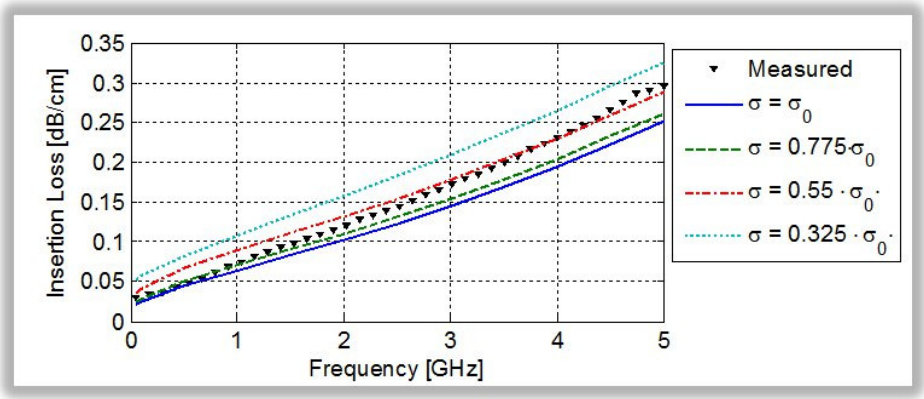

Figure 5.8. Effect of lowering the conductivity of the silver ink on insertion loss [P6].

It can be observed that the curves closest to the measurement result are the 77.5 % and 55 % curves. According to this it is concluded that the fabricated lines may have about 25 % lower conductivity than expected (according to the manufacturer's data sheet). However, even though the 55 % curve would fit the measurement data better at high frequencies, it is not considered that such a great impairment is caused by the non-uniform distribution of the silver ink. In addition, it is seen that the 55 % and 32.5 % curves do not agree as well with the measurements at lowest frequencies as do the other curves. This also favours the proposition of higher than 77.5 % realized conductivity since the effect of other measurement uncertainties due to parasitic effects are expected to grow with frequency. In conclusion, the effective conductivity of the printed film is assumed to be about 0.9 MS/m instead of 1.25 MS/m cited in the ink datasheet [P6].

The effect of conductivity and different conductor materials (silver inks and copper) on losses is also examined in publication [P4]. The impedance of an RFID tag antenna manufactured by screen printing, gravure printing and etching was simulated. Ink conductivity of 4 MS/m was used in gravure-printed tag simulations and 1.25 MS/m in screen printed tag simulations (according to ink manufacturers). Copper conductivity of 58 MS/m was used in etched tags. The substrate of the tags used in simulations was PET foil with loss tangent of 0.002 and relative permittivity of 3. The thickness of the substrate in etched tags and in printed tags was 50 µm and 75 µm respectively (according to materials of prototype tags in article [P4]). Printed film thickness of 3.8 µm with gravure printing and 21.5 µm with screen printing (measured average thicknesses, see Table 4.2) were used. Copper film thickness was set to 20 µm, according to the manufacturer's data [P4].

For the gravure-printed tag, two simulations were performed: "nominal" and "realized". The former term refers to nominal design and the latter to a simulation where the effect of the non-uniform distribution of the conductive ink is taken into account. As Fig. 5.9 illustrates, coverage of the ink is not perfect in the narrow part of the gravure printed antenna [P4].

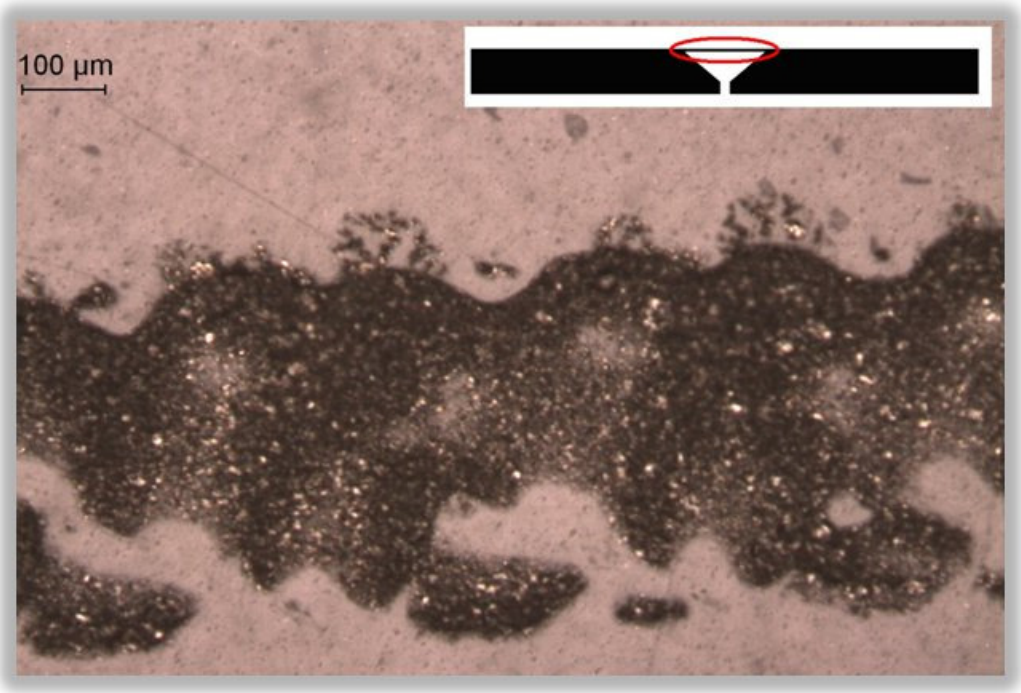

Figure 5.9. Narrow conductive line in tag antenna, printed with gravure printing [P4].

In practice, the non-uniform distribution of the ink becomes apparent when the printed layer is thin, as in the case of the gravure-printed tag. This effect is particularly evident in narrow traces, where the current density is high, such as in the matching loop of the manufactured tag (Fig. 5.9). The effect of the non-ideal print quality in this part of the antenna was modelled by reducing the nominal trace width by 30 % to account for the effect of the ragged edge of the actual printed conductor. Simulated antenna resistances (real part of the antenna input impedance) for different tag antennas are shown in Fig. 5.10.

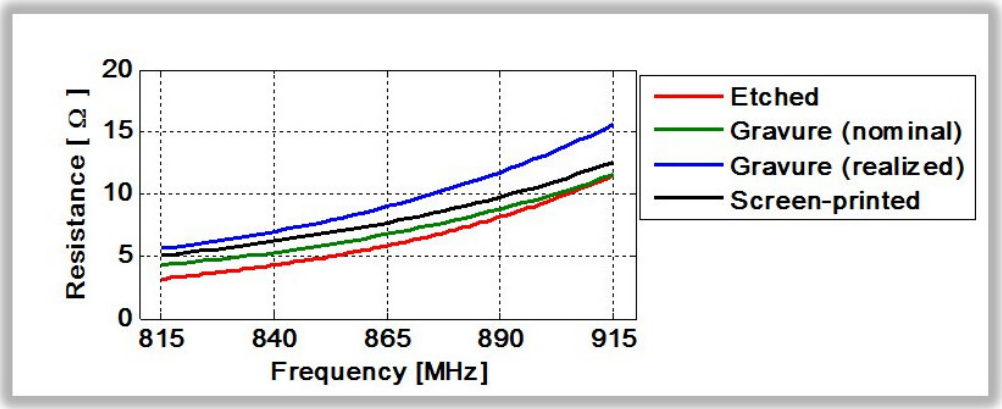

Figure 5.10. Simulated antenna resistances [P4].

Simulation results in Fig. 5.10 predict that the resistances of the tag antennas studied remain within 5 Ω of each other. The skin depth of the ink used in gravure printing (ink "A") is 8.6 µm at 866 MHz. This means that the printed film thickness (3.8 µm) is less than half of the penetration depth, which affects the performance of the gravure printed

film by increasing the ohmic losses. The penetration depth in screen printable ink (ink (B)) is 15 µm at 866 MHz, which means that a thicker film is required when screen printing is used instead of gravure printing. The penetration depth in copper is 2.2 µm at 866 MHz and the 20 µm copper film is more than nine times the penetration depth [P4].

The attenuation of the current density as a function of penetration depth can be solved using Eq. (5-20). The current density decreases by approximately 63 % of its initial value at the surface at one penetration depth and to 86 % and 95 % at two and three penetration depths, respectively. Therefore, in terms of current packing, using a much thicker conducting layer than three penetration depths would be of little use since only 5 % of the total current would penetrate beyond the three penetration depths in the conductor. It can be assumed, therefore, that in copper the current flow is not adversely affected by the structure and the ohmic losses remain low [P4; P5].

The effect of the printed film thickness on the ohmic losses is also discussed in publication [P5]. Here the loss resistance of the tag antennas was investigated for three different film thickness 13.9 µm, 21.5 µm and 50.5 µm, according to the manufactured prototypes (Table 4.2).

The simulations were first performed for silver ink antennas (σ = 1.25 MS/m) in free space, to isolate the loss resistance due to the conductor. The simulation was then repeated for the conductive films (antennas) on substrate in order to take into account the losses arising from the substrate material. The substrate used in simulations was 75 µm PET film with loss tangent of 0.002 and relative permittivity of 3. The simulation results are presented in Fig. 5.11 [P5].

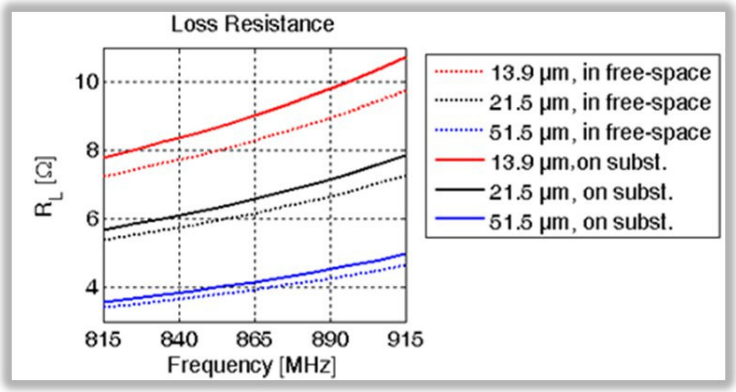

Figure 5.11 The loss resistance of prototype tags in publication [P5].

The results predict that the loss resistance increases for each film thickness studied as a function of frequency. The difference between the conductor loss resistance of the thinnest (13.9 µm) and thickest (51.5 µm) conducting layers is approximately 5 Ω. In addition, for each studied conductor thickness, adding the substrate increases the loss resistance due to dielectric loss, as was expected. The relative change of the loss re-

sistance caused by the added substrate seems to remain fairly constant at 9 % for the studied conductor thicknesses. Because of this, the effect of the substrate increases as the thickness of the conductive layer decreases. This suggests that, in addition to increasing conductor losses, the role of the dielectric losses also increases in structures with thin conductive films [P5; P7].

5.4 The effect of printing process and materials on the performance of passive UHF RFID tags

The foregoing sections (5.1 - 5.3) discussed the characteristics and the electrical performance of the materials used in printed RFID tags. The present section now examines how such materials affect the performance of passive UHF RFID tags. Input impedance of a tag antenna is a decisive factor in tag antenna design since it has to be tuned according to IC impedance in order to maximize power transfer. The input impedance of the antenna depends on the geometry, the conductor material and the substrate material of the antenna, as well as on all other proximate materials. This poses challenges for printed RFID tag fabrication since these issues need to be addressed early in the tag antenna design process in order to achieve prospective antenna performance at the desired frequency [P4].

The radiation characteristics of an antenna depend on its current distribution. The current distribution then depends on the electromagnetic properties of the surrounding media. For example, good conductors near the antenna impair radiation efficiency. When attaching tags to different identified objects, these matters need careful attention. In addition, when the tags are remotely read, the reflections from the environment cause multipath propagation. Since the focus in this study is on the effects of the antennas' conductor material and substrate on the tag operation, there is no further discussion of proximate materials and the environment [P1; P7; Youn_00; Kata_06; Ukko_06].

Tag materials are responsible for three effects: they affect losses, change the feed impedance, and alter the radiation characteristics of the tag antenna. These effects are dependent on the conductor material (i.e., conductivity, thickness, surface roughness) as well as on the substrate material (i.e., permittivity, loss tangent, thickness) [P4; P5; P7; P9; Schm_02].

Since the substrates have low relative permittivity and they are thin sheets, their effect on the radiation pattern is assumed to be minor and it is not evaluated (except in Section 6, (case studies)). Similarly, the conductor material in the antennas is also assumed to cause only a minor effect on the radiation pattern. The main focus of interest in the present section, therefore, is not these minor effects but rather the effect of the conductor

and substrate material properties on the losses and the impedance matching of the tags [P1; P7; Youn_00; Kata_06; Ukko_06].

With regard to conductor thickness, the current in the antenna that creates the radiation also causes ohmic losses. The ohmic losses limit the efficiency of the antenna, causing some of the input power to be lost as heat. One way to reduce ohmic losses is to use thicker conductive film for the antenna, as discussed in Section 5.2.2. The thicker film has less resistance, leading to smaller ohmic losses but the thickness of the film also transforms the feed impedance and has an effect on the radiating behaviour of the antenna. In publication [P5] the effect of the thickness on tag performance was studied by means of simulations and measurements. The same simulation parameters for the materials were also used in loss resistance simulations (Fig. 5.11). The measured power on tag and simulated power reflection coefficients (PRC) of tags on PET substrate (75 µm) with different conductive film thicknesses are presented as a function of frequency in Fig. 5.12. The PRC is the power reflection coefficient between the tag antenna and the IC and it describes the quality of the complex conjugate match (see Eq. (3-19)). The minimum power level at which the IC is activated, and thus the power on tag in 5.12, is heavily dependent on the PRC [P5, Schm_02].

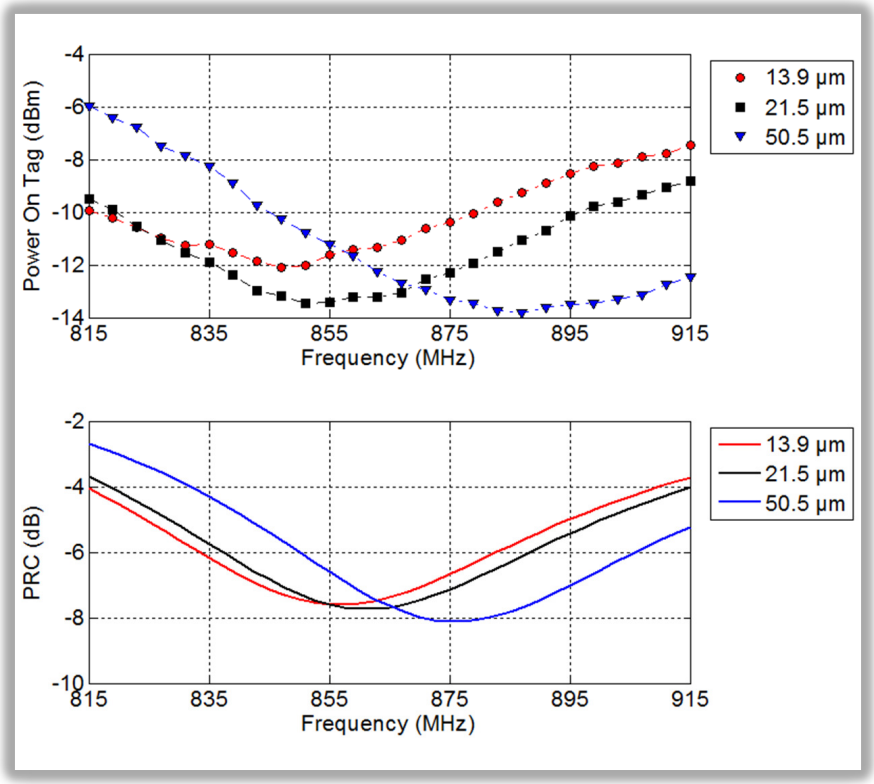

Figure 5.12. Measured power on tag and simulated power reflection coefficient (PRC) with different conductor thickness as a function of frequency [P5].

The power on tag and PRC at the frequency of the best impedance matching both increase slightly as the conductive film thickness decreases as a result of higher ohmic losses (see the minimum values in Fig. 5.12). A decrease in conductor thickness also shifts the operating frequency downwards. This is due to the thickness of the film that affects the antenna input impedance, but since it depends on antenna geometry as well as on the IC's input impedance, no general conclusions can be made about the direction of this shift. Nonetheless, it can be observed that the frequency shift percentage change in the conductor thickness is greater between 50.5 µm and 21.5 µm than between 21.5 µm and 13.9 µm. This could be due to the nonlinear relationship between the loss resistance of the antenna and conductor thickness suggested in Eq. (5-27). It can be seen that the shape of the measured power on tag curves matches that of the simulated PRCs. This is explained by the fact that the impedance of a resonant antenna has strong frequency dependency, whereas the gain of these antennas exhibits weaker frequency dependency within the frequencies studied [P5].

The measured backscattered signal power of the tags as a function of transmitted power is shown in Fig. 5.13. The threshold power for each tag can also be seen in Fig. 5.13 as the value at which the curves begin [P5].

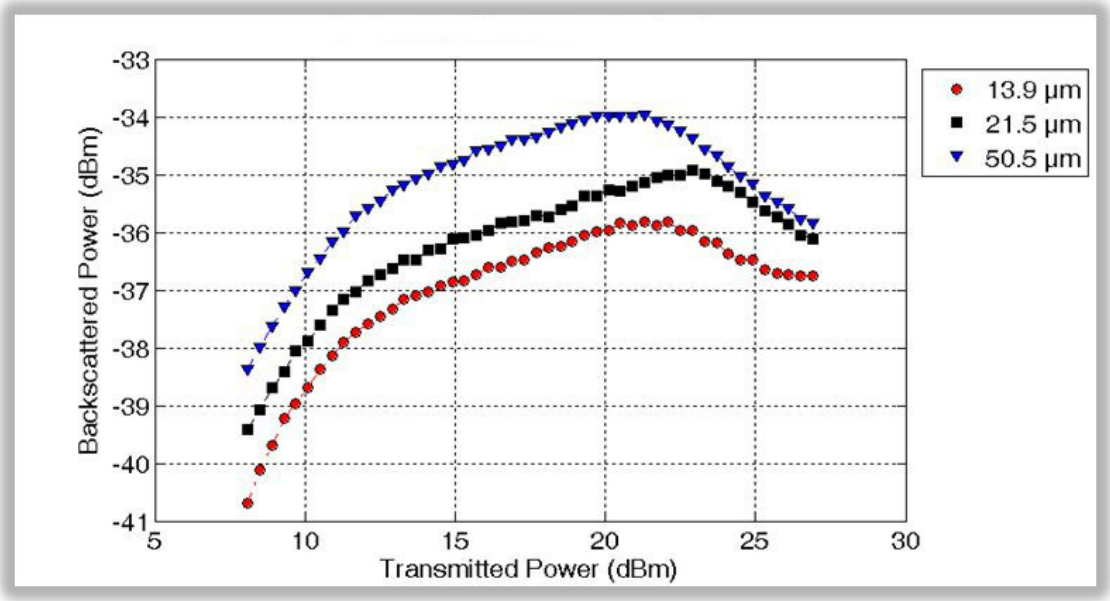

Figure 5.13. Measured backscattered signal power at 866 MHz with different conductor thicknesses as a function of the transmitted power [P5].

According to the measurement results shown in Fig. 5.13, the thickest tag backscatters the strongest signal, regardless of the transmitted power, and the thinnest tag backscatters the weakest response. This agrees with the theory, as the backscattered signal is proportional to the square of the tag antenna gain (see Eq. (3-21)). Gain, in turn, is a product of the directivity and the radiation efficiency of the antenna (see Eq. (3-7)). Since at a given frequency the directivity is completely determined by the antenna struc-

ture, the backscattered signal power is affected by the radiation efficiency which increases as the thickness of the printed film increases due to decreasing conductor losses (see Figs. 5.11 and 5.14). The observed difference between the measured backscattered power curves as a function of the transmitted power is caused by the power dependent input impedance and, consequently, the power dependent modulation efficiency of the tag; the conductor loss itself is not power dependent. In terms of the system, the difference in the backscattered signal powers of the tags is rather modest because, as discussed in Chapter 3, the passive RFID systems are typically limited by the forward link. Though, it should be remembered that due to increasing sensitivity of the ICs also the reverse link might play more important role in the future [P5].

At transmitted powers below 20 dBm the difference between the backscattered signal power from the 13.9 µm tag and 50.5 µm tag remains fairly constant and is therefore expected to be caused by the difference in radiation efficiency rather than a change in the modulation efficiency. The simulated frequency behaviour of the radiation efficiency of the manufactured prototype tags is illustrated in Fig. 5.14. The same simulation parameters used for the materials were also used in the loss resistance simulations (Fig. 5.11).

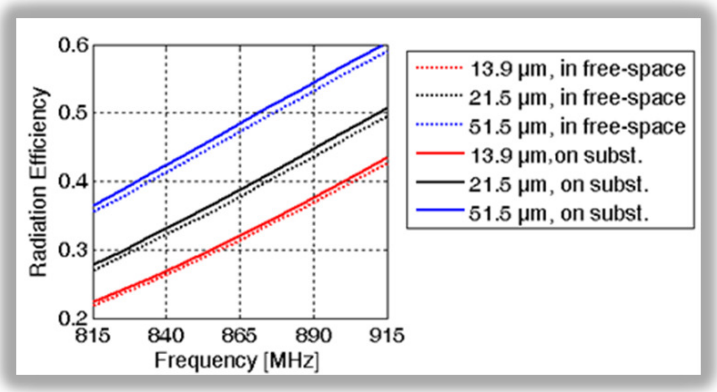

Figure 5.14. Simulated Radiation Efficiencies with different conductor thickness [P5].

For all conductor thicknesses, regardless of whether or not the tag is placed on the substrate, the simulated radiation efficiencies increase as a function of frequency as the antennas become electrically larger. This monotonic behaviour over the frequencies studied is expected since even at the highest frequency, 915 MHz, the antenna length of 97 mm translates to around 0.3λ. The antenna is, therefore, still electrically short enough for current cancellation not to occur in the antenna structure. For electrically small antennas, on the other hand, the achievable radiation efficiency is proportional to the antenna size. Recalling the expression for the radiation efficiency in terms of loss- and radiation resistance (Eq. (3-4)), it is found that the radiation efficiency increases if the radiation resistance increases faster as a function of frequency than the loss resistance [P5; Schm_02].

The role of the antenna efficiency of the tag in a passive RFID system is also discussed in publication [Side_07]. A dipole-type RFID tag antenna was modelled and the effect of decreasing the conductor conductivity from a perfect electrical conductor was investigated. The effect on the ohmic losses, the impedance mismatch and, thereby, the antenna efficiency was studied. The conductor was simulated in a vacuum. It was found that if it is possible to print the tag antenna used in simulations with sheet resistances below 100 mΩ/□, the decrease in efficiency due to an impedance mismatch is negligible. Ohmic losses were found to have a much more adverse effect on antenna efficiency. Sheet resistance of 100 mΩ/□ gave a mismatch efficiency of 99 %, but the conductor efficiency was only 80 % [Side_07].

The effect of the conductor material on the ohmic losses, as well as on the impedance matching, was also examined in publication [P4] by comparing the performance of screen printed and gravure printed silver ink tag antennas and etched copper tag antennas. Since the tag antennas were manufactured with different methods, the thickness and surface structures of the tags are different and consequently there are more variables than the conductor material conductivity. In addition, minor modifications were made to the tag geometry of the printed tag compared to the copper tag. Since realistic parameters are used in the simulations and the measurements are performed from actual prototypes, the results in article [P4] provide a realistic view of the performance of the tags manufactured with different methods.

The simulated antenna resistance of the screen printed tag, gravure printed tag and etched tag from publication [P4] is discussed in Section 5.3 (Fig. 5.10) and the resistances of the tag antennas studied were found to remain within 5 Ω of each other. The reactance values for the same tags are shown in Fig. 5.15. The decreased conductivity due to non-ideal print quality of the tag printed with the gravure method (see Fig. 5.9 in Section 5.3) was taken into account by simulating both “nominal” and “realized” tags, as in the resistance simulations [P4].

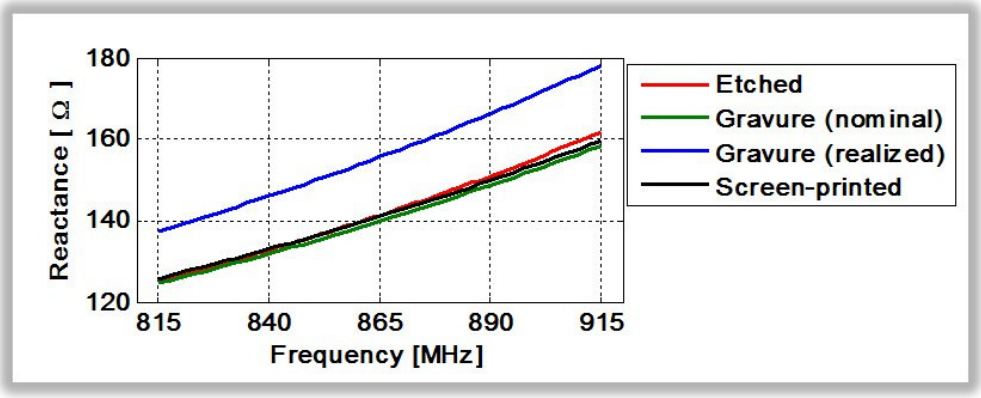

Figure 5.15. Simulated antenna reactance [P4].

The reactance of the realized gravure printed tag displays quite different characteristics because the non-ideal print quality is located on the high current density matching structure. Otherwise the reactance of different designs seems to be very similar across the frequencies studied. According to a simulation in article [P4], ± 3Ω change in chip reactance may shift the operation frequency of the tag some 10 MHz from the nominal case. Similarly, change in antenna reactance is expected to shift the operation frequency if IC impedance is kept constant. This is also seen in Fig. 5.16 which shows the simulated PRCs for the tag antennas [P4].

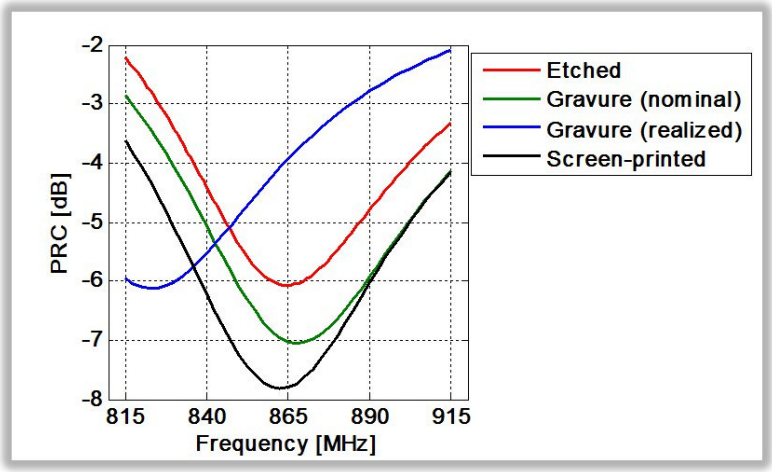

Figure 5.16. PRC's of different antenna models according to the simulated antenna impedances [P4].

From the simulation results it can be seen that the realized gravure tag is tuned at a lower frequency than the other tags, which are reasonably well tuned for operation at 866 MHz (as was intended) [P4].

In addition to simulations, actual prototype tags were manufactured. Ink (B) (see Table 4.1) was used with a screen printed tag and ink "A" (see Table 4.1) with a gravure printed tag. The substrate material was PET and the thickness of the substrate used in the etched and printed tags was 50 µm and 75 µm respectively. Average thickness of the printed film in the gravure printed tag was 3.8 µm and in the screen printed tag, 21.5 µm (Table 4.2). Thickness of the copper film was 20 µm. The power on tag and the backscattered signal power were measured. The measurement results are presented in Figs. 5.17 and 5.18 [P4].

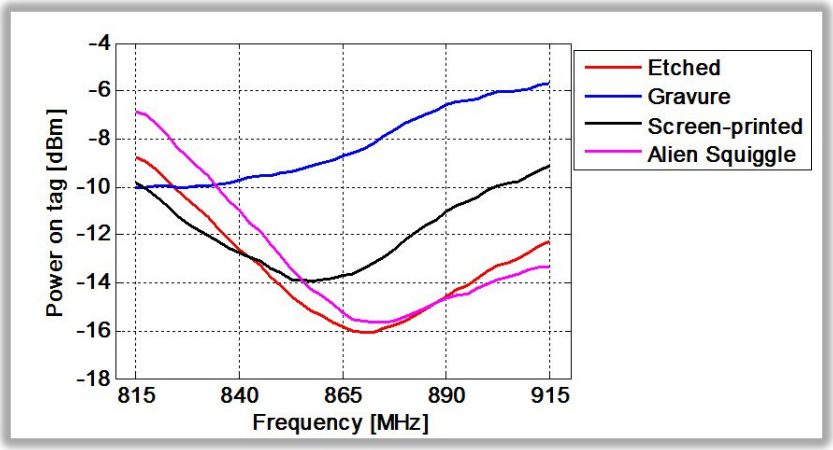

Figure 5.17. Measured power on tag as a function of frequency [P4].

The measured minimum values of the power on tag curves in Fig. 5.17 appear in a different order to the simulated PRCs in Fig. 5.16. This is because in a realistic case conductivity, thickness and surface structure of the conducting film, among other things, affect the radiation efficiency of the tag. These parameters in the fabricated prototype tags differ from the simplified models assumed in the simulations. However, the simulation results can be used to predict fairly accurately the operating frequencies corresponding to the minimum value of power on tag as well as their mutual order: only the measured operation frequency of the screen-printed tag seems to be slightly lower than predicted. This might be due to lower than expected IC reactance, as the simulation results in article [P4] suggest [P4].

The measurement results for backscattered signal power in Fig. 5.18 show that at the threshold power (beginning of the curves), when the IC-chips on the different tags receive approximately equal power, the strength of the responses is almost the same from the etched and screen printed tag as that from the commercial Alien Squiggle tag that was measured as a reference. The response from the gravure-printed tag is about 2 dB weaker [P4].

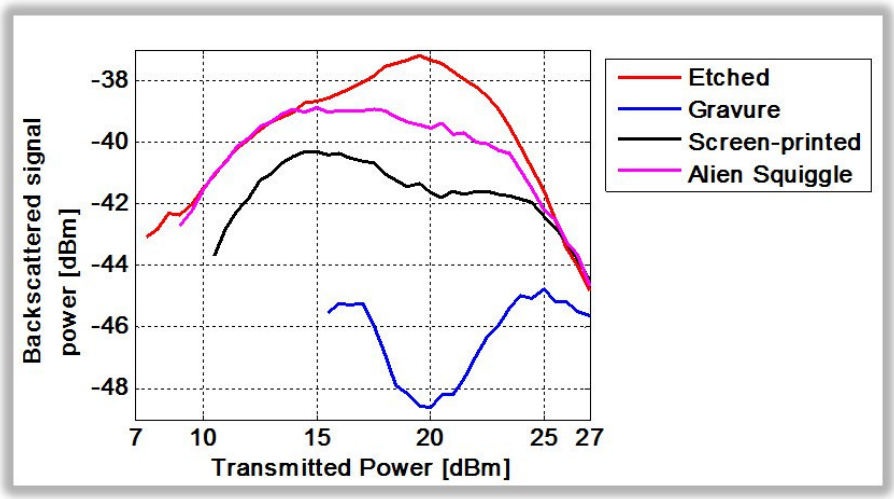

Figure 5.18. Measured backscattered signal power as a function of transmitted power at 866 MHz [P4].

The weaker performance of the tag printed with gravure printing is assumed to be caused by the thinner film and lower print quality. Because of this, ohmic losses increase and antenna impedance changes. The changed antenna impedance affects the operation frequency through the impedance matching. In particular, the poor print quality of the printed film in the narrow conductor in the matching loop is assumed to cause the worst performance because the current density is high in that part of the antenna structure [P4].

In conclusion, the printed tags were tuned at the desired frequency and it was possible to manufacture a printed tag with almost the same geometry as the copper tag; only a minor change was made to optimize the antenna impedance. Thus in terms of tag performance and conductor material, printed tags seem to offer an alternative to copper tags in passive RFID systems [P4; Syed_07; Niki_05; Nils_07; Yang_07]. However, when tags are printed on different substrates, the effect of the substrate on performance should also be taken into account.

In publication [Side_07] losses due to different substrates were simulated. The publication examined thin paper (thickness: 87 µm, relative permittivity ≈ 4 and loss tangent 0.07), plastic foil (thickness 73 µm, relative permittivity ≈ 1.9 and loss tangent 0.031) and thick paper (thickness 600 µm, relative permittivity ≈ 2.2 and loss tangent 0.064). The losses due to these substrates were not considered severe, with the worst case being the thick paper that showed a total radiation efficiency due to substrate of 85 % (with perfect electrical conductor). The losses are quite low, even though the substrates' loss tangents are significantly above zero. The low ohmic losses were mostly due to the low substrate thickness relative to the wavelength. If the substrate had been thicker, but with the same parameters, both the mismatch and losses would have increased. However, if a

specific substrate is considered in the antenna design process, the efficiency due to a mismatch could approximate to 100 % [Side_07].

In publication [P7] the effect of substrate on PTF ink tag performance was evaluated with measurements. Prototype tags were printed with pad printing on different substrates with inks “A” and “B”. Three (3x) and five (5x) printing presses were performed in sample manufacturing. Tags on thin flat substrates and on thicker convex surfaces were analysed. Soft drink bottles and cardboard reels were selected as the convex substrates. The soft drink bottles are made from polyethylene terephthalate and therefore PET foil was selected as one of the substrates. Another substrate is paper, which serves as a comparison to the cardboard reel. The tag sensitivity (power on tag) of the prototypes was measured. Figs. 5.19 and 5.20 present the tag sensitivity measurement results of tags printed on flat substrates with three print presses and five print presses respectively [P7].

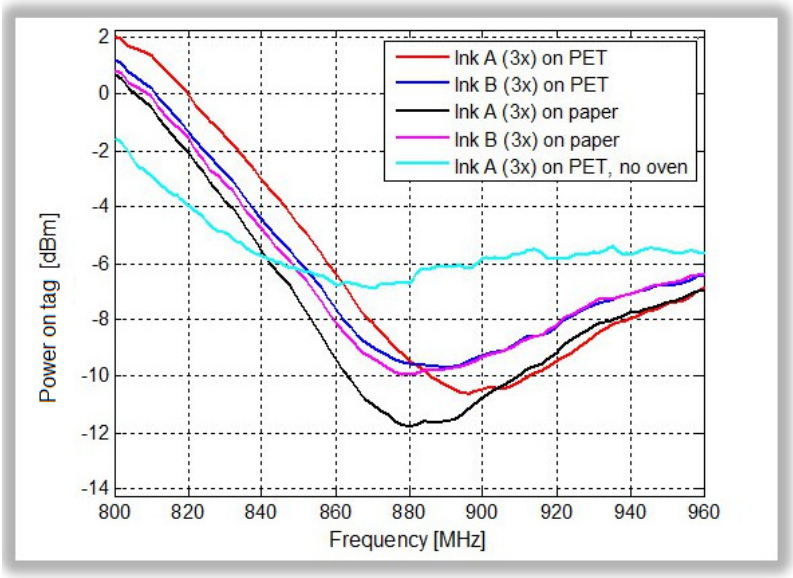

Figure 5.19 Tag sensitivity of tags printed 3x on flat substrates (Ink A is ink “A” in Table 4.1 and similarly with ink B) [P7].

Since the substrates are thin sheets, the effect of their electrical properties on the tag is assumed to be minor. Instead, it is seen from 5.19 that tags printed with ink “A” need less power to activate. This is due to lower ohmic losses (see Table 4.1 and Table 5.3). The high resistance of a sample with no oven curing was found in Section 5.3 (see Fig. 5.4 and Table 5.3) and this can be seen in Fig. 5.19 as weaker tag performance. The ohmic losses of the tag, which was not cured in the oven, increased the required power from the reader to activate the tag [P7].

Fig. 5.20 shows that in tags with five print presses, the ohmic losses are less than in the tags with three print presses. This is due to the increased film thickness. The lower ohmic losses can be seen as decreased power on tag values (see Figs. 5.19 - 5.20) [P7].

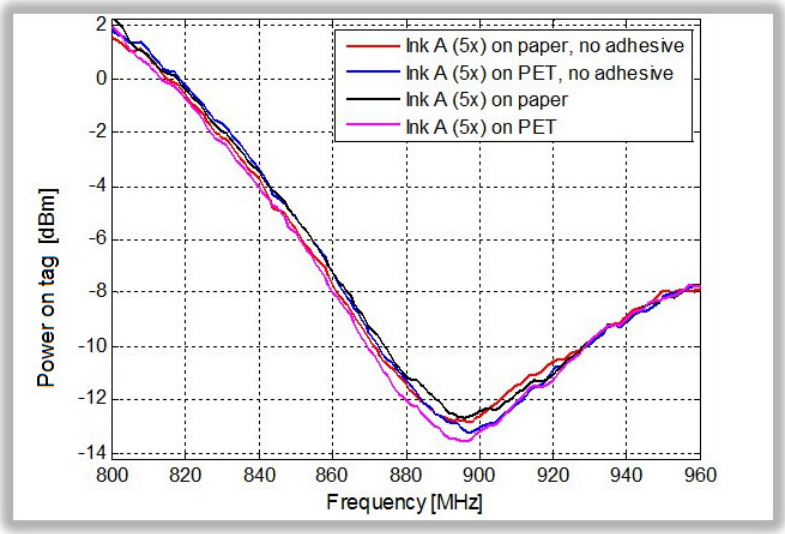

Figure 5.20 Tag sensitivity of tags printed 5x on flat substrates (Ink A is ink "A" in Table 4.1) [P7].

The sensitivity levels of the tags on convex surfaces are presented in Fig. 5.21. The term "vertical" in the legend in Fig. 5.21 means that the longest dimension of the tag runs parallel to the axis of the cylindrical object. "Horizontal" means that the tag's longest dimension is perpendicular to the axis of the cylindrical object.

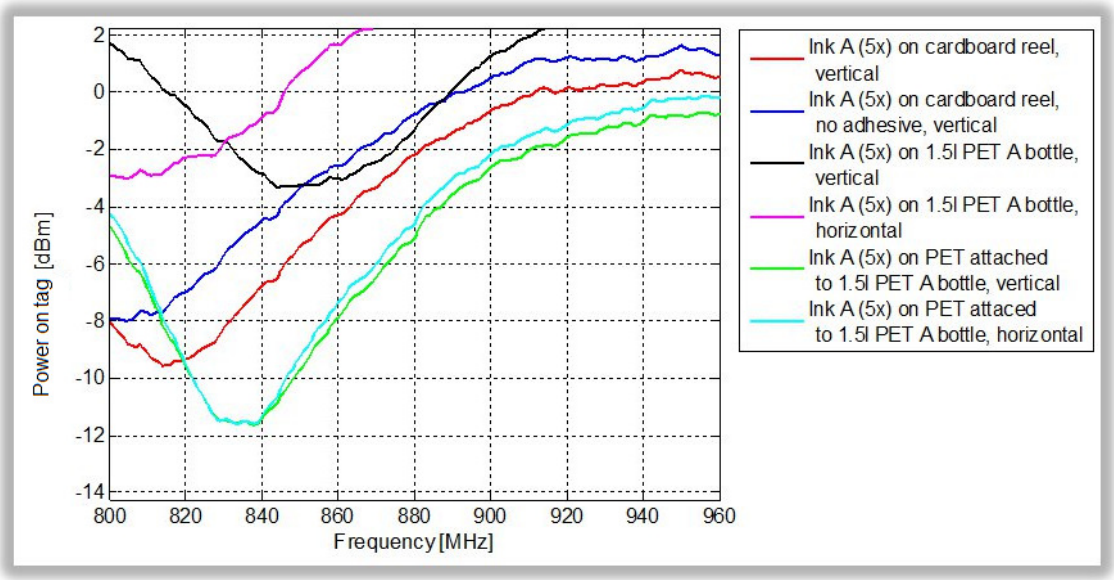

Figure 5.21 Tag sensitivity of tags on convex surfaces (Ink A is ink "A" in Table 4.1) [P7].

On the convex surfaces, the thickness of the substrate is markedly higher than in the case of flat substrates. This affects the impedance of the antenna structure and shifts the frequency where the impedance matching is optimal. A thicker substrate also increases dielectric losses. In addition, as was noted in Section 4.2.2.2 (see Table 4.3), there were large variations in printed film thickness, particularly on convex surfaces. The ink irreg-

ularities and changes in printed film thickness also alter the impedance of the antenna and affect the frequency of the optimal impedance matching as well as the conductor losses. The increase in dielectric and conductor losses leads to decreases in the radiation efficiency of the tag. This can be seen as increased power required in activating the tag. The increased dielectric losses due to the bottle "substrate" are evident when comparing the tag (printed 5x on PET) when it is attached to a bottle (Fig. 5.21) and when it is not (Fig. 5.20). The frequency of optimal impedance matching also shifted to lower frequency when the tag (printed 5x on PET) was attached to a bottle [P7].

The effect of the curing temperature that was already seen in Fig. 5.19 in the case of a tag on flat PET foil can also be found in the samples printed on convex surfaces. Tags which were printed directly onto a bottle required more power from the transmitter to activate them than the planar tags. This is due to the low curing temperature (50 °C) of the samples printed directly onto the bottle, which does not tolerate high temperatures. It is seen that the power on tag is higher than with the tag that is printed on a separate substrate, cured according to the manufacturer's recommendations (120 °C) and placed on the bottle (see Fig. 5.21) [P7].

The tag that was printed directly onto the cardboard reel was cured in an oven. The power on tag at optimal impedance matching was significantly lower compared with the samples that were cured at 50 °C (samples printed on a bottle) because of lower conductor losses. However, compared with tags on thinner substrates, a thicker cardboard substrate increases dielectric losses [P7].

Cardboard and paper both had similar measured relative permittivity (difference 0.85), but the thicker cardboard shifted the optimal operation of the tag to a lower frequency. The effect of the different relative permittivity of the substrate with the same thickness was not apparent from the results because there were too many variables (such as the printed film imperfections). Thus a simulation was performed to evaluate the role of the difference in relative permittivity. Fig. 5.22 shows the power transmission coefficient (1-PRC) between the tag antenna and the IC on the substrates with relative permittivity from 1 to 10 [P7].

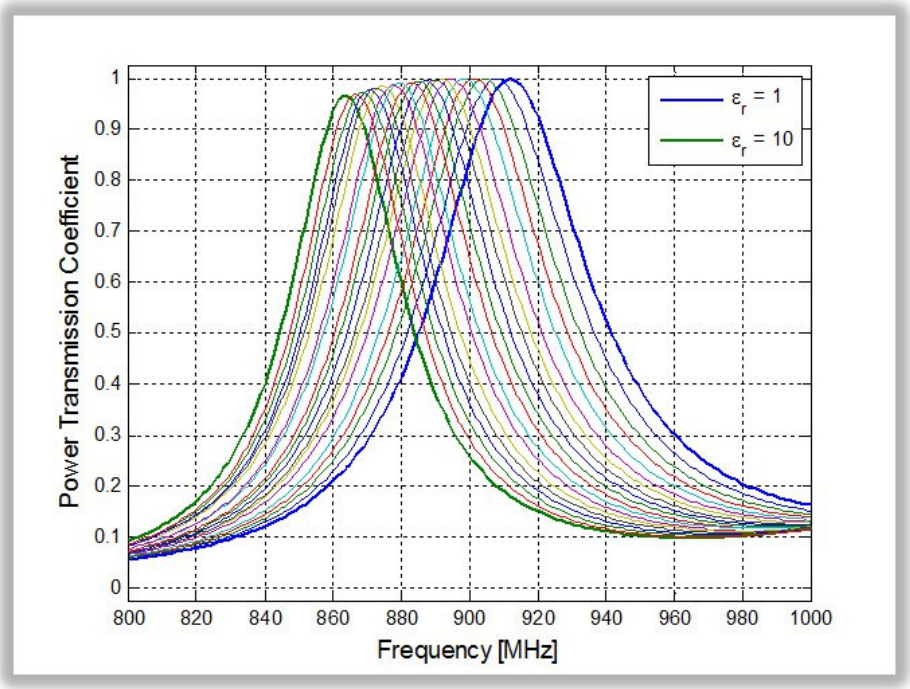

Figure 5.22. The simulated power transmission coefficient between the tag antenna and the IC on substrate with relative permittivity varying from 1 to 10 [P7].

The increase in relative permittivity lowers the optimal operation frequency of the tag. By comparing the tag on the cardboard reel and the tag on the paper, it can be seen that the tag on the cardboard reel operates at lower frequencies. This is assumed to be due mainly to the large thickness of cardboard (3 mm), but the higher relative permittivity of cardboard may also shift the optimum operation frequency downwards. However, the effect on tag operation of the small differences in the relative permittivity of the tested substrates is considered small. The differences in the thickness of the substrates, on the other hand, play a more important role. When comparing a tag on PET when it is placed on a soft drink bottle with a tag on PET in free air, the optimal operating frequency moves downwards from about 895 MHz to 835 MHz (60 MHz) (see Figs. 5.20 and 5.21). If the relative permittivity of a thin substrate (thickness 75 µm) is changed from 1 to 3 (relative permittivity of the substrates in article [P7] are from 1.6 to 2.6), while other parameters remain constant, the operational frequency only moves from about 910 MHz down to 890 MHz (20 MHz) (see Fig. 5.22) [P7].

On the basis of the simulations and measurements on thin substrates, print quality has a greater effect on tag operation than slight changes in the relative permittivity of the substrate. Different materials such as fabrics, papers or plastics have a typical relative permittivity ranging from 1 to 4 and they are widely used as thin sheets in electronic applications. This means that in such cases the indirect effect of the substrate material on tag properties, through conductor morphology and process limitation (like curing), is more significant. When tags are printed on different objects, it is very important to take into account the fact that the thickness of the substrate, as well as the large change in relative

permittivity, has a significant effect on tag operation. In addition, the tags which are directly printed on 3D objects may be slightly distorted in the printing process. This is further discussed in a case study in Section 6.2 [P7].

In summary, it can be concluded that, as well as tag geometry, tag materials are essential factors in performance because the impedance of the tag antenna is affected by them. Both radiation efficiency and impedance matching are affected by the materials. The properties of the conductive medium (ink) have a major role in achieving low ohmic losses and, thereby, adequate tag antenna performance. It is also important to consider the composition of the ink. In addition, the substrate material affects the losses through printed film morphology and dielectric losses. The electrical properties of the substrate affect tag functioning and the effect becomes emphasized as the substrate thickness increases. The curing conditions may also be adversely affected by the substrate. Inadequate curing impairs antenna performance [P7].

The effect of the materials and the geometry on impedance matching can be eliminated by good antenna design. Modifications to the tag antenna geometry according to the materials used are normally sufficient to tune the antenna, though additional ohmic losses cannot be totally eliminated by design alone. Nevertheless, when the losses are known, antenna performance can be correctly predicted.

The fabrication process itself can also set limitations on the tag (for example, the size of the tag and conductive film quality). A potential challenge in printing is the maximum film thickness achieved with different printing methods by a single print press. However, it is possible to increase the conductivity of the ink in various ways, such as by decreasing the particle size and adding particle content of the ink. However, this increases tag cost and affects both the process and the mechanical properties of the ink.

Nevertheless, the results obtained in the study support the usage of the printing process as an alternative to etching in the manufacture of RFID tags. This can be advantageous, for example, when the substrate does not tolerate the use of etching chemicals or when tags need to be embedded into products or packages. The printing method has to be selected according to the tag model and materials. The antenna design process ultimately involves a compromise between numerous factors. The most important of these factors are antenna performance, physical dimensions of the tag, price, materials (substrate material, conductor material, materials nearby during the use of the tag) and manufacturing requirements (process limitations) [P4].

In addition to tag materials and manufacturing process, the objects to which the tags will be attached, should be taken into consideration. The objects affect the impedance of the tag and introduce losses. In addition, the radiation pattern may change in the presence of thick dielectric layers, dielectrics whose relative permittivity is large or if the

tag is near conductive media [P1; P7; Ukko_06]. Impedance mismatch can be avoided by proper design if the object is known in advance. However, objects are seldom known in advance and knowledge of their electrical properties is usually inadequate. One solution could be to use a substrate which has relatively large relative permittivity but low loss tangent. This would decrease the dependence of antenna performance on the identified item, but keep the substrate losses within permitted limits. According to publication [Side_07], antennas having wide band properties could potentially also make the RFID tag more robust to dielectric substrates. Further discussion of this issue is excluded from the thesis [P7; Side_07].

6. Applications of printed passive UHF RFID polymer thick film tag antennas – case studies

In the previous chapter, the effect of the printing methods and the novel materials on passive UHF RFID tags was investigated. Although new manufacturing processes and materials may set challenges, they also provide numerous opportunities. Printing enables new ways of embedding electronics into other structures and the development of novel applications. In this chapter these opportunities are discussed through case studies. The first case deals with paper reel identification by tags which are printed on paper. In the second case, the tags are embedded in items by directly printing them on the convex objects. The third case introduces a new application, a wireless and wearable strain sensor whose operation is based on passive UHF RFID technology and the behaviour of the materials used in the prototype RFID tags.

6.1 Printed passive UHF RFID tags in paper reel identification

In the paper industry there is a growing interest in the use of passive UHF RFID technology for the identification of paper reels [Ukko2_06; Numm_10]. In this application the safest location for the tag would be on the core of the paper roll. This means that the tag is read through a thick paper layer. In publication [P1] screen printing was used to fabricate prototype antennas. Four different paper qualities were selected for the antenna substrate and three PTF silver inks were selected as antenna materials. The prototype tags had an EPC Class 1 Gen 1-based microchip with a 96 bit identification code. The prototype antenna was designed to operate at UHF frequencies, especially through paper. The maximum reliable read range (MRRR) of the tag prototypes was measured through paper reams and also in air because in certain cases identification might also be required in air. The MRRR was measured using both linearly and circularly polarized reader antennas. Since the read range measured with a linearly polarized reader antenna is heavily dependent on the antenna orientation, the tag was aligned with the reader antenna polarization plane [P1].

The average MRRR in air was 134 cm when measured with the linearly polarized reader antenna, and 57 cm with the circularly polarized one. The MRRR values of the samples which were measured with the linearly polarized reader antenna are approximately two times larger than the values measured with the circularly polarized reader antenna (see Table 4 in article [P1]). This is due to power loss, which is caused by the polarization mismatch with the circularly polarized reader antenna, although there is additional loss sources involved as well. In theory the read range with circularly polarized reader (ac-

cording to Friis transmission equation) is $1/\sqrt{2}$ times the read range measured with the linearly polarized reader antenna. Additional loss sources may be caused by multipath propagation and the fact that the circularly polarized reader antenna is in practice slightly elliptically polarized. In addition, the wooden holder might not have been exactly in line with the reader antenna all the time, because the holder was on wheels and there were no rails on the floor. MRRR measurements have been made for similar sized copper bow-tie-antennas on FR-4 laminate and aluminum bow-tie-antenna on plastic foil in article [Scha_05]. MRRR for the copper tag was 139 cm for the linearly polarized reader antenna and 65 cm for the circularly polarized reader antenna. The same values for the aluminium tag were 89 cm (linear polarization) and 35 cm (circular polarization). Thus the reading performance of silver ink antennas is comparable to that of the copper and aluminum tags [P1; Scha_05].

The length of the bow-tie antenna is approximately the half wavelength of the 915 MHz electromagnetic wave when it propagates through paper [Scha_05]. Bow-tie antennas are relatively broadband and thereby the tested tag antenna also operates satisfactorily in air [Kuma_03]. However, to optimize the performance of the antenna design in air, the geometry of the antenna has to be modified to correspond better with the wavelength of the electromagnetic wave in air [P1].

After measuring MRRR in air, the measurements were performed through paper. One to five reams of copy paper were placed in front of the tag. The thickness of a single ream was 55 mm. The measurement results (average MRRRs) are presented in Fig. 6.1 [P1].

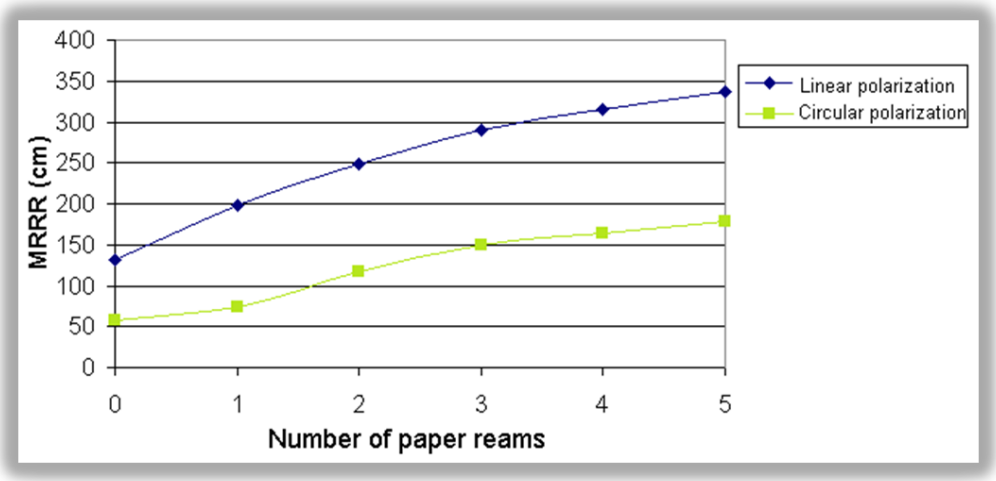

Figure 6.1. The effect of paper reams on MRRR [P1].

Adding paper reams improved the MRRR irrespective of whether a linearly or circularly polarized reader antenna was used. When the reams of paper are placed in front of the tag, the radiation pattern of the bow-tie antenna changes from the form of a typical omnidirectional dipole antenna radiation pattern [Kata_06]. The tag antennas start to direct

the radiation toward the reader (the direction in which paper reams are placed). This is due to the effect of paper as a dielectric material on the radiation pattern. No more than five reams are added because after five reams the wavelength of the 915 MHz electromagnetic waves is reached in paper when ε_r of copy paper is considered to be 3. When the thickness of paper exceeds one wavelength, the main effect of the paper reams is to increase attenuation rather than affect the radiation properties of the tag antenna itself. When three paper reams are placed in front of the tag, the antenna substantially directs the radiation and with five reams, side lobes appear [P1; Kata_06].

It was also noted in publication [P1] that the real part of the input impedance of the bow-tie antenna increases when paper reams are added in front of the antenna (due to dielectric losses). In addition, when the paper reams are added, the imaginary part of the input impedance changes from capacitive to inductive. In addition to the dimensions of the antenna design, which are optimized for functioning through paper, the change in the imaginary part from capacitive to inductive increased the read ranges through the paper due to improved impedance matching [P1].

Paper is cheap, environmentally friendly and it is often used in packaging. Since tag identification behind the paper reams was successful in this study, it can be concluded that the tags can be directly printed on paper in such items as packages where tags may also be located behind thick stacks of cardboard or thick layers of paper. This means that the printing of tags would provide new opportunities for the packaging industry. All tested inks and paper substrates worked satisfactorily. The results also indicate that printed tags could be used in paper industry applications where tags are affixed to the reel core and read through the roll of paper. It should also be noted that especially the sensitivity of the ICs has increased and thus longer read distances than those achieved in publication [P1] are now possible [P1].

6.2 Embedded passive UHF RFID tags

Printing makes it possible for conductive patterns such as RFID tag antennas to be fabricated directly on various materials. This offers a new way to embed electronic structures as integral parts of other objects. The capability of pad printing in passive UHF RFID tag antenna manufacturing and the ability to print on 3D surfaces is investigated in publication [P7]. Passive UHF RFID tags were printed on flat and on convex surfaces and the performance of the tags was studied. The motivation for this work was to promote the embedding of tags directly into the objects to be identified. This would eliminate the need for a substrate. It has already been noted in this thesis that the conductive patterns can be successfully printed on fabric and paper substrates which are typical surfaces of packages and clothes. Those investigations showed promise for further examination of embedding tags onto different objects and substrates which are not traditionally used in electronics manufacturing. Soft drink bottles and cardboard reels were select-

ed as the 3D “substrates” for the tags. A tag on a cardboard reel is presented in Fig. 6.2. Test tags were also printed on flat substrate materials to characterize their nominal performance [P7].

Fig. 6.2. Prototype tag printed directly on cardboard reel with pad printing.

The power on tag measurement results for all the sample tags were presented in Section 5.4 in Figs. 5.19 - 5.21. It was found that the power on tag and the frequency response of the tags were influenced by the electrical properties of the substrate materials due to changed antenna impedance. The substrates also had an indirect effect on tag performance through the print quality and ink curing temperature. Hence, when embedding tags into other structures, it is important to consider the effect of the materials of the particular objects in which the tags are embedded [P7].

If tags are printed on 3D objects, they may be distorted in the printing process. This also affects antenna performance. In our case, the tag may elongate along the circumference of cylindrical objects. The matching structure at the centre of the antenna remains unchanged because the tag only stretches in the areas further away from the mid point of the pad, which is placed in the centre of the antenna during printing. On flat surfaces, there is no additional length on tags due to such stretching. Table 6.1 presents the stretching of tags which are printed directly onto convex surfaces. The samples are the same as in Table 5.3 (samples 9, 10 and 11) [P7].

Table 6.1. The stretching of the tags printed directly onto convex surfaces of cylindrical objects [P7].

Sample	Original measure (mm)	Elongation (mm)	Elongation (%)
9. Ink "A" on soft drink bottle, 5 print presses, printed in horizontal position*	65	7	11
10. Ink "A" on soft drink bottle, 5 print presses, printed in vertical position*	11	≈ 0	≈ 0
11. Ink "A" on cardboard reel, 5 print presses, printed in vertical position*	65	3	5

* "Horizontal position" means that the tag's longest dimension is perpendicular to the cylindrical object's axis. "Vertical position" means that the tag's length runs parallel to the cylindrical object's axis.

A comparison was made between the performance of non-distorted, vertically (parallel to the cylinder axis) printed tags and distorted, horizontally (perpendicular to the cylinder axis) printed tags. A soft drink bottle served as the object of the comparison. As reference, a planar tag which had first been printed on a PET foil substrate was bent around the soft drink bottle, both vertically and horizontally in order to observe the difference between a tag that had been directly printed on a 3D object and a tag which was not distorted [P7].

It can be concluded from the measurement results in Section 5.4 (Fig. 5.21) that the horizontally printed tag on the soft drink bottle works at lower frequencies than the vertically printed tag on the soft drink bottle. This is probably due to the elongation of the tag in the printing process because when a tag printed on PET foil was placed on the bottle, it worked in quite the same way, regardless of its orientation (see Fig. 5.20) [P7].

Based on the elongation and power on tag measurements (Table 6.1 and Fig. 5.21), it is concluded that the tags should be printed vertically on cylindrical surfaces to eliminate elongation due to the printing process. The horizontally printed samples provide an insight into how printed patterns become distorted on such surfaces (for example on spherical surfaces) where the distortion cannot be avoided by tag positioning, and how this distortion affects tag performance [P7].

In addition to such issues, the radiation pattern of the tag may also be changed if it is attached or directly printed onto objects. The power on tag measurements in Section 5.4 are all measured in front of the tag. Small dipole tags in free space typically have radiation patterns which resemble the radiation pattern of an infinitesimal dipole (Fig. 3.3). Omnidirectionality of the radiation pattern is desired in most RFID applications and in the case of dipole tags, it is typically achievable in H-plane. The H-plane radiation patterns were measured for samples 7, 9, 10 and 11 in Table 5.3 and for sample 7, which was vertically and horizontally placed on a soft drink bottle. The radiation pattern measurement was accomplished by rotating the tags in 15^{o} steps around the dipole axis

and measuring the power on tag at each orientation. Since the power on tag is inversely proportional to the tag antenna pattern, the pattern can be obtained by observing the difference of the power on tag over the rotation angles [P7; Ukko_10].

For the flat dipole-type tags in free air, the H-plane radiation pattern is expected to approximate closely to a circle. Thus, the radiation pattern of a planar tag (Sample 7) was measured in free air as a reference in order to investigate how the convex substrate and its material affect the antenna radiation pattern. The radiation patterns of horizontally and vertically printed tags on soft drink bottles (Sample 9 and Sample 10) were measured to investigate the effect of the positioning of the tag. Since the elongation of the tag in the pad printing process may affect the pattern, the radiation patterns were also measured using an unstretched tag on PET foil (Sample 7) attached to the bottle. In this way, direct comparison with the planar sample will be consistent [P7].

The normalized (reference power is the lowest measured power on tag) radiation patterns, based on the tag sensitivity measurements, are presented in Figs. 6.3 - 6.5. Irrespective of whether the tag was printed vertically or horizontally on the bottle, the radiation pattern is the same (see Fig. 6.3). This means that the slight elongation due to horizontal positioning has no significant impact on the radiation pattern of tags; mostly it remains omnidirectional in the dipole H-plane, allowing the tag to be read from all directions in this plane. This result suggests that it should also be possible to print tags directly onto spherical surfaces, provided that the curvature radius is the same order of magnitude as for the PET bottle and cardboard reel investigated in this study. Nevertheless, the tags printed on such specimens work differently from those on thin flat plastic foils or paper because of the increased conductor losses due poor print quality, low curing temperature and the dielectric losses discussed earlier [P7].

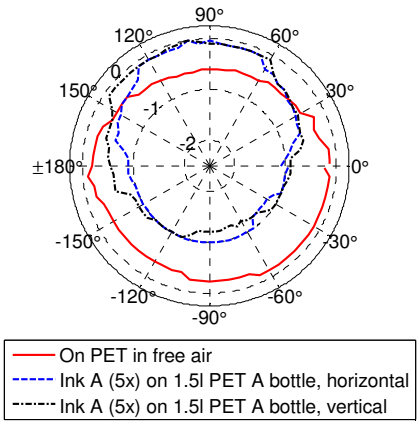

Figure 6.3 Radiation patterns of the tag on PET and the tag printed directly on soft drink bottle (ink A is ink "A" in Table 4.1) [P7].

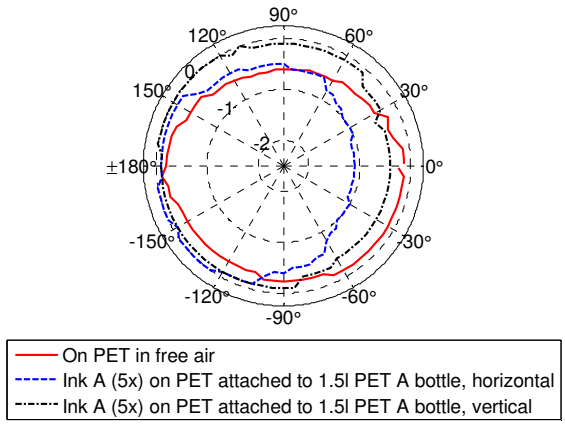

Figure 6.4 The radiation pattern of tag on PET foil in free air and attached to soft drink bottle (ink A is ink "A" in Table 4.1) [P7].

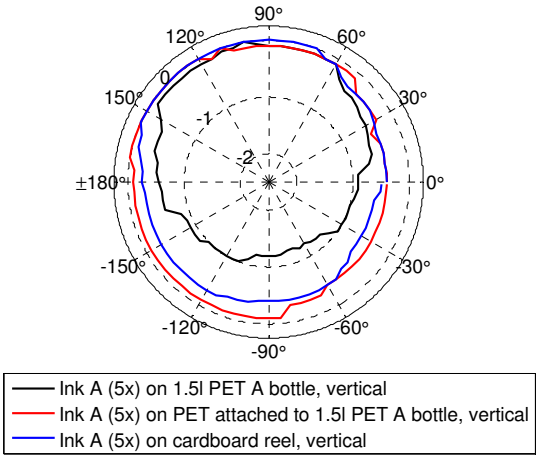

Figure 6.5 Radiation patterns of tags on different substrates (ink A is ink "A" in Table 4.1) [P7].

Measurements made for the tags with 5 print presses on PET foil attached to a bottle are presented in Fig. 6.4. According to Figs. 6.3 and 6.4, it seems that when the tag is placed (not directly printed) on the PET bottle, the measured patterns are different from the patterns of the tags that are directly printed on the bottles. They also resemble more closely the planar tag on PET in free air. This is thought to be due to the additional air gap between the bottle and the attached tag, whereas the tags printed on the bottle are in direct contact [P7].

In a realistic scenario the bottle is filled with liquid whose electrical properties are significantly different from those of a vacuum and so the impedance mistuning will be more considerable. This can be anticipated from the pattern of the tag printed on cardboard, which is shown in Fig. 6.5. The cardboard reel is thicker than the PET bottle and has higher permittivity and thus the radiation pattern of the tag printed directly on cardboard is changed compared to the one printed directly on PET bottle. However, anything about losses in the substrate material cannot be concluded from the patterns since they are normalized quantities. It is expected that the finite conductivity is distributed uniformly in the materials so that the cardboard reel, for instance, appears equally lossy from all directions [P7].

Overall, the measured patterns presented in Figs. 6.3, 6.4 and 6.5 appear very similar, showing less than 1 dB maximum variation among each other, regardless of the orientation or attachment method [P7].

In summary, it can be concluded that if conductive patterns such as RFID tag antennas are embedded into objects, it is always important to take account of the electrical properties of the object's materials as well as the indirect effect of factors such as printed film quality or the manufacturing process. The curvature of the substrates had little significant effect on the antenna functioning in the case of the small tag of the study. All

tags had omnidirectional radiation patterns despite the three dimensional substrate. These studies show that printing offers new ways of embedding electronics such as RFID tags as integral parts of other structures [P7].

6.3 Tag-based sensing – wireless strain sensor

The potential of RFID has been widely recognised and there is now increasing interest in applying the technology to purposes other than identifying objects. One novel field of research in RFID technology is tag-based sensing. RFID tags with a sensing function are expected to become important in the next generation of applications. External sensors have been connected to RFID tags so that the system is used for wireless sensing instead of identification. Even more interesting is the use of a passive RFID tag antenna as the sensing element itself. This would eliminate the need of external sensors and batteries. In addition, printing techniques offer a new way of embedding RFID tags into other structures such as buildings or clothing. These kinds of cost effective, low maintenance, embedded sensors have numerous application possibilities. These applications include health care applications (wearable sensors), structural health monitoring and game applications [P9; Suzu_09; Gao_10; Kiil_10; Meri_10].

In publication [P9] a wireless strain sensor was developed for measuring large strains based on passive UHF RFID technology and printed electronics. The basic idea was to make a stretchable tag whose operation changes when the tag is stretched. The sensor is a new application of printed electronics and it is made of novel materials: polymer thick film silver ink (ink (B)) on stretchable fabric and PVC substrates. The behaviour of the materials during straining was first characterized in publication [P8]. In publication [P9] a strain sensitive stretchable RFID tag was developed on the basis of the behaviour of the selected materials studied in article [P8]. Performance of the tags and the effect of mechanical straining on tag functioning was examined.

The effect of tensile strain on the conductivity of polymer matrix composites such as silver ink has been studied by several researchers. When the polymer matrix composite is strained, several different phenomena are reported to occur. These include the breaking of the 3D network formed by the conductive filler particles, a loss of contact between particles, an increase in the inter filler distance, delamination and reorientation of particles and a decrease in the volume fraction of the filler material as the material extends [Mera_95; Hay_07; Hu_08; Kure_08; Sevk_08]. Sevkat et al. [Sevk_08] have also discovered a decrease in resistance in the tensile test due to the Poisson effect: more contacts in a lateral direction and fewer contacts in a longitudinal direction. Sevkat et al. have reported that the resistance change and the tensile strain follow an exponential or power law. Hu et al. [Hu_08] observed that the change in the resistance is most sensitive to strain at the percolation threshold. During large strain, conditions resemble the state where the content of silver particles is close to the critical volume fraction. Ac-

cording to article [Lin_04], the aspect ratio affects the critical volume fraction due to a wider contact area between the particles with the increasing aspect ratio. Similarly, the aspect ratio may also affect the electrical performance of printed film upon straining. If the particles move away from each other under large strain, the conditions resemble those near the percolation threshold and the role of tunnelling and hopping conductivity increases and they may affect the total conductivity [P8; Hu_08].

Publication [P8] investigates screen printed PTF conductors on stretchable substrates during stretching to observe the above mentioned mechanisms and to evaluate the strength of their effect. The dimensions of the printed rectangular conductors were 97 mm x 8 mm. The width and the length of the conductor are the same as those for the prototype strain sensitive tag antenna geometry used in publication [P9].

Stretchable polyvinylchloride (PVC) sheet proved to be a suitable substrate for printed conductors in article [P2] and thus samples on a PVC substrate were the main study focus of publication [P8]. Fabric was used as substrates to find a reference structure whose behaviour is markedly different from that of the samples on PVC substrate. The aim was to identify different structures which could be utilized in strain sensors [P8].

The stretchability of the PVC substrate is based on the material itself and the elastic behaviour of the substrate called “Fabric 1” is based on the texture of the fabric. There are elastane “rubber bands” inside the woven fabric texture. When the fabric is stretched, the individual fibres do not stretch, though the woven structure does [P8].

The change in DC resistance of the conductor was investigated when the structure was strained. The measured change in resistance of a conductor on PVC is presented in Fig. 6.6. Three sequential stretches are plotted in the same figure. Publication [P8] presents the results for two similar samples [P8].

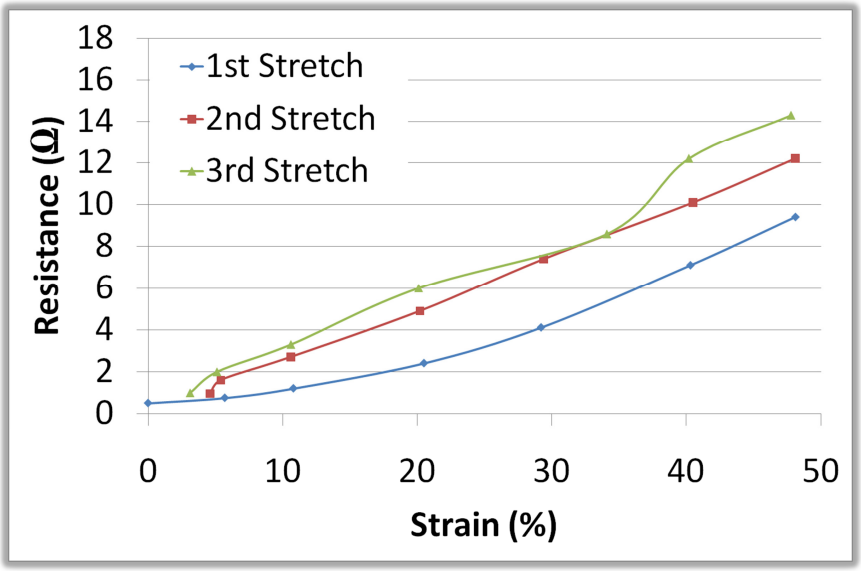

Figure 6.6. Resistance of Sample 3 (ink (B) on PVC) during stretching [P8].

It can be seen from the resistance measurements that the difference in resistance between the first stretch and the two following stretches is larger than the difference between the second and the third stretch. In article [Hay_07] a high degree of hysteresis was found during the first cycle of straining, after which hysteresis reduced dramatically. This supports the findings of Fig. 6.6 when comparing the difference between the first and subsequent stretches. This behaviour is assumed to be due to the emergence of microstructural defects during the first stretch which remain in the structure during the next two stretches. Thus, if the materials are used in sensor applications, the first stretches should be performed before using the sensor. Publication [P8] also showed that the recovery of the samples from very large strains (50 %) is slow from 10 % to 2 - 3 % elongations so that the PVC substrate behaves anelastically. This anelastic behaviour also explains why for the samples in article [P8] the starting resistance of stretch 2 is larger than the starting value of stretch 3. The recovery time is 24 hours before stretch 3 and about 30 minutes before stretch 2. Also about 2 - 3 % plastic deformation was found in the structure after 24 h. Permanent change in resistance (24 h after the stretch) in the unloaded state was 0 Ω - 0.5 Ω for samples 1 – 3 in article [P8].

The effect of tensile strain on the conductivity of the ink on PVC can be explained by microstructural changes in the printed film. Poisson's effect, found in article [Sevk_08], was not observed in our samples because of the non-elastic matrix polymer cracking. Matrix microcracking is shown in Fig. 6.7. Although the printed film partially contains holes (see Fig. 12 in article [P9]), the film remains conductive (Fig. 6.6) [P8].

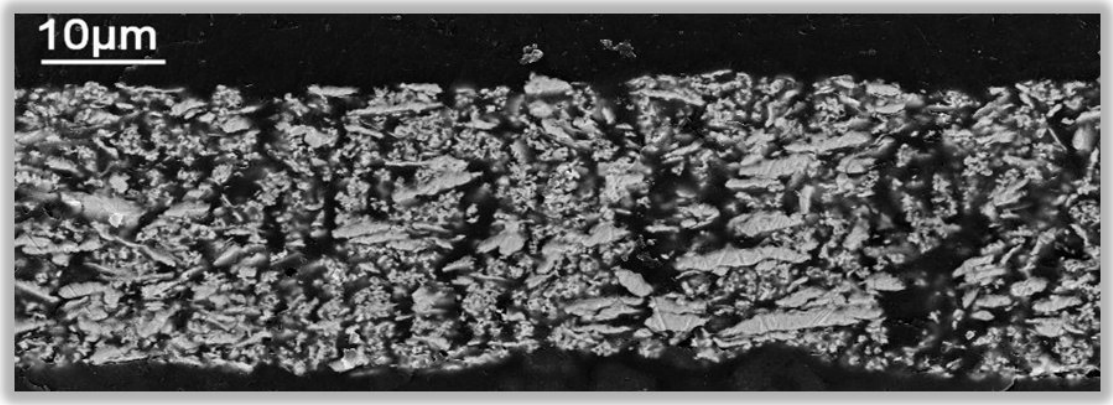

Figure 6.7. SEM micrograph from a cross section of printed film on PVC under 50 % strain.

The cracking of the matrix leads to partial breaking of the 3D network and reduction of the contact area between the particles. The interfiller distance also increases and the delamination of particles occurs. The decrease in the volume fraction of the particles in the printed film was evaluated from the cross section figures of the samples under loading. It was estimated that about 20 % volume fraction reduction under ≈ 50 % strain occurs.

The volume fraction of particles is recovered almost entirely after straining. Similar behaviour was observed in article [P2]. Only particle delamination from the matrix could be seen after recovery. The volume fraction values are approximations from cross section areas of particles relative to the total film cross section area. Since the volume fractions are evaluations from 2-dimensional cross section figures, the values are not absolute. However, comparisons between the samples can still be made. The polymer matrix of the ink is not elastomer, but it would seem that the particles orientate in the direction of the load. More research is needed to confirm this implication. The particle size distribution of the ink of our study is large and strain levels are high. Thus instead of the movement of the particles relative to each other, matrix cracking and its consequences are believed to be the main cause for the increase in resistance. It should be noted that in addition to microstructural changes, change in the physical dimensions (width, length, thickness) affects resistance. It was also found that thickness variation and surface roughness increases under strain [P8].

The behaviour of a similar conductor printed on Fabric 1 was investigated after the samples on PVC. The printed film is very uneven (see Table 4.2 and Fig. 6.8) and the ink is distributed between the fabric fibers, which form gaps in the film. The performance of this kind of film is not the same as the performance of a smooth uniform film [P8].

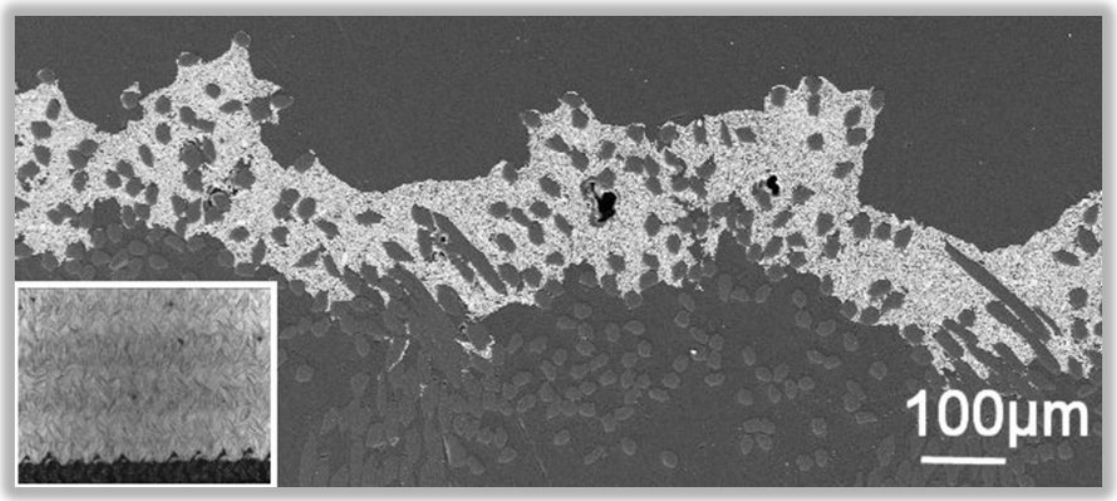

Figure 6.8. SEM micrograph of a cross section of printed film on Fabric 1 under 0 % strain [P8].

The resistance measurement results for the conductor on Fabric 1 substrate during stretching are presented in Table 6.2. A similar fabric, Fabric 2, is used as an antenna substrate in publication [P9] and the results for a similar conductor on Fabric 2 are also presented in the table [P8 - P9].

The resistance of the printed film on Fabric 1 and on Fabric 2 changes more rapidly during straining compared with samples on PVC. It can be seen from Fig. 6.8 and Fig. 6.9

that the decrease in the conductivity of the ink on fabric is due more to the structural change of the fabric than to microstructural changes of the printed film.

Table 6.2. The resistance of printed film on Fabric 1and Fabric 2 during straining.

Substrate	Strain (%)	DC Resistance (Ω)
Fabric 1	0	1
Fabric 1	5	7
Fabric 1	10	12
Fabric 1	20	40
Fabric 1	28	70
Fabric 1	38	200
Fabric 1	48	1200000
Fabric 2	0	1
Fabric 2	5	10
Fabric 2	11	30
Fabric 2	19	100
Fabric 2	28	300
Fabric 2	39	600000
Fabric 2	47	1400000

The printed film does not stretch but when the fabric is strained, the threads move apart from each other as does the printed film on the threads, as is seen in Fig. 6.9. The pictures in the lower left corners of Fig. 6.8 and Fig. 6.9 are taken from above the sample conductors and they illustrate the behaviour of the fabrics. The magnification in Fig 6.9 shows that no microstructural changes occur in the printed film during straining. Since Fabric 2 in article [P9] is similar in structure to Fabric 1, the straining behaviour of the fabrics is also similar [P8].

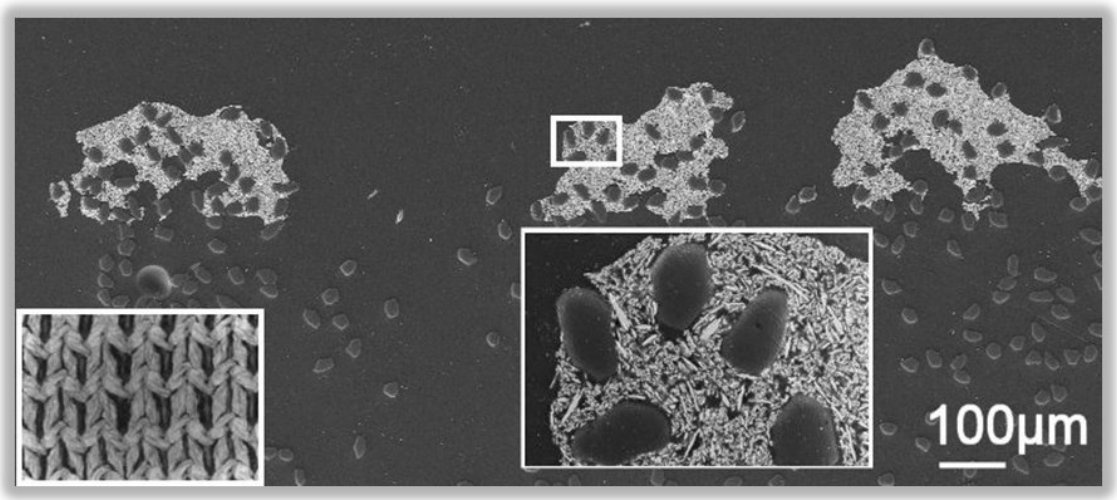

Figure 6.9. SEM micrograph of a cross section of printed film on Fabric 1 under 50 % strain [P8].

It proved rather difficult to measure the resistance of samples on fabrics due to the web-like structure in larger strains (> 30 %, see Fig. 6.9) and it was difficult to attach the measurement heads securely. Every effort, however, was made to overcome these challenges. Though the absolute values may not be entirely precise, the measured values do indicate the right order of magnitude. It can be concluded from the results that the behaviour of the samples on fabrics differs considerably from that of the samples on PVC. They therefore serve as interesting reference structures for the structures on PVC in strain sensing applications [P8].

The strain sensitive behaviour of the structures in publication [P8] was exploited in a wireless strain sensor whose operation is based on passive UHF RFID technology. The tag antenna used as a strain sensor in publication [P9] is a rectangular short dipole, as shown in Fig. 6.10. The dimensions of the tag are L = 97 mm, W = 8 mm, s = 17 mm, t = 0.5 mm, u = 2 mm and v = 5 mm. The geometry is selected because it is simple and the outer dimensions are the same as those of the sample conductors in articles [P8] and [P9].

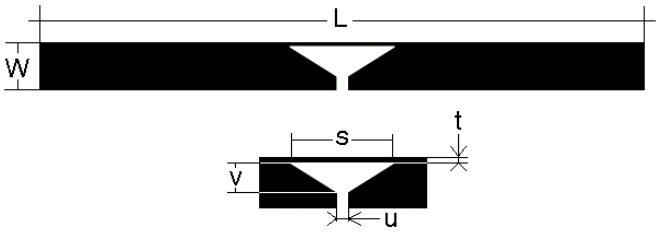

Figure 6.10. Strain sensor tag geometry [P9].

Prototype tags were printed on Fabric 2 and on PVC. The area where the IC chip is attached was shielded and stiffened with epoxy so that the chip does not detach from the structure and the matching structure does not change when the antenna is strained. Thus, only the tag antenna "arms" with same width and thickness as those of the conductors are stretched. For this reason the behaviour of the "arms" can be assumed to be similar to the behaviour of the sample conductors discussed earlier [P9].

EPC Gen 2 protocol-based measurements were performed to study tag performance. The quantities measured were the transmitted threshold power and the backscattered signal power. With the tag on PVC, the measurements were first performed without straining. Then ≈ 5 % strain was applied and the strain was increased from ≈ 10 % up by ≈ 10 % steps until ≈ 50 % strain (like the conductors in Fig. 6.6 and in Table 6.2). Tag on fabric was measured in unloaded conditions, under "small" (5 - 10 %), "moderate" (≈ 30 %) and "large" (> 50 %) strain [P9].

Straining changes the operation of the tag because the dimensions and the impedance of the tag changes. These affect ohmic losses, the power reflection coefficient and the di-

rectivity of the tag during stretching. As Eq. (3-18) shows, the power received by the tag increases by increasing the gain of the tag. Both radiation efficiency and directivity affect the gain (Eq. (3-7)). Straining increases the losses and thus decreases the radiation efficiency. Because change in the antenna geometry affects the current distribution, the directivity is also changed [Saun_07]. According to publication [Saun_07], when the length of a simple dipole antenna is increased from an infinitesimally short dipole to nearly one wavelength, the directivity increases. In publication [P9], when the dipole type tag is stretched, the length increases but it does not exceed one wavelength and the directivity of the antenna increases due to the increasing physical size [P9].

The threshold power showed an ambiguous response to strain at certain frequencies on both PVC and fabric substrates (see Fig. 4 and Fig. 7 in publication [P9]). The power the chip receives is, in addition to tag antenna gain (G_{tag}), proportional to the power reflection coefficient (Γ_{tag}) of the tag antenna (Eq. (3-20)). When the tag antenna is stretched, the power reflection coefficient is increased because the tag antenna impedance changes from the "matched" state. Impedance mismatch and decreased radiation efficiency increase the required threshold power, whereas the increasing directivity decreases it. The ambiguous behaviour of the tag threshold power is caused by impedance matching, which changes the frequency of optimal impedance matching. However, with some form of calibration (using only a certain part of the frequency regime and strain levels) the threshold power could be used in strain sensing [P9].

The backscattered signal power showed far less ambiguous behaviour and thus seems a promising method in strain measuring. In Chapter 3, the backscattered signal power was examined. It can be seen from Eq. (3-21) that the backscattered signal power depends on the power wave reflection coefficient of the tag in chip state 1 and 2 (ρ_1 and ρ_2) as well as the gain of the tag. In publication [P9] these parameters are functions of strain through changed antenna impedance and directivity.

Fig. 6.11 shows the backscattered power as a function of strain at 866 MHz, 915 MHz and 955 MHz for samples on PVC and on Fabric 2. The backscattered signal power of the samples on PVC monotonically increases during stretching, although the conductor loss resistance increases (see Fig. 6.6). This increase in backscattered signal power is due to increased antenna directivity as the length of the dipole increases towards half wavelength. The monotonic increase is clearly an advantage because the power needed from the reader remains below the permissible limit through the UHF RFID band and the sensor could thus be used globally. In addition, the response is fairly linear until 30 % strains. As the ohmic losses start to increase, the increase in backscattered power as a function of strain slows down. Due to changed antenna impedance, the power wave reflection coefficients ρ_1 and ρ_2 are also affected by antenna deformation. However, since the chip impedance varies with frequency and with the power absorbed by the

chip, it is unclear how $|\rho_1 - \rho_2|$ and, thus the differential radar cross section, is affected. If $|\rho_1 - \rho_2|$ increases, this is one of the reasons why backscattered power increases when the antenna is stretched [P9].

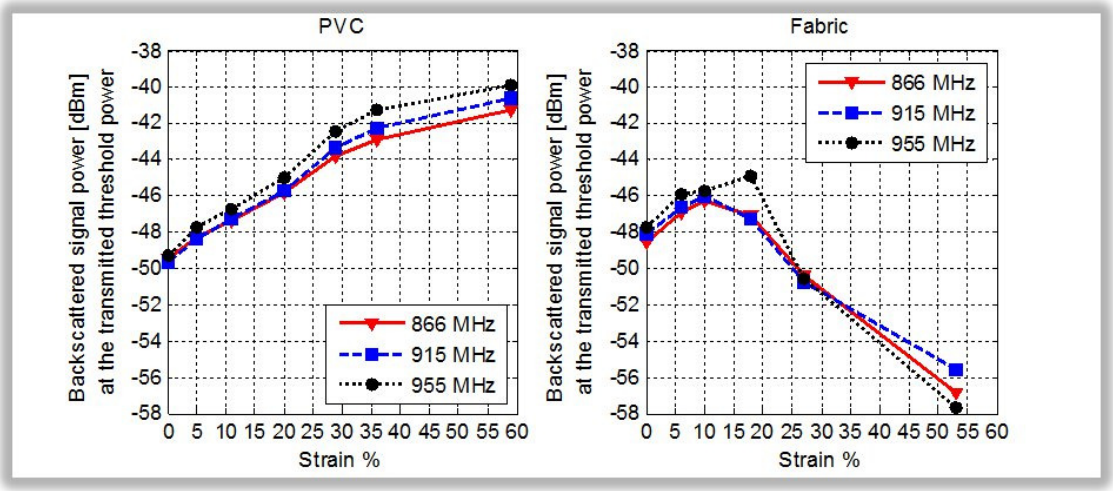

Figure 6.11. The backscattered signal power of tag on PVC and on Fabric 2 as a function of strain at 866MHz, 915 MHz and 955MHz [P9].

In the case of tag on Fabric 2, the backscattered signal power first increases as a result of increasing directivity, but when the ohmic losses increase significantly from 10 % - 20 % strain levels up (see Table 6.2), they start to dominate and backscattered power starts to decrease. The measured DC resistance of silver ink conductor on a PVC substrate at ≈ 50 % strain level corresponds to the DC resistance of samples on fabrics at ≈ 10 % strain level (see Fig. 6.6 and Table 6.2). The difference in the ohmic losses is assumed to be the main reason for the differences in behaviour of the tag on PVC and that on Fabric 2.

Although the backscattered signal power of the tag on Fabric 2 does not change monotonically (Fig. 6.11), it could also be used as a strain sensor. The tag on Fabric 2 could be used in two ranges. It can be used to sense: 1. strain levels which do not exceed 10 % at 866 MHz and 915 MHz (≈ 18 % at 955 MHz), or 2. strain levels from 10 % up at 866 MHz and 915 MHz (≈ 18 % up at 955 MHz). However, some form of calibration is required [P9].

It is seen from Fig. 6.11 that the operation of the sensor can be modified by substrate selection and there are, in fact, other opportunities to modify it. One option is to change the tag geometry [Meri_10]. The characteristics of the ink can also be modified. The sensitivity of the sensor can be improved by decreasing the particle volume fraction near the percolation threshold. In this case, it is impossible to measure large strains because the conductivity eventually disappears [P8; P9].

Overall, the backscattered signal power of the tags shows very promising results in terms of many practical applications such as in monitoring structural health or human bodily functions and movements. The materials used in this study can be embedded into clothing. This means that the sensor can be made wearable and thus it seems a promising solution in many health care applications [Meri_10]. Future work is to evolve the background systems for these applications [P9].

Further work is also required to investigate the long term reliability of the sensors and recovery from cyclic straining. In addition, development of the tag by material modification and tag geometry improvement is another area for future study. In terms of the practical applications, the permitted power levels and read ranges should be determined as well as the effect of the human body and other proximate materials.

7. Final remarks and conclusions

Printing facilitates the manufacture of different electronics applications and thus it holds a good deal of promise for the electronics industry. Flexibility and light weight are typical characteristics of printed applications. Printing can be advantageous, for example, when tags need to be integrated into products, or when developing new applications based on printed electronics materials.

When different printing methods are used in tag fabrication, many factors need to be considered. Firstly, both substrate and conductor materials may differ greatly from the traditional materials used in electronics. The electrical properties of the novel materials may also be relatively unknown. Secondly, the selected printing technique may impose certain constraints on substrate selection, ink composition, thickness and surface roughness, print quality, printable image size and resolution and so on. As a result, the manufacturing method should be taken into consideration already at the tag design stage. It is possible to produce tags with uniform modes of operation, regardless of the printing method selected. This requires knowledge of the materials used and also the process characteristics. However, different printing methods are suitable for fabricating different applications.

Despite the challenges presented by the use of printing methods and novel materials, they provide new and exciting opportunities for tag antenna manufacturing. Printing of PTF inks enable new ways of integrating RFID tags into other structures such as packaging. Embedded tags may also be useful in brand protection and product lifecycle management. If RFID tags are embedded in objects, it is always important to consider the electrical properties of the objects' materials as well as the indirect effects, such as the effect on printed film quality and the manufacturing process.

In this study, flexible and highly stretchable electrically conductive PTF patterns as well as passive UHF RFID tags were developed and produced with printing techniques on various substrate materials. The following conclusions can be drawn:

- Through careful design and the use of electrically conductive polymer thick film silver inks, it is possible to achieve levels of performance that are comparable with traditional etched copper circuit implementations. The use of printing processes and PTF inks are also an option for use in UHF RFID tag antenna fabrication.

- The printed film and the substrate characteristics both have an effect on the operation of the passive UHF RFID tag. The characteristics of these materials affect the impedance of the tag antennas which, in turn, has an effect on the losses (conductor and dielectric) of the tag antenna and the impedance matching between the antenna and the IC. As a result, the required power and the operating frequency are also affected. In addition, the materials have a bearing on the radiation characteristics of the tags.

- The ink plays a very major role in achieving adequate tag antenna performance. In dipole type passive UHF RFID tags, the effect of the conductor material on the normalized radiation pattern is minor. Instead, the conductivity of the printed film affects the impedance of the tag and, thus, ohmic losses and impedance matching. The ink composition is a critical factor in the electrical conductivity of the PTF ink.

- The morphology of the printed films is another important factor. Using conductor film thicknesses more than one penetration depth yields significant improvement to the electrical performance of the tag, but reducing the film thickness can be a favourable trade-off to improve cost effectiveness through savings in materials. However, the thickness of the conducting film also affects the input impedance of the tag antenna and this must be considered in tag antenna design in order to tune the antenna to the right frequency and to achieve sufficient performance.

- Printed films are irregular and, in addition to the ink composition, both substrate material and the printing process affect the film morphology. Thickness variations occur even if the substrate material is smooth. The non-uniformities increase ohmic losses. For very thin conductor layers, possible non-uniform distribution of the conducting material also detunes the antenna significantly when the irregularities occur in a high current density region. Print quality, therefore, needs special attention when UHF RFID tags are printed using very thin conducting layers or narrow traces.

- Substrate materials produce effects on tag performance similar to those of the properties of the printed film. The substrate properties affect the losses of the tag as well as the impedance matching. The substrate may also affect the radiation pattern. The effect of the substrate is marked when the thickness, relative permittivity or loss tangent of the substrate increases. In addition, the substrate may have indirect effects on the tags. The curing conditions, for example, may be limited by the substrate. Inadequate curing impairs antenna performance due to residues in the printed film which increase the loss resistance of the film.

- The curvature of the substrates has no significant effect on the functioning of the antenna in the case of the small tag used in this study. All embedded convex tags had omnidirectional radiation patterns regardless of the 3D substrate.

- The use of PTF inks in tag antennas enables the development of new applications for RFID. These include RFID-enabled sensors. In this thesis screen printed PTF structures were found to maintain electrical conductivity under heavy strain. The resistance of the structures increased as a function of strain. The resistance change during straining depends on the PTF ink composition as well as on the substrate material. This means that strain sensitivity can be controlled by modification of the substrate and the ink. The materials were utilized in a wireless strain sensor that was developed in the study. The operation of the sensor was based on passive UHF RFID technology and the behaviour of the materials during straining. A stretchable tag was manufactured and the threshold power, as well as the backscattered signal power of the tag, changed when it was strained. The measurement results indicate that large strains can be successfully measured wirelessly by using stretchable RFID tag as a strain sensitive element. It was possible to measure strains up to 50 %.

Further work is required to improve the strain sensor and also to evolve other novel applications. The applications should also be tested in real situations. In addition, there is a need for more research to create background systems for the applications. New tag geometries also need to be developed for embedding tags into different objects and to minimize the consumption of conductive ink. Depending on the application, environmental and burn-in testing may be necessary.

Although printing methods offer new opportunities for RFID manufacturing, adaptation of the item level RFID requires a reduction in the costs of conductor materials. Printing methods themselves are already cost effective and the electrical performance of materials is also satisfactory. In addition, the development of cost-effective semiconductor inks would assist the use of printed electronics through fully printed products. Nowadays the products are typically hybrids of printed structures and traditional components (such as ICs).

References

[Auto_02] Auto-ID Center technical report, 860MHz–930MHz Class I Radio Frequency Identification Tag Radio Frequency & Logical Communication Interface Specification Candidate Recommendation, Version 1.0.1, Auto-ID Center, 2002

[Bala_05] Balanis C.A., Antenna Theory - Analysis and Design (3rd Edition), John Wiley & Sons, 2005

[Bala_89] Balanis C. A., Advanced Engineering Electromagnetic, John Wiley & Sons, 1989

[Baye_04] Bayes M., Horn A., Effects of Conductor Surface Condition on Signal Integrity, Circuit World, Volume 30, Issue 3, 2004, pp. 11–16

[Bhat_09] Bhattacharyya R., Floerkemeier C., Sarma S., Towards Tag Antenna Based Sensing – An RFID Displacement Sensor, IEEE International Conference on RFID, Orlando, Florida, USA, 2009, pp. 95 - 102

[Blay_05] Blayo, A., Pineaux, B., Printing Processes and their Potential for RFID printing. Joint sOc- EUSAI conference, Grenoble, France, 2005, pp. 27 - 30

[Brom_97] Brom H.B., Adriaanse L.J., Teunissen P.A.A., Reedijk J.A., Michels M.A.J., Brokken-Zijp J.C.M., Frequency and Temperature Scaling of the Conductivity in Percolating Fractal Networks of Carbon-Black/Polymer Composites, Synthetic Metals Volume 84, Issues 1 - 3, 1997, pp. 929 – 930

[Busc_01] Buschow K.H. J. (editor), Cahn R. W. (editor), Flemings M. C. (editor), Ilschner B. (editor), Kramer E. J. (editor), Mahajan S. (editor), Encyclopedia of Materials - Science and Technology, Volumes 1 - 11, Elsevier, 2001

[Cagl_10] Caglar U., Studies of Inkjet Printing Technology with Focus on Electronic Materials, Tampere University of Technology doctoral thesis, TUT Publication 863, Tampere, Finland, 2010

[Camp_08] Campo E. A., Selection of Polymeric Materials - How to Select Design Properties from Different Standard, William Andrew Publishing/Plastics Design Library, 2008

[Carr_01] Carr J. J., Practical Antenna Handbook, McGraw-Hill Professional Publishing, 2001

[Chan_05] Chang K. (editor), Encyclopedia of RF and Microwave Engineering, Volumes 1 - 6, John Wiley & Sons, 2005

[Chen_07] Chen Z. N., Antennas for Portable Devices, John Wiley & Sons, 2007

[Chen_93] Cheng D. K., Fundamentals of Engineering Electromagnetics, Addison-Wesley publishing company, 1993

[Coom_01] Coombs C. F., Coombs' Printed Circuits Handbook, McGraw-Hill Publishing, 2001

[Cost_05] Costenoble J., Rotary Screen Printing: The Productive Solution for HF/UHF RFID Labels, SGIA Journal, fourth quarter 2005, pp. 7 - 10

[Cous_01] Cousins K., Polymers for Electronic Components, Smithers Rapra, 2001

[Deep_09] Deepa K. S, Kumari Nisha S., Parameswaran P., Sebastian M. T., James J., Effect of Conductivity of Filler on the Percolation Threshold of Composites, Applied Physics Letters, Volume 94, Issue 14, 2009, pp. 142902 - 142902-3

[Denl_80] Denlinger, E. J., Losses of Microstrip Lines, IEEE Transactions on Microwave Theory and Techniques, Volume 28, Issue 6, 1980, pp. 513 - 522

[Djor_01] Djordjevic, A. R., Biljie, R. M., Likar-Smiljanic V. D., Sarkar T. K., Wideband Frequency-Domain Characterization of FR-4 and Time-Domain Causality, IEEE Transactions on Electromagnetic Compatibility, Volume 43, Issue 4, 2001, pp. 662- 667

[Dobk_08] Dobkin D., RF in RFID - Passive UHF RFID in Practice, Elsevier, 2008.

[Dzie_01] Dziedzic A, Snarskii A. A., Percolation Theory and its Application in Materials Science and Microelectronics (part I – theoretical description), Informacije MIDEM, Volume 31, 2001, pp. 1–9

[Dzie_07] Dziedzic A., Carbon/polyesterimide Thick-Film Resistive Composites - Experimental Characterization and Theoretical Analysis of Physicochemical, Electrical and Stability Properties, Microelectronics Reliability, Volume 47, Issues 2-3, 2007, pp. 354 – 362

[Dzie_95] Dziedzic A., Polymer/conductive Filler Composites - Chosen Properties and Application, Proceedings of SPIE 2780, 5th International Workshop on Electronic Properties of Metal/Non-Metal Microsystems, Polanica, Poland, 1995, pp. 18 - 24

[Dzie2_01] Dziedzic A, Snarskii A. A., Percolation Theory and its Application in Materials Science and Microelectronics (part II – experiments and numerical simulations), Informacije MIDEM, Volume 31, 2001, pp. 141–152

[EPC_08] EPC Radio-Frequency Identity Protocols, Class 1 Generation-2 UHF RFID protocol for Communications at 860MHz – 960 MHz, Version 1.2.0, 2008, Available: http://www.epcglobalinc.org/standards/uhfc1g2/uhfc1g2_1_2_0-standard-20080511.pdf (Accessed 25.8.2010)

[Evans_97] Evans, P. S. A, Ramsey, B. J, Harrison, D. J., Shepherd, P.R., Further Developments of Microwave CLFs', Proceedings of Automated R.F. and Microwave Measurement Society Conference, Malvern, England, 1997

[Evans2_97] Evans, P.S.A., Ramsey, B. J. and Harrison, D. J., A Comparison of the Characteristics of Conductive Lithographic Films and Screen Printed Circuits, CARTS-Europe 97, 11th Annual European Passive Components Conference, Prague, Czech Republic, 1997, pp. 24-28

[Fink_03] Finkenzeller K., RFID Handbook, 2nd Edition, John Wiley & Sons, 2003

[Flew_03] Flewitt P. E. J., Wild R. K., Physical Methods for Materials Characterisation, 2nd Edition, IOP Publishing Ltd., 2003

[Fore_01] Forest Products Laboratory U.S. Department of Agriculture, Wood Handbook - Wood as an Engineering Material, 2001

[Fors_54] Forsythe W. E., (1954), Smithsonian Physical Tables (9th Revised Edition), Knovel, 2003

[Frad_04] Fraden J., Handbook of Modern Sensors - Physics, Designs and Applications (3rd Edition), Springer – Verlag, 2004

[Gao_10] Gao J., Siden J., Nilsson H-E., Printed Temperature Sensors for Passive RFID Tags, Progress in Electromagnetics Research Symposium Proceedings, Xi'an, China, 2010, pp. 845 – 848

[Golo_96] Golovanov V., Solis J. L., Lantto V., Leppävuori S., Different Thick-Film Methods in Printing of One-Electrode Semiconductor Gas Sensors, Sensors and Actuators B: Chemical Volume 34, Issues 1 - 3, 1996, pp. 401 - 406

[Gooc_97] Gooch J. W., Analysis and Deformulation of Polymeric Materials: Paints, Plastics, Adhesives and Inks, Kluwer Academic Publishers, 1997

[Hahn_01] Hahne P., Hirth E., Reis I.E., Schwichtenberg K., Richtering W., Horn F.M., Eggenweiler U., Progress in Thick-Film Pad Printing Technique for Solar Cells, Solar Energy materials & Solar Cells, Volume 65, Issues 1-4, 2001, pp. 399 - 407

[Hay_07] Hay G., Southee D., Evans P., Harrison D., Simpson G., Ramsey B., Examination of Silver-Graphite Lithographically Printed Resistive Strain Sensors, Sensors and Actuators A: Physical, Volume 135, Issue 2, 2007, pp. 534 - 546

[Hick_80] Hicks W. T., Allington T. R., Johnson V., Membrane Touch Switches: Thick Film Materials Systems and Processing Options, IEEE Transactions on Components, Hybrids and Manufacturing Technology, Volume 3, Issue 4, 1980, pp.518 - 524

[Hoff_97] Hoff, S. B., Screen Printing – A Contemporary Approach, Delmar Publishers, 1997

[Hu_08] Hu N., Karube Y., Yan C., Masuda Z., Fukunaga H., Tunneling Effect in a Polymer/Carbon Nanotube Nanocomposite Strain Sensor, Acta Materialia, Volume 56, Issue 13, 2008, pp. 2929 - 2936

[Impi_11] Impinji Inc, Available: http://www.impinj.com/products/monza4specs.aspx (Accessed 18.4.2011)

[Jing_00] Jing X. , Zhao W., Lan L., The Effect of Particle Size on Electric Conducting Percolation Threshold in Polymer/conducting Particle Composites, Journal of Materials Science Letters, Volume 19, Issue 5, 2000, pp. 377 - 379

[Jylh_07] Jylhä L., Sihvola A., Equation for the Effective Permittivity of Particle-Filled Composites for Material Design Applications, Journal of Physics D: Applied Physics, Volume 40, Issue 16, 2007, pp. 4966–4973

[Jylh_08] Jylhä, L., Modelling of Electrical Properties of Composites, Thesis for the degree of Doctor of Science in Technology, TKK Radio Science and Engineering Publications, Espoo, Finland, 2008

[Kata_06] Kataja J., Ukkonen L., Schaffrath M., Sydänheimo L., Kivikoski M., Modelling the Effects of Stacked Paper on the Radiation Pattern of Bow-Tie RFID Tag Antennas, IEEE Antennas and Propagation Society International Symposium with USNC/URSI Radio Science and AMEREM Meetings., Albuquerque, New Mexico, USA, 2006, pp. 3225 - 3228

[Kiil_10] Kiili K., Merilampi S., Developing Engaging Exergames with Simple Motion Detection, Proceedings of the 14th International Academic MindTrek Conference: Envisioning Future Media Environments, Tampere, Finland, 2010, pp. 103-110

[Kipp_01] Kipphan H, Handbook of Print Media, Springer, 2001

[Knot_04] Knott E. F., Shaeffer J. F., Tuley M. T., Radar Cross Section (2nd Edition), SciTech Publishing, 2004

[Kovi_11] Kovio Ltd, Available: http://kovio.com (Accessed 11.4.2011)

[Kuls_02] Kulshreshtha A. K.(editor), Vasile C. (editor), Handbook of Polymer Blends and Composites, Smithers Rapra Technology, 2002

[Kuma_03] Kumar G., Ray K. P., Broadband Microstrip Antennas, Artech House, USA, 2003

[Kure_08] Kure K., Kanda T., Suzumor K., Wakimoto S., Flexible Displacement Sensor Using Injected Conductive Paste, Sensors and Actuators A, Volume 143, Issue 2, 2008, pp. 272 - 278

[Kuro_65] Kurokawa K., Power Waves and the Scattering Matrix, IEEE Transactions on Microwave Theory and Techniques, Volume 13, Issue 2, 1965, pp. 194 - 202

[Laht_99] Lahti M., Seppävuori S., Lantto V., Gravure-Offset Technique for the Fabrication of Solid Films, Applied Surface Science, Volume 142, Issues 1-4, 1999, pp. 367 - 370.

[Land_94] Landers T. L., Brown D. B., Fant E. W., Malstrom E. M., Schmitt N. M., Electronics Manufacturing Processes, Prentice Hall, 1994

[Laug_03] Laughton M. A. (editor), Warne, D. F. (editor), Electrical Engineer's Reference Book (16th Edition), Elsevier, 2003

[Lear_69] Learmonth G. S., Pritchard G., Electrical Resistivity and Crosslinking in Thermosetting Resins, Industrial & Engineering Chemistry Product Research and Development Volume 8, Issue 2, 1969, pp 124–127

[Lehp_07] Lehpamer H., RFID Design Principles, Artech House Incorporated, 2007

[Lin_04] Lin Y-S., Chiu S-S., Effects of Oxidation and Particle Shape on Critical Volume Fractions of Silver-Coated Copper Powders in Conductive Adhesives for Microelectronic Applications, Polymer Engineering and Science, Volume 44, Issue 11, 2004, pp. 2075 - 2082

[Loo1_08] Loo C-H., Elmahgoub K., Yang F., Elsherbeni A., Kajfez D., Kishk A., Elsherbeni T., Ukkonen L., Sydänheimo L., Kivikoski M., Merilampi S., Ruuskanen P., Impedance Matching for RFID Tag Antennas, Applied Computational Electromagnetics (ACES) Conference, Hilton Fallsview, Niagara Falls, Canada, 2008

[Loo2_08] Loo C-H., Elmahgoub K., Yang F., Elsherbeni A., Kajfez D., Kishk A., Elsherbeni T., Ukkonen L., Sydänheimo L., Kivikoski M., Merilampi S., Ruuskanen P., Chip Impedance Matching for UHF RFID Tag Antenna Design, Progress In Electromagnetics Research, Volume 81, 2008, pp. 359-370

[Loo3_08] Loo C-H., Elmahgoub K., Yang F., Elsherbeni A., Kajfez D., Kishk A., Elsherbeni T., Ukkonen L., Sydänheimo L., Kivikoski M., Merilampi S., Ruuskanen P., RFID Tag Antenna Matching to Frequency Dependent MicroChip Impedance, IEEE Antennas and Propagation Society International Symposium, APS 2008, San Diego, California, USA, 2008, pp. 1-4

[Love_97] Love G. R., Maher G., Lambrecht R. A., Pad Printer, Proceedings of IEEE 47th Electronic Components and Technology Conference, San Jose, California, USA, 1997, pp. 972-978

[Marr_08] Marrocco, G., The Art of UHF RFID Antenna Design: Impedance-Matching and Size-Reduction Techniques, IEEE Antennas and Propagation Magazine, Volume 50, Issue 1, 2008, pp.66 - 79

[Mehr_08] Mehrjerdi Y. Z., RFID-Enabled Systems: A Brief Review, Assembly Automation, Volume 28, Issue 3, 2008, pp. 235-245

[Mehr_09] Mehrjerdi Y. Z., RFID-Enabled Supply Chain Systems with Computer Simulation, Assembly Automation, Volume 29, Issue 2, 2009, pp. 174-183

[Mena_07] Menachem L., Handbook of Fiber Chemistry 3rd Edition, CRC Press, 2007

[Mera_95] Meraghnia F., Benzeggagha M. L., Micromechanical Modelling of Matrix Degradation in Randomly Oriented Discontinuous-Fibre Composites, Composites Science and Technology, Volume 55, Issue 2, 1995, pp. 171 – 186

[Meri_06] Merilampi S., RFID-tunnisteantennien valmistustekniikat ja paperille painettujen tunnisteiden arviointi (RFID Tag Antenna Manufacturing Techniques and the Characterization of Printed Tags on Paper Substrate), Diploma Thesis, Pori, Finland, 2006

[Meri_10] Merilampi S., Björninen T., Ukkonen L., Ruuskanen P., Sydänheimo L., Printed Passive UHF RFID Tags as Wearable Strain Sensors (invited paper), 3rd International Symposium on Applied Sciences in Biomedical and Communication Technologies, ISABEL, Rome, Italy, 2010

[Meye_07] Brown M., Patadia S., Dua S., Mike Meyers' Comptia RFID+ Certification Passport, McGraw-Hill Osborne, 2007

[Mole_06] Molesa S. E., Ultra-Low-Cost Printed Electronics, Electrical Engineering and Computer Sciences, Technical Report No. UCB/EECS-2006-55, University of California at Berkeley, 2006

[Morg_49] Morgan S. P., Effect of Surface Roughness on Eddy Current Losses at Microwave Frequencies, Journal of Applied Physics, Volume 20, Issue 4, 1949, pp. 352-362

[Moya_07] Moya J. S., Lopez-Esteban S., Pecharroma´n C., The Challenge of Ceramic/metal Microcomposites and Nanocomposites, Progress in Materials Science, Volume 52, Issue 7, 2007, 1017–1090

[Mänt_09] Mäntysalo M., Mansikkamäki P., An Inkjet-Deposited Antenna for 2.4 GHz Applications, International Journal of Electronics and Communications, Volume 63, Issue 1, 2009, pp. 31 - 35

[Nils_07] Nilsson H.-E., Siden J., Olsson T., Jonsson P., Koptioun A., Evaluation of a Printed Patch Antenna for Robust Microwave RFID Tags, IET Microwaves, Antennas & Propagation, Volume 1, Issue 3, 2007, pp. 775-781.

[Niki_05] Nikitin P. V., Lam S., Rao K. V. S., Low Cost Silver Ink RFID Tag Antennas, IEEE Antennas and Propagation Society International Symposium, Volume 2B, 2005, pp. 353 - 356

[Niki_06] Nikitin P. V., Rao K. V. S., Theory and Measurement of Backscattering from RFID Tags, IEEE, Antennas and Propagation Magazine, Vol. 48, Issue 6, pp. 212 – 218, 2006

[Niki_07] Nikitin P. V., Rao K. V. S., Martinez R. D., Differential RCS of RFID Tag, Electronic Letters Volume 43 Issue 8, 2007, pp. 431 - 432

[Niki_08] Nikitin P. V., Rao K. V. S., Antennas and Propagation in UHF RFID Systems, IEEE International Conference on RFID, Las Vegas, Nevada, USA, 2008, pp. 277 – 288

[Niki2_05] Nikitin P. V., Rao K. V. S., Lam S. F., Pillai V., Martinez R., Heinrich H., Power Reflection Coefficient Analysis for Complex Impedances in RFID Tag Design, IEEE Transactions on Microwave Theory and Techniques, Volume 53, Issue 9, 2005, pp. 2721 - 2725

[Numm_10] Nummela J., Studies Towards Utilizing Passive UHF RFID Technology in Paper Reel Supply Chain, Tampere University of Technology doctoral thesis, TUT Publication 876, Tampere, Finland, 2010.

[Pard_04] Pardos F., Plastic Films in Europe and the Rest of the World, Smithers Rapra, 2004

[Pill_06] Pillai V., Impedance Matching in RFID Tags: To Which Impedance to Match?, IEEE Antennas and Propagation Society International Symposium, 2006, pp. 3505 - 3508

[Prud_94] Prudenziati M. (editor), Thick Film Sensors, Elsevier, 1994

[Psar_06] Psarras G. C., Hopping Conductivity in Polymer matrix–metal particles Composites, Composites Part A: Applied Science and Manufacturing Volume 37, Issue 10, 2006, pp. 1545 - 1553

[Puda_05] Pudas M., Halonen N., Granat P., Vähäkangas J., Gravure Printing of Conductive Particulate Polymer Inks on Flexible Substrates, Progress in Organic Coatings Volume 54, Issue 4, 2005, pp. 310 – 316

[Purs_08] Pursula P., Vähä-Heikkilä T., Müller A., Neculoiu D., Konstantinidis G., Oja A., Tuovinen J., Millimeter-Wave Identification—A New Short-Range Radio System for Low-Power High Data-Rate Applications, IEEE Transactions on Microwave Theory and Techniques, Volume 56, Issue 10, 2008, pp. 2221 - 2228

[Radi_06] Radivojevic Z., Andersson K., Hashizume K., Heino M., Mäntysalo M., Mansikkamäki P., Matsuba Y., Terada N., Optimised Curing of Silver Ink-jet Based Printed Traces, 12th International Workshop on THERMal INvestigation of ICs and Systems, Côte d'Azur, France, 2006, pp. 163 - 168

[Rao_99] Rao K. V. S., An Overview of Backscattered Radio Frequency Identification System (RFID), IEEE 1999 Asia Pacific Microwave Conference, Volume 3, 1999, pp. 746 – 749

[Rims_04] Rimska Z., Kresalek V., Spacek J., AC Conductivity of Carbon Fiber-Polymer Matrix Composites Carbon Fibers., Polymer Composites, Volume 23 Issue 1, 2004, pp. 95 - 103

[Roth_03] Rothon R., Particulate-Filled Polymer Composites (2nd Edition), Smithers Rapra, 2003

[Saha_06] Sahalos J. N., Orthogonal Methods for Array Synthesis - Theory and the ORAMA Computer Tool, John Wiley & Sons, 2006

[Saun_07] Saunders S., Aragón-Zavala A., Antennas and Propagation for Wireless Communication Systems (2nd Edition), John Wiley & Sons, 2007

[Scha_05] Schaffrath M., Ukkonen L., Sydänheimo L., Kivikoski M., RFID Antenna Design for Paper Industry Applications: Passive Bow-tie Transponder Performance Analysis, Proceedings of Second IASTED International Conference: Antennas radar and wave propagation, Banff, Alberta, Canada, 2005, pp. 348 – 353

[Schm_02] Schmitt R., Electromagnetics Explained - A Handbook for Wireless/RF, EMC, and High-Speed Electronics, Elsevier, 2002

[Sevk_08] Sevkat E., Li J., Liaw B., Delale F., A Statistical Model of Electrical Resistance of Carbon Fiber Reinforced Composites under Tensile Loading, Composite Science and Technology, Volume 68, Issues 10-11, 2008, pp. 2214 - 2219

[Side_05] Siden J., Olsson T., Fein M., Koptioug A., Nilsson H-E., Reduced Amount of Conductive Ink with Gridded Printed Antennas, Polytronic 2005, 5th International IEEE Conference on Polymers and Adhesives in Microelectronics and Photonics, Wroclaw, Poland 2005, pp. 86 - 89

[Side_07] Siden J., On the Design, Characterization and Optimization of RFID Tag Antennas, Mid Sweden University doctoral thesis, Sundsvall, Sweden, 2007

[Side2_07] Siden, J., Fein, M. K., Koptyug A., Nilsson, H-E., Printed Antennas with Variable Conductive Ink Layer Thickness, IET Microweves, Antennas & Propagation, Volume 1, Issue 2, 2007, pp. 401–407

[Simp_02] Simpson W. S. (editor), Crawshaw G. H. (editor), Wool: Science and Technology, Woodhead Publishing, 2002

[Stor_06] Storey N., Electronics A System Approach, 3rd Edition, Pearson Education Ltd., 2006

[Stut_98] Stutzman W. L., Thiele G. A., Antenna Theory And Design, 2nd Edition, Wiley, 1998

[Suzu_09] Suzuki S., Okamoto H., Murakami H., Asama H., Morishita S., Mishima T., Lin X., Itoh H., Force Sensor System for Structural Health Monitoring Using Passive RFID Tags, Sensor Review, Volume 29 Issue 2, 2009, pp. 127 - 136

[Syed_07] Syed A., Demarest K., Deavours D.D., Effects of Antenna Material on the Performance of UHF RFID Tags, IEEE International Conference on RFID, Grapevine, Texas, USA, 2007, pp. 57 - 62

[Swed_10] Swedberg C., In the U.K., Libraries Switch to Self-Serve, RFID journal Inc., 2010

[Taya_98] Taya M., Kim W., Ono K., Piezoresistivity of a Short Fiber/Elastomer Matrix Composite, Mechanics of Materials Volume 28, Issues 1-4, 1998, pp. 53–59

[Tudo_07] Tudorache M., Bala C., Biosensors Based on Screen-Printing Technology and Their Applications in Environmental and Food Analysis, Analytical and Bioanalytical Chemistry, Volume 388, Issue 3, 2007, pp. 565 - 578

[Ujii_06] Ujiie H., Digital Printing of Textiles, Woodhead Publishing, Limited, 2006

[Ukko_06] Ukkonen L., Development of Passive UHF RFID Tag Antennas for Challenging Objects and Environments, Tampere University of Technology doctoral thesis, TUT Publication 621, Tampere, Finland, 2006

[Ukko_07] Ukkonen L., Sydänheimo L., Kivikoski M., Read Range Performance Comparison of Compact Reader Antennas for a Handheld UHF RFID Reader, IEEE International Conference on RFID, Grapevine, Texas, USA, 2007, pp. 63 - 70

[Ukko_10] Ukkonen L., Sydänheimo L., Threshold Power-based Radiation Pattern Measurement of Passive UHF RFID Tags, Progress In Electromagnetics Research Symposium (PIERS) Online, Volume 6, Issue 6, 2010, pp. 523 - 526

[Ukko2_06] L. Ukkonen, M. Schaffrath, J. Kataja, L. Sydänheimo and M. Kivikoski, Evolutionary RFID Tag Antenna Design for Paper Industry Applications, International Journal of Radio Frequency Identification Technology and Applications (IJRFITA), Inderscience, Vol. 1, Issue 1, 2006, pp. 107 – 122

[Vacc_02] Vaccari J. A., Brady G. S., Clauser H. R., Materials Handbook (2nd Edition), McGraw-Hill, 2002

[Virt_10] Virtanen J., View to RFID Market Opportunities, RFIday 2010, Advances and Challenges in RFID Technology Workshop, Tampere, Finland, 2010

[Viss_05] Visser H. J., Array and Phased Array Antenna Basics John Wiley & Sons, 2005

[Voya_10] Voyantic Ltd, http://www.voyantic.com/, (Accessed: 25.8.2010)

[Whee_99] Wheeler I., Metallic Pigments in Polymers, Smithers Rapra Technology, 1999

[Will_03] William E., Practical RF System Design, Wiley-IEEE Press, 2003

[Worz_07] Worzakowska M., Study of Polymerization Kinetics of the Unsaturated Polyester Resin Using Acetyl Aceton Peroxide and Co(II)octoate, Journal of Thermal Analysis and Calorimetry, Volume 88, Issue 2, 2007, pp. 441–448

[Yang_06] Yang L., Basat S., Rida A., Tentzeris M. M., Design and Development of Novel Miniaturized UHF RFID Tags on Ultra-Low-Cost Paper-Based Substrates, Microwave Conference APMC 2006, Asia-Pacific 2006, Yokohama, Japan, 2006, pp. 1493 - 1496

[Yang_07] Yang L., Rida A., Vyas R., Tentzeris M. M., RFID Tag and RF Structures on a Paper Substrate Using Inkjet-Printing Technology, Microwave Theory and Techniques, IEEE Transactions on Volume 55, Issue 12, Part 2, 2007, pp. 2894 - 2901

[Youn_00] Young H. D., Freedman R. A., University physics, 10th Edition, Addison Wesley Longman, Inc., 2000

[Zebr_07] Gen 2 Implications for Smart Label Printing A ZEBRA BLACK & WHITE PAPER, ZIH Corporation, 2007, Available: http://www.mobilityexperts.com/media/Gen_2_Implications_for_Smart_Label_Printing.pdf, (Accessed 25.8.2010)

[Zebr_10] Available: http://www.zebra.com/id/zebra/na/en/index/rfid/faqs/epc_rfid_technology.html#FAQ_53090, (Accessed 25.8.2010)

Publication 1

Analysis of Silver Ink Bow-Tie RFID Tag Antennas Printed on Paper Substrates

Merilampi S., Ukkonen L., Sydänheimo L., Ruuskanen P., Kivikoski M.

Publication 2

The Characterization of Electrically Conductive Silver Ink Patterns on Flexible Substrates

Merilampi S., Laine-Ma T., Ruuskanen P.

© Microelectronics Reliability, Volume, 49, Issue 7, 2009, pp. 782 - 790

Publication 3

Printed RFID Tag Performance with Different Materials

Merilampi S., Haukka V., Ukkonen L., Ruuskanen P., Sydänheimo L., Kivikoski M.,
Loo C-H, Yang F., Elsherbeni A. Z.

Publication 4

The Effect of Fabrication Methods on Passive RFID Tags

Björninen T., Merilampi S., Ukkonen L., Sydänheimo L., Ruuskanen P.

Publication 5

The Effect of Ink Layer Thickness on RFID Tag Performance

Merilampi S., Björninen T., Vuorimäki A., Ukkonen, L., Ruuskanen P., Sydänheimo L.

Publication 6

Performance Comparison of Silver Ink and Copper Conductors for Microwave Applications

Björninen T., Merilampi S., Ukkonen L., Ruuskanen P., Sydänheimo L.

Publication 7

Characterization of UHF RFID Tags Fabricated Directly on Convex Surfaces by Pad Printing

Merilampi S., Björninen T., Ukkonen L., Ruuskanen P., Sydänheimo L.

Publication 8

Analysis of Electrically Conductive Silver Ink on Stretchable Substrates under Tensile Load

Merilampi S., Björninen T., Haukka V., Ruuskanen P., Ukkonen L., Sydänheimo L.

© Microelectronics Reliability, Volume 50, Issue 12, 2010, pp. 2001-2011

Publication 9

Embedded Wireless Strain Sensors Based on Printed RFID Tag

Merilampi S., Björninen T., Ukkonen L., Ruuskanen P., Sydänheimo L.

© Sensor Review, Volume 31, Issue 1, 2011, pp. 32-40